URBAN LAND COVER CLASSIFICATION FROM HIGH RESOLUTION GEOEYE-1 IMAGERY USING A LIDARBASED DIGITAL SURFACE MODEL

by
ULRICH PAVLIQUE ETOUGHE KONGO

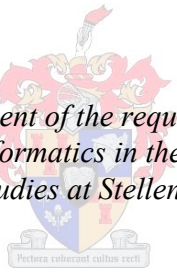

Thesis presented in fulfilment of the requirements for the degree of Master of Science in GeoInformatics in the Faculty of Geography and Environmental Studies at Stellenbosch University

Supervisor: Mr, Nitesh Poona
Co-supervisor: Prof, Adriaan van Niekerk

March 2015

DECLARATION

By submitting this research report electronically, I declare that the entirety of the work contained therein is my own, original work, that I am the owner of the copyright thereof (save to the extent explicitly otherwise stated), that reproduction and publication thereof by Stellenbosch University will not infringe any third party rights and that I have not previously in its entirety or in part submitted it for obtaining any qualification.

March 2015

SUMMARY

Urban planning and management require up-to-date information about urban land cover. Producing such geospatial information is time consuming as it is usually done manually. The classification of such information from satellite imagery is challenging owing to the difficulties associated with distinguishing urban features having similar spectral properties. Therefore, this study evaluates the combination of a digital surface model (DSM) derived from LiDAR data and very high-resolution GeoEye-1 satellite imagery for classifying urban land cover in Cape Town. The value of the DSM was assessed by comparing a land cover product obtained from the GeoEye-1 image to a map produced using both the GeoEye-1 image and the DSM. A systematic segmentation procedure for the two classifications scenarios preceded a supervised (using a support vector machine, K nearest neighbour and classification and regression algorithm tree classifiers) and rule-based classification. The various approaches were evaluated using a combination of methods.

When including the DSM in the supervised and rule-based classifications, the overall accuracy and kappa vary between 80% to 83% and 0.74 to 0.77 respectively. When the DSM is excluded, the overall accuracy ranges between 49 to 64% whereas kappa ranges between 0.32 to 0.53 for the two classification approaches. The accuracies obtained are always about 20% higher when the DSM is included. The normalised DSM (nDSM) enabled accurate discrimination of elevated (e.g. buildings) and non-elevated (e.g. paved surfaces) urban features having similar spectral characteristics. The nDSM of at least one-metre resolution and one metre vertical accuracy influenced the accuracy of the results by correctly differentiating elevated from non-elevated.

The rule-based approach was more effective than the supervised classification, particularly for extracting water bodies (dams and swimming pools) and bridges. Consequently, a rule-based approach using very high spatial resolution (EHSR) satellite imagery and a LiDAR-derived DSM is recommended for mapping urban land cover.

KEY WORDS AND PHRASES

Urban land cover, GeoEye-1 imagery, LiDAR, digital surface model and object-based image analysis, Cape Town.

OPSOMMING

Stedelike beplanning- en bestuur vereis dat inligting oor grondbedekking (*land cover*) op datum moet wees. Die vervaardiging van hierdie georuimtelike inligting is tydrowend omdat dit gewoonlik met die hand gedoen word. Die onttrekking van sulke inligting vanuit satellietbeelde bied 'n groot uitdaging omdat stedelike voorwerpe met soortgelyke spektrale eienskappe moeilik is om van mekaar te onderskei. Hierdie studie evalueer die kombinasie van 'n digitale oppervlak model (DOM) afkomstig van LiDAR-data en 'n baie hoë resolusie GeoEye-1-satellietbeeld om stedelike grondbedekking in Kaapstad te klassifiseer. Die waarde van die DOM word bepaal deur 'n grondbesettingsproduk wat vanuit 'n GeoEye-1-beeld verkry is te vergelyk met 'n grondbesettingsproduk wat verkry is deur beide die GeoEye-1-beeld en die DOM te gebruik. Sistematiese segmentasie word op die twee benaderings uitgeoefen en dit word gevolg deur 'n gekontroleerde klassifikasie (steunvektormasjiene, k-naaste aangrensende waarde en klassifikasie en regressie algoritme) en 'n reël-gebaseerde algoritme. Hierdie verskeie benaderings is geëvalueer met behulp van 'n kombinasie van kwalitatiewe en kwantitatiewe metodes.

Toe die DOM in die gekontroleerde en reël-gebaseerde klassifikasie ingesluit is, het die algehele akkuraatheid en kappa tussen 80% en 83%, en 74% en 77% gewissel. Toe die DOM uitgesluit is, het die algehele akkuraatheid en kappa tussen 49% en 64%, en 32% en 53% vir die twee klassifikasiebenaderings gewissel. Die behaalde akkurraatheidswaardes is altyd 20% hoër as die DOM ingesluit word. Dit is hoofsaaklik omdat die DOM akkurate onderskeiding tussen hoë (bv. geboue) en plat (bv. geplaveide oppervlaktes) stedelike bakens met gelyksoortige spektrale eienskappe in staat stel. Die kwaliteit van die DOM beïnvloed die akkuraatheid van die resultate. 'n DOM van ten minste een meter resolusie, met een meter of beter vertikale akkuraatheid, word benodig om te verseker dat geboue en ander beboude bakens korrek van mekaar onderskei kan word.

Die reël-gebaseerde benadering was meer effektief as die gekontroleerde klassifikasie, veral om waterliggame (damme en swembaddens) en brûe te identifiseer. Gevolglik word 'n reël-gebaseerde benadering met die hoë resolusie satellietbeelde en 'n LiDAR-afgeleide DOM aanbeveel om stedelike grondbesetting te karteer.

TREFWOORDE EN -FRASES

Stedelike grondbesetting, GeoEye-1-beelde, LiDAR, digitale oppervlakmodel en objekgebaseerde beeldanalise OBIA, Cape Town.

ACKNOWLEDGEMENTS

Firstly, I thank almighty God for making me who I am and giving me the opportunity to further my studies at Stellenbosch University.

I sincerely thank my supervisor, Mr Nitesh Poona, for his patience in assisting me any time I needed help. Thank you for being my supervisor and for investing his precious time and effort to improve my research.

I specially thank my co-supervisor, Prof Adriaan van Niekerk, for his insight and suggestions that inspired my research; for his guidance on how to conduct quality research and write scientific papers.

I thank Marianne Cronje for her kindness, help and encouragement during all the years that I have been at Stellenbosch University.

To Theo Pauw and Garth Stephenson, I say thank you for your availability and guidance, and for providing me with the necessary data and assistance.

I also sincerely thank Dr. Sydoine Moudouma and Wasiu Sonibare for their encouragement as well as offering assistance with editing my reports.

I thank Vieky, Emmanuel, Andrea, Nyasha and all my fellow students in the department, who equally felt the pressure and spent nights together with me, working and chasing submission deadlines. Special thanks to Gatien, Stephane, Emmanuel and Blanchard for having joined hands with me; praying together each year for our funding to be supplied.

I wish to thank my partner, Mireille Moussounda, for always cheering me up when I was down, for her encouragements and continued assistance.

Finally, I thank my entire family for the love and kindness they have for me and especially my mother for her love and my brothers and sisters for assisting her.

I dedicate this thesis to all my family members and hope they will quickly forget the pain, which they endured all these years due to my absence from them.

CONTENTS

TABLES

FIGURES

ACRONYMS AND ABBREVIATIONS

ALS	airborne laser scanning
ATCOR	atmospheric and topographic correction
AVHRR	advanced very high resolution radiometer
CART	classification and regression algorithm tree
CBD	central business district
CD: NGI	Chief Directorate National Geo-Spatial Information
CGA	Centre for Geographical Analysis
CIR	colour infrared
CTCC	Cape Town city centre
DEM	digital elevation model
DN	digital number
DSM	digital surface model
DTM	digital terrain model
EHSR	Extremely high spatial resolution
GCP	ground control point
GIS	geographical information system
GLCM	grey-level co-occurrence matrix
GPS	global positioning system
IMU	inertial measurement unit
INS	inertial navigation system
InSAR	interferometric synthetic aperture radar
KNN	K nearest neighbour
LASER	light amplification by stimulated emission of radiation
LiDAR	light detection and ranging
LO19	longitude of origin using the 19th central meridian as reference
MLC	maximum likelihood classifier
MRS	multiresolution segmentation
MS	multispectral
NBI	new built up index
NDBI	normalised difference built-up index
nDSM	normalised digital surface model
NDVI	normalised difference vegetation index

NDWI	normalised difference water index
NIR	near infrared
NOAA	National Oceanic and Atmospheric Administration
OA	overall accuracy
OBIA	object-based image analysis
PA	producer accuracy
PPO	parent process objects
RADAR	radio detection and ranging
RBC	rule-based classification
RF	region of interest
RF-SVM	random forest-support vector machine
RGB	red green blue
RMSE	root mean square error
ROI	region of interest
RPC	rational polynomial coefficient (or camera)
RS	remote sensing
SANBI	South African National Biodiversity Institute
SBC	SPOT 5 building count
SMA	spectral mixture analysis
SVM	support vector machine
UA	users accuracy
UN	United Nations
UTM	universal transverse Mercator

1 CHAPTER 1 INTRODUCTION

1.1 BACKGROUND

Land cover mapping can be used to identify environmental factors that contribute to environmental change (Giri et al. 2011). Such mapping is used to determine the composition and distribution of landscape types and is subsequently used as the basis for assessing ecosystem change (Reyers et al. 2009). As an example, mapping impervious surface is a key input for understanding the urban hydrological system for flood control, while vegetation remains a critical structure component in the urban environment in that the amount of vegetation is closely related to quality of urban life and surface biophysical processes (Weng & Quattrochi 2006). To provide accurate and current land surface characterization and its change at global and regional scales, maps of land cover are increasingly being created through the classification of remotely sensed data (McIver 2001). For example, Schoeman et al. (2013) reported an increase of 1.2 % in transformed land specifically associated with urban, cultivation, plantation forestry and mining between 1994 and 2005 during their study of South African land cover change maps.

A number of South African studies have focused on urban land cover expansion and its consequences (Ros Gordon & Bertoldi 2007; Schoeman et al. 2013), and land management and spatial planning in towns and cities (Kitchin & Oven 2009). For example, Ros Gordon & Bertoldi (2007) discovered rapid expansion of irregular housing that caused servicing problems for the authorities. The research methodology applied was based on a strategic approach and qualitative review of data such as surveyor general, census data and land cover data that were made available. To cope with urban related issues, Kitchin & Oven (2009) suggested the use of effective land management to guarantee poverty alleviation, urban efficiency and long-term sustainability, as well as increased access to land by the poor. According to Kitchin & Oven (2009), high demand for middle-income housing, lack of favourable social housing opportunities and urban agriculture, can be mitigated through the effective management of land. This emphasizes the significance of land cover information, which is a key component for effective land management (Yuan et al. 2005).

“In urban planning, the land use map generated by thematic classification of satellite images can be considered as an end-product, since it is used as a document showing the prevailing situation before any planning action, and as a starting point for further analyses that will propagate the qualities and the errors inherent in the classification” (Donnay et al. 2003:5). Over the last few

decades, the expansion of urban areas in South Africa has accelerated because of the rural-urban migration of black communities due to lack of infrastructure and poor service delivery as well as unemployment in rural areas (Cox, Hemson & Todes 2004). The resulting rapid increase in population in urban areas stimulated new urban management challenges, mainly in the housing sector with the Breaking New Ground housing programme (Charlton & Kihato 2006). Land cover information has the potential to ensure effective land management because it is a key for the success for such programmes.

Remote sensing (RS) provides an excellent basis for cost-effective, up-to-date, and large-area mapping and monitoring of urban land cover at multiple scales (Berger et al. 2013). Furthermore, RS offers an important means of detecting and analysing temporal changes occurring within urban areas (Taubenbock et al 2010). Hence, the technology has been widely used for urban environmental research, natural resources management, and urban land cover investigation (Li, Zhang & Sun 2009). A major contribution of RS is the production of a synoptic view of the earth from the space (Holland, Boyd & Marshall 2006), which has become an essential data source for landscape analysis (Burnett & Blaschke 2003). RS has the advantage of providing geospatial data that cannot be collected using field methods (Turner et al. 2003); and has been used to produce valuable land cover and land use information in various applications (e.g. Benz et al. 2004; Kasetkasem & Varshney 2011; McIver & Friedl 2001; Samad et al. 2009). A wide variety of maps portraying vegetation, land cover and land use have been created. Nowadays, RS has witnessed tremendous applications in areas like geology and mineral exploration, oil and mining, oceanography, agriculture and forestry, hazard assessment mainly at the post-disaster phase, land degradation and environmental monitoring (DigitalGlobe 2014; Sabins 2007). In the past decade, important resources have been discovered through RS. For example, the first commercial oil fields in Papua New Guinea were discovered using aerial RADAR images, and in Saudi Arabia, new oil production trend was discovered using Landsat imagery (Sabins 2007).

More recently, researchers have paid increased attention to investigating automated urban feature extraction from high spatial resolution imagery and height information in order to facilitate the development of methodological approaches for the fast acquisition of accurate geospatial data (Hermosilla et al. 2011; Kabolizade, Ebadi & Ahmadi 2010). For example, Kabolizade, Ebadi & Ahmadi (2010) extracted building automatically from a combination of aerial image and the nDSM generated from LiDAR data. The author proposed an improved snake model which he defined as an energy minimizing spline guided by external constraint forces and influence by image forces that pull it towards features such as edge or line. According to Kabolizade, Ebadi &

Ahmadi (2010), the improved model increased the accuracy of the building extraction up to 96 % against the gradient vector flow (GVF) which extracts buildings with 81 % accuracy.

1.2 PROBLEM FORMULATION

As metropolitan areas grow and change at an unprecedented rate (Fraser, Dial & Grodecki 2006), the provision of spatial and temporal data that illustrate where changes are occurring becomes imperative (Eurosense 2011). RS has specific potential for detailed and accurate mapping of urban areas at different spatiotemporal scales, and has long been used to map urban growth and urban morphology (Murayama & Bahadur Thapa 2011). An understanding of emerging spatial patterns of urban form is a necessity as the spatial configuration of the urban landscape provides a snapshot of various economic, social and political factors that influence land use decisions (Netzband, Stefanov & Redman 2007). The use of remotely sensed data and techniques can convey such knowledge at different spatial scales with greater cost-efficiency. Although remotely sensed data are made available to the public through commercial companies, operational applications and the use of appropriate RS technologies are barely used effectively in developing and emerging countries (Feldkotter 2007) due to a lack of suitable competencies (DIANE Publishing Company 1995).

In South Africa, ESKOM (a South African electricity public utility, established in 1923 as the Electricity Supply Commission (ESCOM) by the government of South Africa) produced a building count dataset using SPOT 5 imagery (SANBI 2009). This 2006/2007 data set provided the location of all electrifiable dwelling units and buildings in South Africa. Semi-automated extraction of residential buildings from SPOT 5 imagery is impractical in high-density areas essentially dwelling units in informal settlement, due to the relatively low spatial resolution (2.5 m) of the imagery (Durieux, Lagabrielle & Nelson 2008; Weng & Hu 2008). Therefore, the 2006/2007 SPOT 5 building count (SBC) produced by ESKOM was used via digitisation of points. Such methods are labour intensive and expensive. New techniques are thus required for a fast and cost effective acquisition of such spatial information with the advance of extremily high spatial resolution imagery (EHSR).

Several studies have explored land cover extraction from aerial photographs and very high spatial resolution (VHSR) imagery and achieved satisfactory results (Siart, Bubenzer & Eitel 2009; Myint et al. 2011). Due to spectral similarities between features, the land cover maps often contain errors. New approaches such as the use of height information have been developed given

the growing demand for accurate geospatial information (Potsiou et al 2010). Such information can potentially accelerate the differentiation of features of similar spectral information based on their height.

A variety of EHSR sensors and platforms are now available. This data combined with complementary data such as DSM, are suitable for the detection of buildings (Ioannidis, Psaltis & Potsiou 2009). Remote sensing imagery and high-resolution DEMs of South Africa are generated by many institutions such as the Centre for Geographical Analysis (CGA) (Stellenbosch University) and the Chief Directorate: National Geo-spatial Information (CD: NGI). For example, the CGA has developed a 5-metre resolution DEM of the Western Cape (van Niekerk 2012) while the NGI intensifying the production of high-resolution red green blue (RGB) and colour-infrared (CI) aerial imagery. Although the DEMs data are made available across the country as well as high quality remotely sensed imagery, the techniques to generate and to use them effectively are still exceptional skills for many users across the world.

The availability of EHSR imagery such as GeoEye-1 and LiDAR offers opportunities for investigating the semi-automated extraction of urban land cover. However, such datasets require new approaches because existing methods cannot readily convert them to useful information. Furthermore, their strengths and limitations in the stream of urban land cover extraction are still being discovered and understood by RS users through new research applications.

1.3 RESEARCH AIM AND OBJECTIVES

The aim of this research is to determine the benefits of combining a high-resolution nDSM with GeoEye-1 satellite imagery to extract urban land cover using an object-based image analysis approach. The specific objectives of the research are to:

1. Review from the literature the various approaches for extracting urban land cover information from GeoEye-1 imagery and nDSM;
2. Generate a high definition nDSM from LiDAR data;
3. Produce urban land cover maps from GeoEye-1 imagery using a supervised and rule-based approach;
4. Integrate the high-resolution nDSM as a complementary source for mapping urban land cover; and

5. Evaluate the capabilities for the nDSM to optimise the accuracy of urban land cover extraction.

1.4 METHODOLOGY AND RESEARCH DESIGN

Kothari (2011) defines the research methodology as a systematic way to solve the research problem. For the author, the research methodology includes the various steps that are generally adopted by a researcher in studying his research problem along with the logic behind them.
This research tests different methods with various feature sets to classify urban land cover through a qualitative and a quantitative approach. According to Kuma (2014), a quantitative approach of a study aims to quantify the extent of the variation in a phenomenon, measures objectively the variables of the process, gives importance to the validity and reliability of the findings; whereas a qualitative approach aims to explore the diversity; emphasises the description. This research attempts to measure the extent of the land cover accuracy's variation when adding a nDSM to the EHSR GeoEye-1 image classification.

This study has been conducted following the research design in Figure 1.1. The research problem in Chapter 1 has motivated the first objective covered by the literature review in Chapter 2. Chapter 3 describes the technique of data collection and preparation in line with the second objective; while Chapter 4 addresses the third and fourth objectives in the description of land cover classification methods sections. Finally, Chapter 5 and Chapter 6 addresses the last objective.

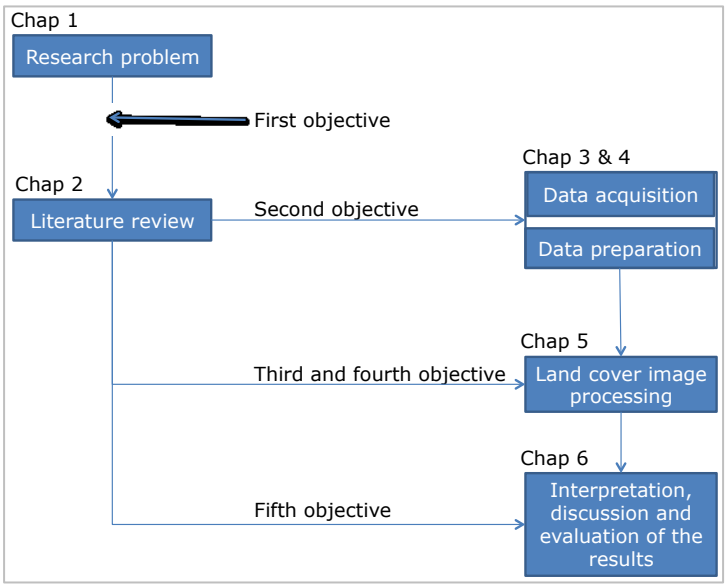

Figure 1.1 Research design

1.5 THESIS STRUCTURE

This thesis is organised into six chapters. Chapter 1 is the general introduction that includes the research aim and objectives, and provides a description of the methodology. Chapter 2 presents a review and significance of urban land cover information, covers the basics of object-based image analysis (OBIA) and a review of LiDAR technology. Chapter 3 addresses the pre-processing and the generation of the nDSM. Chapter 4 describes the segmentation process and the data processing method used. Chapter 5 introduces the results, followed by a discussion. Chapter 6 provides a summary of the findings, with conclusions and recommendations.

2 CHAPTER 2 LITERATURE REVIEW

2.1 SATELLITE IMAGERY

Earth observation (EO) plays a key role in weather prediction, mapping as well as environmental and urban applications where intensive use of imagery acquired from satellites, aircraft or ground based RS platform is evident (Carbonneau & Piegay 2012). "Until recently, maps and land-survey records from the 1960s and 1970s were used for urban studies, but now the trend has since shifted to using digital imagery acquired by EO" (Netzband et al. 2007: 171). Urban studies using RS data began with the first generation of satellite sensors such as Landsat (Netzband et al. 2007). With the latest generation of satellite such as WorldView 3 providing 30 cm spatial resolution imagery, urban and regional planners are increasingly using RS to derive information on the urban environment in a timely, detailed and cost-effective way to accommodate various planning and management activities (Yang 2011).

EO data have specific properties as defined by Wulder & Franklin (2006): (1) spatial resolution provides an indication of the size of the minimum area that can be determined by a detector at an instant in time, (2) temporal resolution provides an indication of the time it takes for a sensor to return to the same location on earth's surface, (3) spectral resolution provides an indication of the number and width of the spectral wavelengths capture by a particular sensor, and (4) radiometric resolution provides an indication of the actual information content of an image and is referred to as the number of intensity levels that a sensor can use to record a given signal.

With the continue advancement of RS technologies, Bhatta (2010) has proposed the current scale for satellite imagery (Table 2.1). According to Ling, Li & Vang (2012), the spatial extent of urban areas has been classified and mapped successfully for a long time using RS data. Currently, EHSR images are increasingly being used for studies of urban land cover mapping providing more detailed information. The classification methods being used for such studies can be divided into three groups namely, sub pixel, pixel-based and object-oriented methods (Ling, Li & Vang 2012). In addition, the use of object-based methods offers the advantage of integrating ancillary data and other RS data such as LiDAR and nDSM.

Table 2.1 Application scale for various remote sensing images

Pixel size (m)	Definition	Platform /Sensor	Application scale
0.1-0.5	Extremely high spatial resolution	Airbone scanne, aerial photos, GeoEye-1 (pan), WorldView 1 (ms), WorldView 2 (ms)	1:500-15000
0.5-1	Very high resolution	Ikonos (pan), QuickBird (pan), Orbview (pan)	15000-10 000
1-4	High resolution	Ikonos (ms), QuickBird (ms), Orbview (ms), GeoEye-1 (ms), IRS (pan)	1:10.000-1:15.000
4-12	Medium resolution	IRS (pan), IRS (LISS-IV ms), SPOT 5 (pan, ms)	1:15.000-1:25.000
12-50	Low resolution	ASTER, IRS (ms), Landsat-TM/ETM+(pan, ms), SPOT 4 (ms)	1:25000-1:100.000
50-250	Very low resolution	Landsat MSS	1: 100.000-1:500.000
250	Extremely low resolution	NOAA	>1: 500.000

Source: Bhatta 2010: 54

2.2 LiDAR AND ANCILLARY DATA

2.2.1 Definition and characteristics of LiDAR

LiDAR is an optical remote-sensing technique that uses laser (light amplification by stimulated emission of radiation) to densely sample the surface of the earth by making highly accurate x, y, z measurements (ESRI 2013a). The major hardware components of a LiDAR system are a collection vehicle (aircraft, helicopter, motor vehicle, or tripod), a laser scanner system, a GPS (global positioning system) and an inertial navigation system (INS) (ESRI 2013a). LiDAR is an active optical sensor that transmits laser beams toward a target while moving through specific survey routes (Figure 2.1). The emitted laser pulses strike objects on the ground and the return echo is received by a light-sensing device. A single emitted laser pulse can return to the LiDAR sensor as one or many returns (Fowler 2001). In addition to recording returned pulse range values, some scanners provide signal intensity, amplitude and pulse angle (Renslow, Greenfiel & Guay 2000). The reflection of the laser from the target is detected and analysed by receivers within the LiDAR sensor. These receivers record the precise time, starting from the laser pulse emission by the sensor to the return echo, in order to calculate the range distance between the sensor and the target (Esri 2013a).

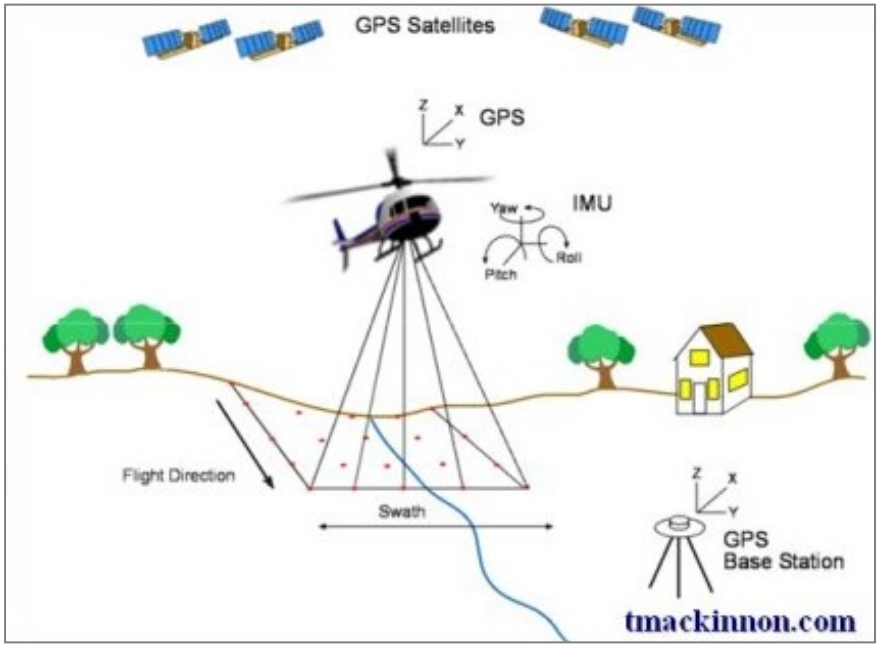

Source: tmackinnon.com

Figure 2.1 Helicopter LiDAR vehicle, satellites and GPS base station representing the entire LiDAR system.

Combined with the positional information (GPS and INS), distance measurements are transformed to measurements of actual three-dimensional points of the reflective target in object space (ESRI 2013a). Following the collection of LiDAR data, the mass point cloud data sets produced are post-processed by analysing the laser time range, laser scan angle, GPS position, and INS information into highly accurate georeferenced x, y, z coordinates (ESRI 2013a).

Each LiDAR system is developed with a software component that visualizes (Figure 2.2) and processes the complete data set to filter irrelevant data, such as a point on top of a flag pole (Fowler 2001). As the produced mass cloud of points can be managed, visualised and analysed, the quality control mechanism can be achieved, either using the GPS tagged video or the digital frame camera integrated to each LiDAR system. Fowler (2001) reported that the processing technician can scroll through the tape or photo record and view what is beneath the LiDAR at any given point as illustrated in Figure 2.2 and Figure 2.3.

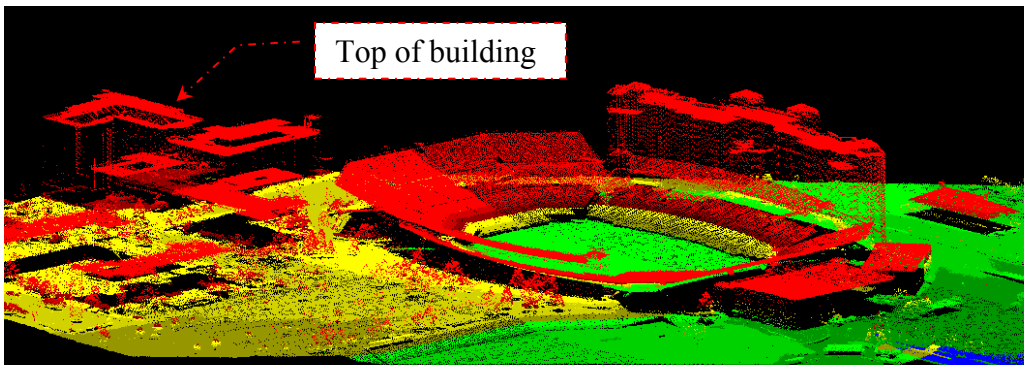

Source: Richmond (2013)

Figure 2.2 A 3-D view of LiDAR cloud point's model of the University of Nebraska's Memorial Stadium.

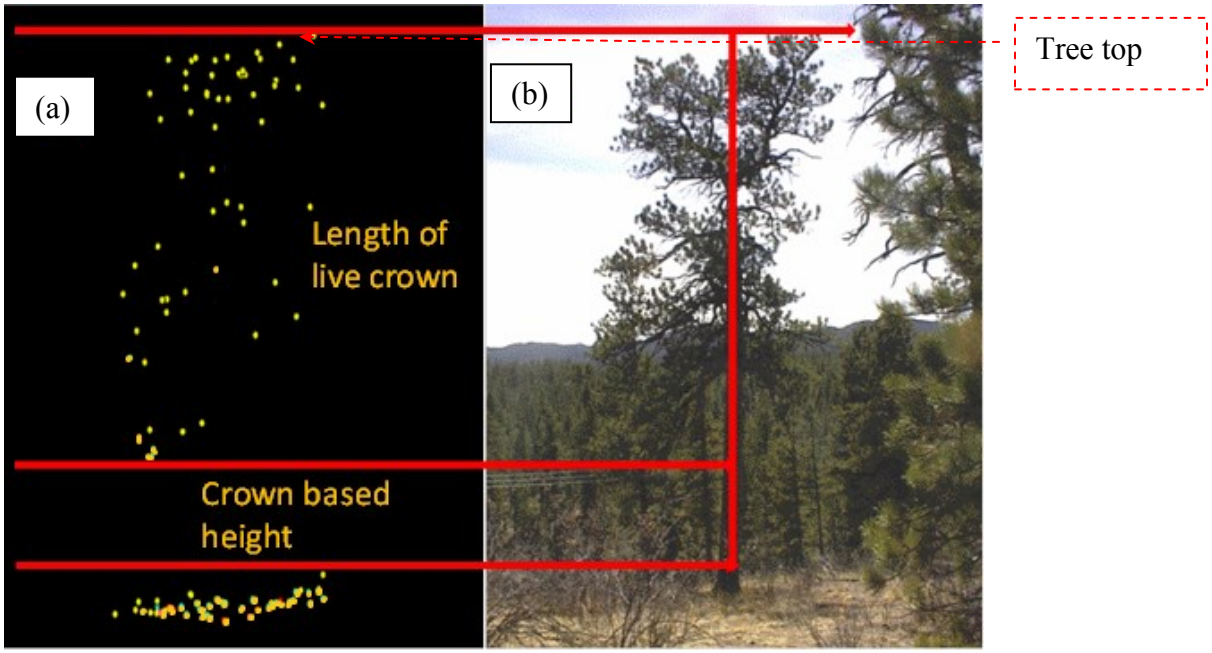

Source: Adapted from Dutton e-Education Institute (2014)

Figure 2.3 LiDAR cloud points captured for forest and bare soil representing in 3-D space (a) and (b) real world.

The first return laser pulse is the most significant return and will be associated with the highest feature in the landscape such as the top of a building (e.g. red cloud points in Figure 2.2) or treetop (e.g. yellow point on top of Figure 2.3). The first return can also represent the ground in which case only one return will be detected by the LiDAR system.

Figure 2.4 illustrates the multiple return pulses of a LiDAR beam. The time trip of the laser pulse increases as the pulse travel towards the ground. In Figure 2.4a, the cloud points are classified

according to the travelling time of the return pulse from the target to the sensor. Consequently, the first return cloud point will represent the shortest time while the last return takes the longest time to reach the sensor. The height of the point cloud increases as the distance to the sensor either reduces or increases relative to the ground points produced by the LiDAR sensor (Figure 2.4b). Points are classified in first, second, third up to last return based on their height above the ground (Esri 2013a).

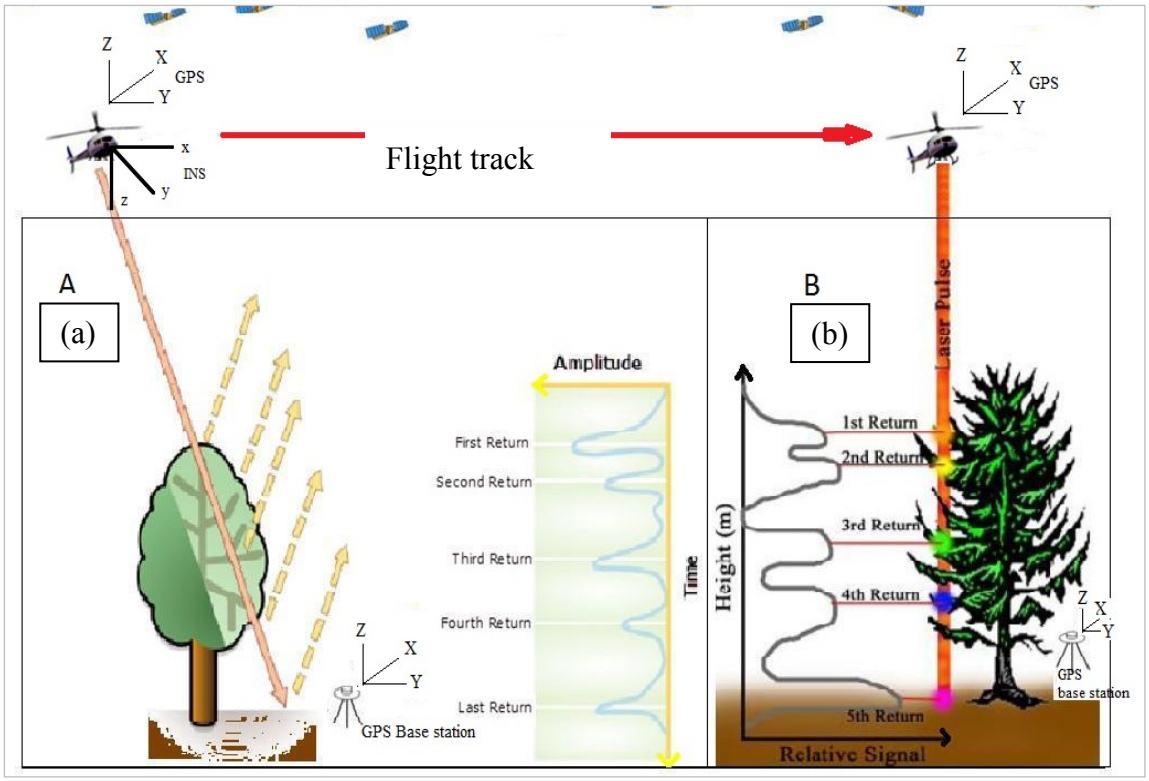

Sources: Adapted from ESRI (2013a)

Figure 2.4 Multiple-return LiDAR technology displaying multiple returns from a beam oblique laser (a) and multiple vertical laser beam (b).

In summary, LiDAR has become an accepted means of acquiring accurate terrain elevation data because of the rapid and cost-effective data acquisition and short processing time, compared to survey based DSM acquisition methods (Charaniya, Manduchi & Lodha 2005; ESRI 2013b; Gehrke et al. 2010). Furthermore, the precision and accuracy of LiDAR exceeds that of traditional remotely sensed imagery (Gatziolis & Andersen 2008).

2.2.2 LiDAR and the digital elevation model

While the need for large scale mapping of urban areas using EHRS imagery continues to grow, LiDAR technology offers the advantage of being used to derive accurate high- resolution digital surface models (DSMs) which can support the extraction of urban features (Gamba & Houshmand 2000; Renslow, Greenfiel & Guay 2000). Both airborne and terrestrial LiDAR are revolutionising the domain of EO for a wide range of applications including the mapping of canopy gaps in continuous cover forest (Gaulton & Malthus 2010), providing information about the ecosystem structure for understanding and monitoring of environmental change (Béland, Widlowski & Fournier 2014), the city modelling and surface reconstruction (Habib et al. 2005), and building extraction (Niemeyer, Rottensteiner & Soergel 2014).

LiDAR technology has emerged as the most appropriate means of generating DEM by providing high-resolution vertical and horizontal spatial data (Brennan & Webster 2006; Owechko, Medasani & Korah 2010). LiDAR has subsequently become a powerful tool in EO as it offers great potential for mapping tree canopies as well as the bare earth, while also providing information about canopy heights and volumes at much less fieldwork and manpower time than required by traditional methods (Renslow, Greenfiel & Guay 2000). Within an urban context, LiDAR has been used in many applications including automated extraction of roads (Clode, Kootsookos & Rottensteiner 2004; Clode et al. 2006), building footprint extraction (Li et al. 2013; Rottensteiner & Briese 2002; Wang, Lodha & Helmbold 2006). Meng, Curri & Zhao (2010) concluded that LiDAR is arguably superior to traditional methods such as photogrammetry techniques, automated image matching and elevation extractions techniques because:

(1) dense LiDAR point clouds enable the generation of highly accurate high-resolution nDEM;

(2) surface features can be extracted on the base of a height context analysis of the LiDAR points, thus enabling accurate mapping of surface features like buildings, trees, power lines, and pipelines;

(3) dense LiDAR point clouds provide the easiest way to identify small changes in elevation, hence making it easier to map regions with little textural variations, including variations in the surface of vegetation canopies;

(4) LiDAR pulses penetrate the vegetation canopy creating multiple returns which can be used to facilitate vegetation classification in different seasons;

(5) multiple returns of LiDAR enable the mapping of ground elevations, even in regions of dense vegetation.

2.3 ELEVATION MODELS

A DEM is defined as any digital representation of the continuous variation of relief over space in which the value of each grid cell can be the elevation of the centre point of the grid cell or the average height of the area covered by the grid cell (Ramesh 2012). DEMs are categorised in two types, namely digital terrain models (DTM) in which pixels represent the surface of the earth, and DSM in which pixels represent the height of the earth's surface including features on the ground. Previously, DEM was largely used for geographic correction of remotely sensed imagery and to visualise the earth's surface in three dimensions. During the last two decades, DEM have been subsequently integrated into land feature classification from remotely sensed data (Weidner 1997) due to the limitations of pixel-by-pixel classification based essentially on spectral information.

2.4 APPLICATIONS USING nDSM

During the last two decades, DEM have been subsequently integrated into land feature classification from remotely sensed data (Weidner 1997) due to the limitations of pixel-by-pixel classification based essentially on spectral information. DEM have since been used to extract buildings (Koc & Turker 2005, Krauβ, Reinartz & Stilla 2007), roads (Clode, Kootsookos & Rottensteiner 2004) and trees (Kim & Muller 2011), either as a single dataset or combined with remotely sensed imagery. The literature indicates that elevation data resolves the difficulties related to spectral similarities of land features having different height, for example parking lots and buildings, grass and trees (Koc & Turker 2005; Gamba & Houshmand 2000). For example, Gamba & Houshmand (2000), Iovan, Boldo & Cord (2008), Koc & Turker 2005, and Wei, Zhao & Song 2004 reduced the misclassification error of roads and buildings by integrating a DEM into the classification process, and achieved more accurate information.

In general, urban land cover analysis is based on the extent, spatial distribution, and the importance of spatial information to the users on the ground in line with the classification purpose (Duadze 2004). Buildings and impervious surfaces such as roads and parking lots cover the largest part of urban areas (Lu & Weng 2006). The available green space is shared by trees and grass designed mostly to regulate heat and moisture (Pauleit, Ennos & Golding 2005; West et al. 2010).

2.4.1 Buildings

Urban planning, infrastructural development, and roof modelling require building footprints (Li et al. 2013; Wang, Lodha & Helmbold 2006), which are defined as the area within the perimeter of a building measured at the foundation (Borough of Mendham 2009). Buildings and their footprints are becoming more important with new 3-D technologies like ESRI CityEngine (ESRI 2013b), which transforms 2-D GIS data into smart 3-D city models making the virtual 3-D visualisation as real as possible. The generation of 3-D building models from point clouds provided by LiDAR have also gained importance (Wang, Lodha & Helmbold 2006). Both the urban spatial extent and the building volume provide an indirect measure of population density, which is an essential parameter in impact assessment that drives emergency response action (Brunner et al. 2010).

Buildings are impervious areas with high economical, humanitarian and geographical interest for human being. Spatial information of buildings plays a key role for not only decision makers but also for spatial analysts which triggers differentiating them from other impervious areas. Building extraction is complex and significant in urban land cover mapping providing key information for settlement analysis (Gamba & Herold 2010; Shackelford & Davis 2003). Buildings can be rather complex structures having many architectural details and may be surrounded by obstructive objects, making extraction difficult (Wei, Zhao & Song 2004). Areas with high building density are more complex, making building extraction even more difficult (Small 2003). However, EHSR offers a possibility to extract building in such areas (Moran 2010) and offers the potential of extracting details of smaller features (Gamba et al. 2011). EHSR has been shown to enable building extraction regardless of building size (Siart, Bubenzer & Eitel 2009; Baraldi et al. 2010).

The use of DSM has improved the discrimination of building from other features (Gamba & Houshmand 2000). A survey of the literature indicated that Brunn & Weidner (1997) were

among the first researchers to investigate building extraction using a DSM together with the differential geometric properties of the surface and roof extraction. Rottensteiner & Briese (2002) proposed a method for building extraction in urban areas using high resolution LiDAR data, and showed that high-resolution DSM enable a more accurate extraction of building features.

The DSM not only provides a geometric description for building extraction (Brunn & Weidner 1997), but also provides height information essential for distinguishing objects with similar spectral information, such as building, roads, water, coal piles, and different vegetation types (Yu et al. 2011). According to Koc & Turker (2005), the basic idea behind using a DSM for building extraction is that man-made objects with different heights can be detected by applying a height threshold to a nDSM. The height threshold is defined according to *a priori* knowledge regarding the minimum height of the building (Frédéricque et al. 2008). When comparing sensors, Gamba & Houshmand (2000) found that LiDAR data provided a better shape characterisation of buildings than radio detection and ranging (RADAR) data. Their approach started by applying mathematical morphology filters to the original LiDAR data to extract the terrain surface, after which the objects higher than ground level were retrieved using a thresholding procedure.

Brunn & Weidner (1997) used the global threshold of the nDSM which refers to the height of objects on the ground, to extract information on building and vegetation from the DSM. The author applied the standard deviation of the nDSM to distinguish buildings from trees. The surface roughness, measured by different geometric quantities like gradient and curvature, combined with size evaluation were used as criteria. Koc & Turker (2005) also used a DSM with Ikonos imagery to extract buildings. The authors first split the data into elevated and non-elevated classes based on the DSM mean value. Building and trees were subsequently discriminated using NDVI. Similarly, Zhou (2013) used the contrast-split segmentation algorithm based on nDSM to separate tall and short objects for urban land cover classification using LiDAR height and intensity data. Splitting the data into elevated and non-elevated classes using a nDSM was found to be efficient in separating spectrally similar features based on their height in an object-based environment.

Theng (2006) employed Ikonos and the DSM to extract building footprint using the snake energy function approach and a circular casting algorithm. The method improved the root mean square (RMS) and the standard deviations from the ground truth data. Other methods were used such as

the morphological building index (MBI) which based on image properties (spectral and spatial information including texture). Huang & Zhang (2011) achieved satisfactory results in terms of accuracy and visual inspection for extracting building from multispectral GeoEye-1 imagery using the MBI. Despite the efficiency of the methods proposed by previous studies (object-based, pixel-based or hybrid) to extract land cover, many of these studies were applied within a small area leading to uncertainly about their successfulness in larger areas.

Automated techniques, for building extraction, are becoming increasingly needed as the traditional manual approaches of building extraction from raw imagery are labour intensive, time consuming and sometimes very expensive (Ren et al. 2008). Although several studies have successfully extracted building footprints (Kock & Turker 2005; Ren et al. 2008; Theng 2006), the methods employed require improvement for rapid acquisition of more accurate results.

2.4.2 Impervious surfaces

As cities grow and develop, the natural landscape is replaced by built-up areas (roads, buildings, housing developments, sidewalks and parking lots), that constitutes impervious surfaces (Milheim et al. 2007; Weng & Hu 2008). Impervious surfaces refer to any surface covered by materials such as concrete, asphalt, brick, and stone that obstruct the infiltration of water into the soil Bauer, Loffelholz & Wilson (2008). These surfaces greatly impact urban areas by raising pollution levels and urban land surface temperatures (Yuan & Bauer 2007). Impervious surfaces can affect local streams, both in water quality and streamflow as well as by altering flooding characteristics (Bauer, Loffelholz & Wilson 2008). Furthermore, impervious surfaces have the ability to eliminate rainwater infiltration and natural groundwater recharge (Weng & Hu 2008). The measurement of impervious surfaces is thus an important indicator of environmental and habitat quality in urban areas (Bauer, Loffelholz & Wilson 2008). Therefore, it is vital to map and estimate impervious surfaces for environmental management and to inform and support urban planning (Weng & Hu 2008).

With the advent of very high spatial resolution (VHSR) imagery from sensors such as QuickBird and Ikonos, many studies for mapping impervious surfaces in urban areas have emerged. For example, Yuan & Bauer (2006) also investigated classification techniques of mapping impervious areas using QuickBird satellite data. The authors reported that QuickBird provides the ability for mapping complex urban features in high detail but again the drawback was the extraction of shadows. Lu & Weng (2009) extracted impervious areas from Ikonos imagery

using a hybrid approach incorporating the decision tree and unsupervised ISODATA classifiers. The study highlighted some weaknesses in this approach in that dark impervious surfaces areas were often confused with shadows and water.

Shackelford & Davis (2003) however noted that road network extraction directly from Ikonos imagery, was difficult due to spectral variation in road surfaces as well as noise present in the data. The narrowness of street surfaces further made road extraction difficult. The authors employed a line segment match method in which they performed a classification using a hierarchical pixel-based fuzzy classification. This was later refined by applying an object-based analysis. The accurate extraction of roads can further be facilitate by the use of ancillary data such as OpenStreetMap (Bennett 2010), which is available for many countries (Haklay 2010).

2.4.3 Urban green areas

Vegetation communities forming green areas are of particular interest in certain studies as it presents a resource for managing and moderating various urbanization associated problems such as urban heat (Tooke et al. 2009). Indeed, Weng, Lu & Schubring (2004) found a higher level of latent heat exchange with more vegetated areas, while sensible heat exchange was more favoured by sparsely vegetated such as urban areas. Vegetated land cover information helps to evaluate the extent of urban land covered by vegetation communities. The spatial distribution and abundance of vegetation in urban areas is recognised as a key factor influencing numerous biophysical processes including air and water quality, temperature, moisture, and precipitation regime (Tooke et al. 2009). Urban greening is the most commonly used strategy to mitigate the increasing risk of urban heat waves in cities (La Rosa & Privitera 2013).

Except the use of NDVI for vegetation extraction, other methods have been used to extract vegetation in urban areas. For example, Iovan, Boldo & Cord (2008) extracted urban vegetation using high-resolution colour infrared (CIR) digital images and a DSM within a high density urban area. Tooke et al. (2009) used high-resolution QuickBird imagery to extract urban vegetation using field observation and linear spectral mixture analysis (SMA). The SMA divided each pixel of the QuickBird imagery used into the representative fraction of end member (selected spectra that represent materials on the ground).

Several studies have produced successful results using a DSM for extracting urban vegetation. For example, Priestnall, Jaafar & Duncan (2000) used the standard deviation of DSM to

differentiate buildings from trees after the study area was split into above-surface information and surface information. Kick & Turkey (2005) discriminated grass from tree plantations using the DSM mean value.

2.5 DATA PRE-PROCESSING

Once sensors have scanned remotely sensed data, the resulting images require meaningful pre-processing to remove noise, caused by atmospheric interferences, and topographic effects. Campbell (2006) emphasised the role of pre-processing, in enhancing the quality of satellite imagery. Pre-processing includes georeferencing, mosaicking, subsetting, and radiometric normalisation. Geometric and radiometric corrections are mostly concerned with improving image quality (Chuvieco, Li & Yang 2010). Several studies have focussed on optimizing pre-processing workflows to improve data quality and ensure good land cover extraction for example. For example Leiss et al. (1995) reported that classification errors induced by insufficient radiometric and geometric precision can be reduced by appropriate geometric and radiometric correction. The author used a DEM to correct the influence of topography on irradiance components and atmospheric parameters.

2.6 IMAGE TRANSFORMS

Image transforms can be simple arithmetic operations on images or complex mathematical operations which convert images from one representation to another (IgorPro 2014). GEOBIA with the use of geometric, shape and size properties of objects proposes numerous operations of image transforms.

2.6.1 Band ratios and Texture

Band ratio is calculated with the criteria being associated to the form, height, texture or distance to neighbouring image objects (Cai et al. 2010). According to Lein (2011), band ratio can also be employed to produce specialized results that give prominence to unique features or materials in a remotely sensed image. Indices are used in rule set at a given threshold to derive predefined feature classes for extraction (Cai et al. 2010; Chen et al. 2011). Vegetation indices, which are linear combinations of *n* spectral bands (Jackson & Huete 1991) have been widely used in quantitative and qualitative assessments of vegetation cover and growth activity (Cai et al. 2010). The use of NDVI is an effective measure to extract vegetation cover given that vegetation has

unique spectral properties that differentiate it from other land cover types (Iovan, Boldo & Cord 2008). NDVI has also been used to extract non vegetation classes. Other indices such NDWI have been used for waterboby extraction. For example, Yu et al. (2011) successfully used the NDWI together with a DSM to extract water and coalpile fields from GeoEye-1 imagery with an overall accuracy more than 90%.

Texture refers to the relationship between grey-levels in neighbouring pixel which contribute to the overall appearance or visual characteristics of an image (Ward 2008). In addition to indices, many studies have incorporated texture measures into the classification process. For example, Pesaresi & Gerhardinger (2011) extracted built-up features from high resolution QuickBird imagery, using anisotropic rotation-invariant grey-level co-occurrence matrix (GLCM) statistics and achieved a 68% overall accuracy. Although, the accuracy of the result were improved to 70 % overall accuracy using the vegetation index, the texture provided standard results.

2.6.2 Edge detection

In many applications, it is important to find boundaries of objects in the image. Edge detection improves the detectability of features in the image (Dwivedi & Sreenivas 1998). The edge detection technique is the process of identifying and locating sharp discontinuities (abrupt changes in pixel intensity that characterise boundaries of objects) in an image (Alshennawy & Aly 2009; Vincent & Folorunso 2009) in order to determine the boundaries of its homogeneous regions (Mather & Koch 2011). An edge represents the boundary between an object and its background (Feng, Wang & Liu 2008). Nain et al. (2006) described edges as regions of interest where there is a sudden change in intensity. The authors indicated that change can mark the end of one object and the starting point of another object within a scene.

The segmentation approach involving edge detection has proved to be effective for deriving significant objects (Koc & Turker 2005; Martin et al. 2001; Wu & Li 2010). That insertion of edge detection in image segmentation contributed to create homogenous objects by stressing their boundaries (Jayachandran et al. 2010). That technique is thus intensively used in image segmentation (Vincent & Folorunso 2009). Among existing edge detection methods, the canny edge detection algorithm is one of the most implemented because of its ability to detect edges even in images that is severely contaminated by noise (Gentsos et al. 2010). Nonetheless, Vincent & Folorunso (2009) found the canny edge detector to be complex and slow to compute, recommending the Sobel operator as an alternative.

Many works have used the canny edge detectors and induced suitable results for the extraction of buildings (Koc & Turker 2005; Wu & Li 2010) as well as for the land cover (Kodge & Hiremath 2010). Due to the value of edge detection algorithms in OBIA, the latest versions of GEOBIA software such as eCognition software (Nussbaum & Menz 2008) have integrated such techniques.

2.7 DATA FUSION

As outlined by Shackelford & Davis (2003), the imagery to map urban areas must have a spatial resolution in the metre to sub metre range to derive geospatial data with a large amount of detailed ground information suitable for many types of GIS applications (Huang, Zhang & Gong 2009). Features such as buildings, pavements, and trees are better distinguished by their spatial properties than by their spectral reflectance properties (Al-Khudhairy, Caravaggi & Glada 2005). Consequently the use of spatial properties (form, texture, and area) in object-based image analysis, offers possibilities to optimise land cover mapping accuracy (Belgiu, Dragu & Strobl 2014).

The use of very high spatial resolution (VHSR) imagery is not without limitations. For example, Huang, Zhang & Gong (2009) reported that the VHSR can reduce the statistical ability to separate the different land cover classes in the spectral domain by increasing the internal spectral variability (intra-class variability) of each land cover class and decrease the spectral variability between classes (inter-class variability). The spectral heterogeneity of land cover types in VHSR imagery thus presents an inconvenience for spectral classification methods based on pixel-by-pixel information (Cots-Folch, Aitkenhead & Martinez-Casasnovas 2007). However, an object-based image analysis approach can readily exploit the spatial and spectral information of high resolution data by using texture and geometric properties associated with these images (Belgiu, Dragu & Strobl 2014; Cots-Folch, Aitkenhead & Martinez-Casasnovas 2007). Many studies have therefore combined the panchromatic high spatial resolution image with the high multi spectral component.

Image fusion methods intend to improve the quality of information contained in the output image. According to Mitchell et al. (2011), the benefits of image fusion include extended range of operation, extended spatial and temporal coverage, reduced uncertainty, increased reliability, and compact representation of information.

A comparison study of per-pixel and object-based approaches for urban land cover extraction using QuickBird imagery indicated higher accuracy for land cover extracted with object-based approach (Myint et al. 2011). The author demonstrated that the spatial resolution of remotely sensed data used to map urban land cover needs to be at least one half of the size of the smallest object to be identified in the image. Mapping objects such as buildings, low vegetation, trees, fences, and cars require multispectral EHSR imagery often acquired through data fusion.

2.8 IMAGE CLASSIFICATION

Image classification attempts to assign raw pixel values to specific classes of information called thematic information (American planning association 2006). Image classification has been processed for the last two decades providing decision tool for urban planners and many others geospatial information users. The advance of the extremely high spatial and spectral resolution with the creation of third generation satellite sensors has triggered tremendous discovery of significance methods of image processing. Nowadays one of the most experimented techniques is the rule-based method associated with automated processing which aims to achieve rule set transferability.

2.8.1 Land cover classification scheme

Land cover refers to the physical surface of the earth, and is often confused with land use (South Africa (Republic of) 2010). For example, grass is not only a land cover, but it can also be a land use where grass was grown for recreational purposes. There is a growing need for land cover information related to the capacity for the land to provide goods and services, including the spatial arrangement of land use (Verburg et al. 2009). The characterisation of land cover schemes to specific users' needs must be established prior to carrying out classifications from satellite imagery so as to match the output with standardised land types.

In the case of South Africa, Thompson (1996) proposed a framework for land type classification that gives standardised baseline specifications to ensure consistency and conformity between data mapped from satellite imagery by various governmental organisations and the specific needs of South African environments. Currently, the CD: ING has taken the lead in mapping of land cover and land use at a national level establishing a recent land cover scheme and over 180 classes were defined. The Department of Agriculture, Forestry and Fisheries (DAFF) and Eskom have expressed their willingness to assist in the compilation of the classification and their

eagerness to use it (rural development and land reform 2013). The CD: NGI has proposed a land cover land use scheme together with other government agencies and private sectors (mainly regional planners). The apparent solution condensed the classification legend into 8 super-classes and 32 sub-classes which can be extracted with modern remote sensing techniques. The condensed classification legend can be found in appendix A.

Large-scale land cover mapping involves greater detail (Steiner, Butler & American planning association 2012); especially in urban areas covered by various types of man-made structures that need pinpointing. A decision to portray detailed urban information increases the importance of high-resolution satellite imagery known to be suitable for supplying such data (Myint et al. 2011; Sawaya et al. 2003). The mass of corresponding information to be extracted is interrelated to the spatial resolution of the satellite sensor imagery used as illustrated in Table 2.2 (Tarek & Jurgens 2010).

Table 2.2 Land cover classification levels

Level	Resolution	Example of class
I	≤100	Built-up urban
II	≤20	Residential, industrial, commercial, etc.
III	≤5	Single family units, apartments, etc.
IV	≤1	Additional information, e.g. condition of the building

Given that different end users requires different information, and that the classification scheme relies on the spatial resolution of the image, VHSR imagery will often lead to large scale information such as building, roads network, trees, waterbody, bare soil and grass.

2.8.2 Rule-based classification

Rules are organised human-understandable knowledge used to predict classes of records that have no class information (Li & Jones 2006). Each rule associates a pattern with a class (Aggarwal 2014). The rule-based classification (RBC) is related to the decision tree (DT) approach (Mather & Koch 2011). Its implementation is based on the feature-specific parameter criterion that produces a unique feature, i.e. each feature is classified using specific criteria with specific parameters (Smith, Paron & Griffiths 2011). According to Li & Jones (2006), RBC involves two stages, the training stage, which refers to the generation of rule set, and the test

stage representing their implementation. The implementation stage consists of testing if the predictive class is the class that a record is supposed to belong to.

2.8.3 Supervised classification

The supervised classification contains a learning process through training data selectable in the same image (Düzgün & Demirel 2011). During the classification procedure, supervised classification comprises user interaction where the analyst selects the training data (i.e. pixels already assigned to informational classes) for each class from the image to classify pixels of unknown identity (i.e. to assign unclassified pixels to one of several information classes). (Campbell & Wynne 2011; Mountrakis, Im & Ogole 2011). Pixels located within the training data or areas of interest (AOI), are the training samples which are used to guide the classification algorithm to assign specific spectral values to appropriate information classes (Campbell & Wynne 2011).

2.9 TRAINING AND REFERENCE DATA COLLECTION METHODS

Training data are areas of known identity that are identified in the digital imagery (Gupta 2003). According to Kumar (2005) the training data is a set of measurements (points from an image) whose category membership is known by the analyst. The reference data is either acquired through remotely sensed products such as aerial photographs, satellite imagery, and thematic maps, or field visit (Masialetti 2008). Even if the collection methods of reference data vary, the author describes four steps whereby the collection process is always performed: (1) choosing the primary source of reference data, (2) pre-selection of field sites, (3) interpretation of features in remotely sensed image and (4) field visit or ground truth. Once the choice on the source of reference data collection has been made, Masialetti (2008) proposed the following steps:

- The pre-selection of field sites are done by image interpretation as a way of minimising staff time in the field and ensuring that useful ground site are captures.
- The visual interpretation step consists for the interpreters, of locating each site on the remotely sensed product; examine the area around the site using conventional photo-interpretation keys and determine the class for each site according to the selected classification scheme.
- The field visit is organised later by navigating to pre-selected reference sites using the Global Positioning system (GPS).

Previous studies have used field data as training data collection. However, Gupta (2003) suggested keeping the training data set small in size, but large enough to characterise the classes as the collection of such data set is a costly affair. According to the author, the training sample size varies for a minimum of 10b (10*number of bands) per class, to 100b per class, where b is the number of bands. Many others have used the aerial photograph of similar date for collecting training data. The advance of the technology offering aerial photograph of higher resolution (case of the 15 cm available aerial photograph of Cape Town) enables the collection at lower cost of reliable training data.

2.10 GEOBIA

Research on urban mapping has gained momentum, chiefly due to the availability and accessibility of VHSR imagery, and successful results using object-based image analysis (OBIA) (Pinho et al. 2008; Zhou 2013). The OBIA approach incorporates spatial contexts and mutual relationships between objects, and is often referred to as GEOgraphic object-based image analysis (GEOBIA) when used in EO (Conchedda, Durieux & Mayaux 2008). According to Blaschke, Lang & Hay (2008: 78) GEOBIA is proposed to replace OBIA "because the term OBIA encompassed techniques used in many different disciplines such as biomedical imaging, Astronomy, Microscopy, Computer vision and others". Being considered as a bridge between a raster domain of RS and a vector domain of GeoInformation Science (GIS), GEOBIA is defined by Blaschke, Lang & Hay (2008: 77) as "a sub-discipline of GIS devoted to developing automated methods to partitioning RS imagery into meaningful image-objects, and assessing their characteristics through spatial, spectral and temporal scales, so as to generate new geographic information in GIS-ready format".

One of the key elements of the GEOBIA approach is that it can integrate all data types including DEM (DTM, DSM and nDSM), shapefiles, and LiDAR data in combination with image data as opposed to the traditional pixel-based approach (Koc & Turker 2005; Wang 2009; Zhou 2013). GEOBIA combine spectral information (tone and colour), with spatial arrangements (size, shape, texture and pattern) in association with neighbouring objects (Campbell & Vynne 2012; Laliberte et al. 2004; Rahman et al 2013). The spatial relationship among image objects allows for more than one level of analysis through multiple segmentations with different parameter settings (Navulur 2007). GEOBIA has been shown to provide better classification results than pixel-based approaches (Moran 2010).

The difference between object-based and pixel-based classification methods revolves around two aspects of the classification problem, namely classification units and classification features. Classification units are individual pixels used for pixel-based classification, whereas classification units are individual image objects used for object-based classification (Liu & Xia 2010). In GEOBIA parlance, an object is a grouping of pixels of similar spectral and spatial properties (Moran 2010; Navulur 2007). The large volume of information contained in the relationship between adjacent pixels, including texture and shape information, allows for the identification of individual objects rather than single pixels (Laliberte et al. 2004).

Object-based classification routinely starts with segmenting the image into meaningful objects (Darwish, Leukert & Reinhardt 2003). It is noteworthy that the successful production of land cover maps is dependent on the quality of image segmentation (Ban, Hu & Rangel 2010). A strong correlation exists between GEOBIA and the segmentation process as it aims to group spatially adjacent pixels into homogeneous objects thereby deriving meaningful objects (Huang, Zhang & Gong 2009).

Segmentation is defined as the division of remotely sensed images into discrete regions or image objects that are homogenous with regard to spatial or spectral characteristics (Laliberte et al. 2004). There are several segmentation algorithms available, including chessboard segmentation, quadtree-based segmentation, spectral difference segmentation, and multiresolution segmentation (MRS). A limitation of many of the segmentation algorithms is the problem of under- or over-segmentation regarding the extraction of meaningful image objects (Taubenböck et al. 2010). To analyse and capture the small variations within a dataset, multilevel segmentation with varying parameters that is scale, shape and compactness are thus used (Wang 2009).

The most widely used segmentation algorithm is MRS (Asmare 2013; Ban, Hu & Rangel 2010; Chen et al. 2007; Krause et al. 2004; Mbaabu 2012; Salehi et al 2012; Zhou 2013). For example, Gang et al. (2010) implemented a multiscale segmentation approach with the MRS to cope with large size differences between feature classes of the same type. The authors used a large scale of 300 to segment larger buildings and a small scale of 90 was used for smaller buildings. The results showed that multiscale segmentation cannot avoid incorrect segmentation between low-rise buildings and peripheral courtyards. The results further showed that on a large scale, edge segmentation of high-rise buildings is more challenging, while on a small scale, the characterisation of building distribution is done satisfactorily in regions of high density. The

work of Gang et al (2010) indicated that a number of segmentations at various scales may need to be performed in order to get meaningful image objects that lead to improve classification. The effectiveness of object-based classification thus relies on the quality of the segmentation. Particular attention must consequently be given to the assessment and improvement of the segmentation (Myint et al. 2011).

Navulur (2007) introduced several segmentation algorithms, most of which face the problem of uncertainty around the reliability of images objects. That uncertainty emerges with what Blaschke, Lang & Hay (2008) call the lack of consensus and basis to believe that segmentation-derived objects are fine representation of landscape. The author raised the following questions: (i) how do you know when your segmentation is good? (ii) Is there a formally stated and accepted conceptual foundation? Those questions triggered research on methods to evaluate segmentation results. Bouziani, Goita & He (2010) proposed two measures of quality to assess an image segmentation, the first measure uses the ratio between a number of generated segments and the number of segments from the reference segmentation done by a skilled interpreter who obtained it by digitising the scene manually, the ration is calculated as followed:

$$Rseg = \frac{Nseg}{Nref} \qquad \text{Equation 2-1}$$

where *Nseg* is the number of segment for the segmentation;
Nref represents the number of segment in the reference segmentation;

The measure uses the error (*E*) of segmentation is given by the proportion of pixels wrongly segmented in the image in relation to the total number of pixels in the image. Bouziani, Goita & He (2010) calculated E as follows:

$$E = \frac{\sum_{i=1}^{N}\sum_{j=1}^{N} NPi,j - \sum_{k=1}^{N} NPk,k}{\sum_{i=1}^{N}\sum_{j=1}^{N} NPi,j} \qquad \text{Equation 2-2}$$

where *NPi,j* is the number of pixels in the *j* segment that has been assigned to the *i* segment;
NPk,k represents the number of pixels assigned to the good segments;
n is the number of segments from the reference segmentation.

After an image has been segmented into appropriate image objects, the image is classified by assigning each object to known and defined classes. To be assured of the final classified image's quality, the process of the accuracy assessment is carried out.

3 CHAPTER 3 METHODS 1: STUDY AREA, DATA COLLECTION AND DATA PREPARATION

3.1 STUDY AREA

The study area lies within the City of Cape Town metropolitan area, comprising the Cape Town City Centre as well as a portion of six suburbs, namely Schotschekloof, Zonnebloem, Vredehoek, Oranjezicht, Gardens, and Tamboerskloof (Figure 3.1). The selected suburbs show a heterogeneous urban structure with a coexistence of commercial and residential districts as well as open spaces. The Cape Town City Centre, Zonnebloem, Vredehoek, and Oranjezicht are relatively flat, whereas the areas of Schotschekloof, Gardens, and Tamboerskloof have varying topography. The study area is approximately 460 hectares, and is characterised by a complex array of varied building heights. The topography varies from sand flats to a moderately-high elevation, and is dominated by sandstone plateaux and ridges that reach a maximum altitude of 1113 metres on Table Mountain. Rainfall is mainly in the winter months, from April to September (Cowling, MacDonald & Simmons 1996). The study area was selected because of (i) the availability of data, and (ii) its morphology which includes a large number of different built-up features (buildings, road networks and greened areas).

3.2 DATA COLLECTION

3.2.1 GeoEye-1 imagery

Launched on 6th September 2008, GeoEye-1 is one of the latest in a series of commercial very high spatial resolution EO satellites (Grigillio & Fras 2011). GeoEye-1 collects four-band multispectral images (Table 3.1) at nadir, with 0.41 m panchromatic and 1.6 m multispectral resolution. The panchromatic band is resampled to 0.5 m, which is used with the information from the multispectral image to produce the pan-sharpened imagery with the final full-colour image of 0.5 m resolution (Land info World Mapping, LLC 2013). The GeoEye-1 image used for this study was captured on 20th February 2011 and provided with the rational polynomial coefficient (RPC) model with a UTM projection.

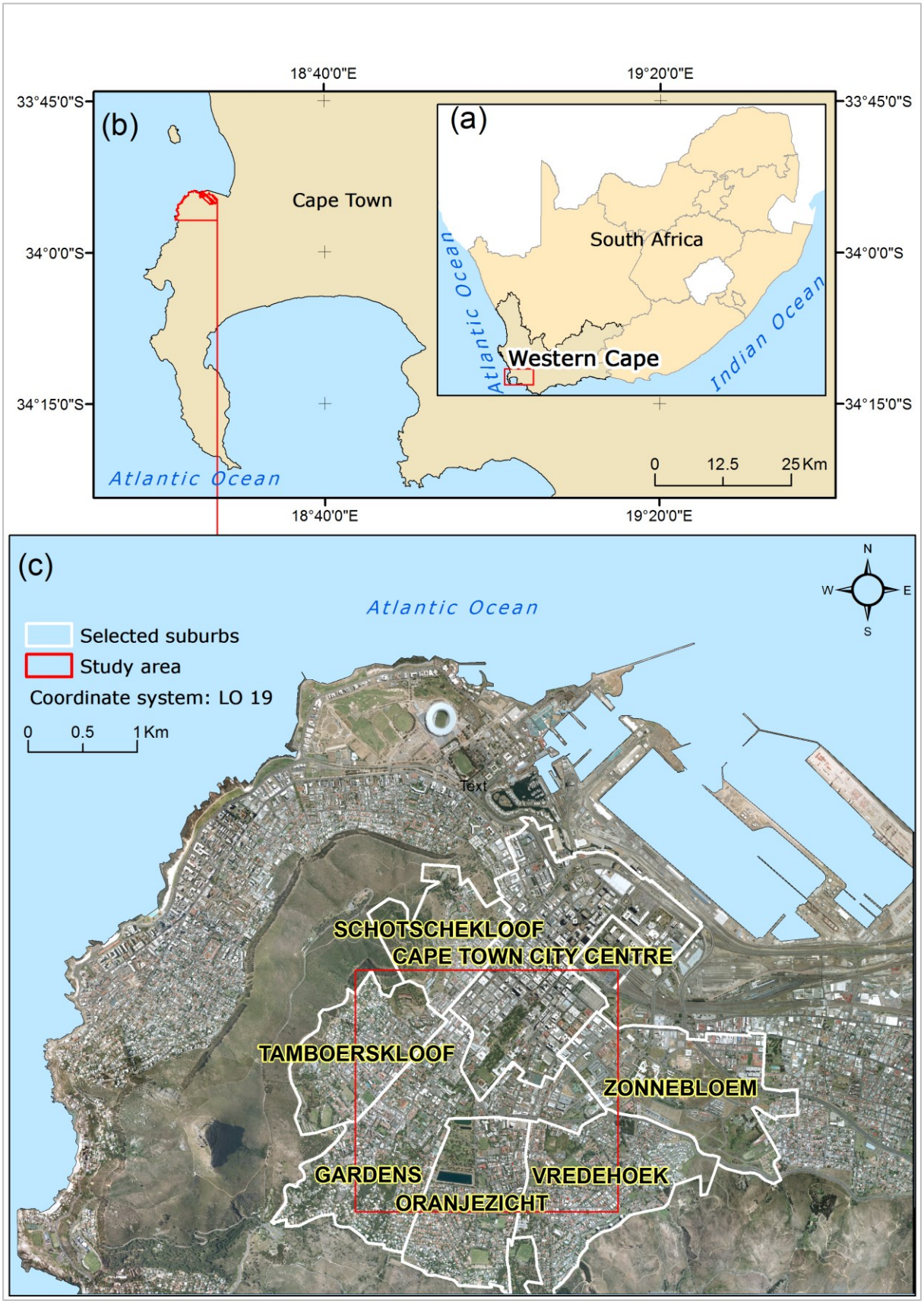

Figure 3.1 The study area location in (a) the Western Cape of South Africa particularly in (b) Cape Town metropolitan area. The red boundary in (c) defines the study site.

Table 3.1 Characteristics of GeoEye-1 imagery

Bands	Resolution
Pan resolution at nadir	0.41 metres
Spectral range (pan)	450-800 nanometres
Multispectral resolution at nadir	1.65 metres GDS at nadir
Blue band	450-510 nanometres
Green band	510-580 nanometres
Red band	655-690 nanometres
Near Infrared band	780-920 nanometres

Source: DigitalGlobe Inc 2014

GeoEye-1 imagery has been used in several large-scale research applications, including building footprint extraction (Dey, Zhang & Zhong 2011; Grigillio & Fras 2011; Hussain et al. 2011), gully mapping (Shruthi, Kerle & Jetten 2011) and the canopy mortality (Dennison, Brunelle & Carter 2010). Its properties make it a suitable data set for the extraction of urban information given that the imagery can provide accurate object boundaries and vegetation information (Yu et al. 2011).

3.2.2 Aerial photograph

The aerial photograph of 12.5 cm resolution was provided by the National Geospatial Information (NGI) in several scenes. That aerial photograph was collected in 2010 and served as a reference data for this project. The training data collection was carried out using the aerial photographs.

3.2.3 LiDAR and ancillary data

The LiDAR data was captured in May 2010, and provided by the City of Cape Town municipality. The LiDAR data was provided in LAS format produced using three different sensors: the Leica ALS40, the Leica ALS50, and the FLI-MAP 400 sensor. The flying heights of the sensors range from 200 m to 6 000 m for the Leica systems, from 50 m to 400 m for the FLI-MAP system (Lemmens 2007). The point density calculated was approximately seven points per square metre. Topographic maps and survey marks (Table 3.2) were used to pre-process the GeoEye-1 imagery. Topographic maps were made available by the CD: NGI Department, and used to identify trig beacons. A total of 1111 survey marks, provided by the Geomatics Services

department of the City of Cape Town municipality were used to orthorectify the GeoEye-1 imagery and to calculate the accuracy of the DSM produced from the LiDAR data.

Table 3.2 The collected study materials

Data	Resolution or Accuracy	Source
GeoEye-1 imagery	Panchromatic: 0.41 metre Multi spectral: 1.61 metre	City of Cape Town
Survey marks	10 cm accuracy	Geomatics Services department of the City of Cape Town Municipality
Topographic maps (3318CD and 3318DC)		CD: NGI
LiDAR data		City of Cape Town

3.2.4 Training and reference data

The land cover scheme categorises the training samples to be collected. The traditional classes of urban land cover are buildings, road networks, trees, grass, natural vegetation, bare soil, shadow, water, and agriculture (Shackelford & Davis 2003). Recent literature cites buildings, shadow, water, bare soil, impervious surfaces, trees and grass/shrub as land cover classes (Berger et al. 2013; Esch et al. 2013; Wurm, Taubenböck & Dech 2010). In this study, the land cover scheme comprises buildings, trees, water bodies, impervious surfaces, grass, shadow and impervious surfaces. Roads usually made of asphalt or concrete along with parking areas, tennis courts and other ground surfaces were classified as impervious surfaces (Weng & Hu 2008). Of all impervious surfaces, buildings constituted the most important part of urban land cover within the study area.

In this study, buildings were not classed as impervious surfaces because they represent valuable information for many urban analyses. For example, in South Africa, the housing units are important because of their demand in many applications such as the building count survey implemented by Eskom (SANBI 2009). Geospatial data on buildings are thus essential as buildings occupy the larger part of impervious surfaces in within the study site.

The relatively low sun elevation produced long shadows in the GeoEye-1 imagery of Cape Town. These shadows obscure much of the information in high spatial resolution satellite

imagery (Dare 2005). Consequently, allowance was made for the classification of shadow in this study.

Both the GeoEye-1 imagery and the aerial photographs provided the green area extent of Cape Town, which comprised mostly grass and trees. Except for the Atlantic Ocean on the west coast of the City, dams and swimming pools were the main water features found in the centre of Cape Town

The supervised classification used the user defined training sites or regions of interest (ROIs) selected during the training process. In object-based environments, a region of interest pertains to image objects created during the segmentation process. They were randomly collected across the entire image.

The ROIs' separability was generated and then examined in eCognition. Afterwards, the supervised classification was computed with three classifiers (K nearest neighbour KNN, support vector machine SVM and decision tree CART). Each classifier was first run with the GeoEye-1 imagery on its own and secondly with a combination of the nDSM and the GeoEye-1 imagery. The same training samples were used for all the supervised classifiers computed.

3.3 DATA PREPARATION

The data preparation for this study included the generation of the nDSM from the LiDAR data, the pre-processing of the GeoEye-1 image and the aerial photograph as detailed in Figure 3.2.

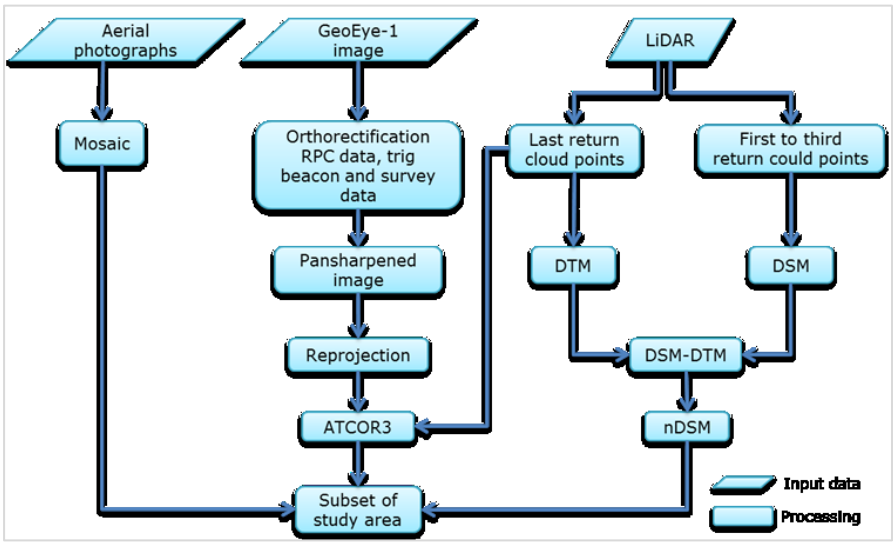

Figure 3.2 Pre-processing of the GeoEye-1 imagery and LiDAR data

Image mosaicking of the aerial photograph, the pre-processing of the GeoEye-1 imagery, as well as the generation of the nDSM from the LiDAR data contribute to prepare the data for urban land cover extraction. The next section describes the workflow of the extraction of the DEMs as described into Figure 3.2.

3.3.1 Generating the DTM, DSM and nDSM from LiDAR data

The nDSM was generated from LiDAR data using ArcGIS (Esri 2014). The LiDAR data contains an intensity image and cloud points (Fowler 2001). Two DEMs (DTM, and a DSM) were first created from the cloud points using an interpolation algorithm (Vögtle & Steinle 2003). The LiDAR cloud points were stratified in four levels of return points. The last returns which correspond to the ground were used to generate the DTM. All remaining returns (from first to before last return) were used to generate the DSM (De Koc & Turker 2005). In areas on the ground, without objects, the first return will correspond to the ground level because it is always associated to the highest feature (Fowler 2001). The nDSM was calculated by subtracting the DTM from the DSM using Raster Calculator in ArcGIS (Figure 3.2). The vertical error of the nDSM described by the vertical root-mean-square error (RMSE) of the sample of vertical errors (Zri) is calculated by (Congalton & Green 2009) as follows:

$$RMSE=\sqrt{\sum_i^n (Zri - Zdi)^2 / n} \quad \text{Equation 3-1}$$

where Zr_i is the reference elevation of survey point

Zdi is the vertical elevation of the corresponding point calculated using the DSM and;

n is the number of points used

The vertical error's value calculated for the DSM generated is 1.04 metre. That DSM was also generated with 1 metre spatial resolution. In addition, the DSM was generated in the LO19 projection system as the original data. .

3.3.2 Pre-processing

Remotely sensed data are most often provided in their recorded raw form with various degrees of distortion (mostly radiometric and geometric) making them less valuable for classification processes (Varshney & Arora 2004). Ancillary data, acquired to assist image classification, usually have a projection system different from that of satellite imagery. Consequently, an array

of data processing procedures, called pre-processing, had to be undertaken before land cover extraction process could proceed (Campbell & Vynne 2011).

3.3.2.1 Image mosaicking

To produce a single aerial photograph covering the study area, an image mosaic of 12.5 cm resolution aerial photographs was prepared using Erdas imagine (Erdas, Inc 2011). Image mosaic was used to create an orthophoto (one single large scene from all small scenes covering the area and having overlapping areas among consecutive scenes) of the study area.

3.3.2.2 Geometric correction and image registration

The GeoEye-1 image was supplied with the rational polynomial camera (RPC) data, which integrate the RPC model. The RPC model relates the object space (latitude, longitude and height) coordinates to image space (line, sample) coordinates (Dial & Grodecki 2002; Grodecki 2001). The accuracy of the RPC data has been tested often since the concept's introduction in 2000 with Ikonos sensors. Dial & Grodecki (2002) noted that RPC data provides a mathematical equation that simply and accurately describes the object image relationship. To model and subsequently compensate for the biases inherent in the RPC model, the bundle adjustment was computed using the trig beacon points and 3D survey marks as ground control points (GCPs). Trig beacon points were extracted from the digital topographic maps and registered to the same projection as the GeoEye-1 image.

Aerial and satellite images of land surfaces commonly contain spatial distortions due to terrain relief and off-vertical imaging geometry (MicroImages 2013). Orthorectification is a procedure that removes these distortions, creating an ortho-image where objects lie in the correct planimetric position (Xu 2012). The RPC files contain information needed to determine interior and exterior orientation of the camera, as well as supplemental information such as the UTM coordinates associated with the imagery (Kliarchuk & Collins 2011). Thus, the orthorectification was carried out to spatially correct the imagery so that each point of the image matches each corresponding point on the ground.

3.3.2.3 Image Fusion

Image fusion, also referred to as image pan-sharpening is a process of merging data from multiple sources to achieve refined information (Gupta 2003). The subtractive resolution merge combined the multispectral GeoEye-1 imagery data of fine spectral resolution with the structure information from the panchromatic band of fine spatial resolution, resulting in 50 cm pan-sharpened colour image. The image fusion was computed using Erdas imagine (Erdas 2010a). The output was a multispectral (MS) GeoEye-1 image that retained the colours of the MS image while maintaining the spatial detail of the panchromatic image.

3.3.2.4 Projection

To be useful, images must be geometrically corrected to the same coordinate system. As the aerial photograph was in Longitude of origin 19 coordinate system (LO19), and the pan-sharpened GeoEye-1 imagery in UTM, the registration process was carried out to reproject the pan-sharpened imagery to the LO19 projection. The LO19 is grounded in the "Gauss conformal projection" used to define the South African national coordinate system. It is a UTM projection with the longitude 19 degree for origin and two zones of 2 degree each as opposed to 6 degree wide for UTM (Surveying and land information Department 2011).

3.3.2.5 Radiometric correction and normalisation

Haze removal and atmospheric correction are important steps prior to conducting land and ocean surfaces mapping using images of space borne sensors (Wen & Yang 2008), because such images strongly depend on atmospheric conditions and solar zenith angle in the spectral region of 0.4 - 2.5 μm (Kneubühler et al. 2005). ATCOR3 (Erdas 2011a) was used for atmospheric correction of the GeoEye-1 image. ATCOR3 was designed for rugged terrain, and calibrates image pixel values from digital numbers to reflectance (Richter & Schlapfer 2014). A DEM generate by the LiDAR data was used. ATCOR3 was thus suitable for atmospheric and topographic correction of the imagery of Cape Town which is crossed by Table Mountain, Devils Peak, and Lion's Head (Cowling, MacDonald & Simmons 1996).

3.3.3 Image transformation

The pan-sharpened GeoEye-1 image transformations were carried out in eCognition. The first transformation was the generation of edge detection file using the canny edged detection function. Other transformations were carried out using the indices such as NDVI, NDWI and the texture (GLCM). These transformations were done prior to the image classification during which the output were tested.

4 CHAPTER 4 METHODS 2: DATA ANALYSIS

4.1 FEATURE SETS

In this study, data analysis was undertaken using three independent experiments. For each experiment, two segmentation processes were first implemented, followed by a supervised and a rule-based classification. For each of the segmentation and classification processes, a feature set was defined (Table 4.1). The key difference between experiment A, experiment B, and experiment C is the difference in the feature sets used. In experiment A and experiment B, a nDSM was used to split the resulting image objects into elevated and non-elevated image objects prior to classification. The difference between experiment A and experiment B is that experiment A uses only the nDSM to segment the GeoEye-1 imagery whereas in experiment B, both the nDSM and the GeoEye-1 imagery were used. In experiment C no nDSM was employed. This was done in order to elucidate the effect of using a nDSM for segmentation and classification and the impact of using a nDSM on overall classification accuracy. The idea of including the nDSM in both level 1 and level 2 of experiment B as opposed to experiment A, was: (1) to ensure that the nDSM can be used alone at level 1 segmentation and provide as good results as using both the two data input (nDSM and the GeoEye-1 imagery), and (2) because using the two data inputs for the segmentation level 2 produced good results.

4.2 EXPERIMENTAL DESIGN

Figure 4.1 provides an overview of the experiments A, B and C conducted for the supervised and the rule-based classifications of urban land cover.

4.3 IMAGE SEGMENTATION

In this study the segmentation of the GeoEye-1 imagery was undertaken using eCognition (Trimble 2011). eCognition provides several approaches to segmentation, ranging from very simple algorithms (chessboard and quad tree) to highly sophisticated methods such as MRS and contrast filters (Trimble 2011). After testing all the available segmentation algorithms, the MRS was used given its ability to produce meaningful desired objects.

As explained by Trimble (2007) and by Blaschke, Lang & Hay (2008), the MRS algorithm (segmentation level 1) starts with a single image object of one pixel and repeatedly merges it in several iterations, in pairs, to form larger units, as long as an upper threshold of homogeneity is not exceeded locally. This homogeneity criterion is defined as a combination of spectral homogeneity and shape homogeneity. The algorithm uses a scale factor to stop the object from getting too heterogeneous so that homogenous areas result in larger objects and heterogeneous areas result in smaller objects (Trimble 2007). According to Trimble (2007), image objects become highly homogenous, as the value of the scale factor tends to zero. The MRS algorithm was used at segmentation level 1 to produce the first set of image objects.

The MRS region-grow algorithm was used to grow regions by combining neighbouring pixels or image objects (Bhattacharyya & Dutta 2012) according to the multi-resolution segmentation criteria (Trimble 2011). The MRS region grow algorithm was used at segmentation level 2 to refine the objects produced by the MRS algorithm (segmentation level 1) by resizing image objects in order to produce new image objects that better represent real world features. The MRS region-grow algorithm grouped image objects produced by the previous segmentation to yield more meaningful objects (Lein 2011). To achieve this, the region-growing function of the MRS was run with a larger scale on both elevated and non-elevated image objects with edge detection file and the pansharpened bands as input layers.

Using the nDSM to differentiate between ground and non-ground objects

In order to split the object into elevated and non-elevated objects, the analyst's knowledge of the area is necessary to select the appropriate threshold value of the nDSM. Different mean threshold values of the nDSM were tested and the lowest height threshold value of one metre was set to ensure the integrity of building extraction. This was particularly important for buildings on steep slopes. The height threshold value of one metre enabled the extraction of entire buildings, irrespective of slope steepness.

Table 4.1 Feature sets used for the supervised classification of different experiences

Experiment	Segmentation L1		Segmentation L2		Classification			
					Supervised classification		Rule-based classification	
	Feature set	Features	Feature Set	Features	Feature set	Features	Feature set	Features
A	A_{L1}	nDSM	A_{L2}	Pan-sharpened bands, edge detection file	A_1	Pan-sharpened bands, edge detection file, nDSM, NDVI, NDWI	A_2	Pan-sharpened bands, edge detection file, nDSM, NDVI, NDWI, geometry (shape index, length/width, rectangular fit), Haralicks texture (homogeneity), class-related features (border to, distance to, real border to)
B	B_{L1}	Pan-sharpened bands, edge detection file, nDSM	B_{L2}		B_1		B_2	
C	C	Pan-sharpened bands, edge detection file	C		C_1	Pan-sharpened bands, edge detection file, NDVI, NDWI	C_2	Pan-sharpened bands, edge detection file, NDVI, NDWI, geometry (shape index, length/width, rectangular fit, density), Haralicks texture (homogeneity), class-related features (border to, distance to, real border to)

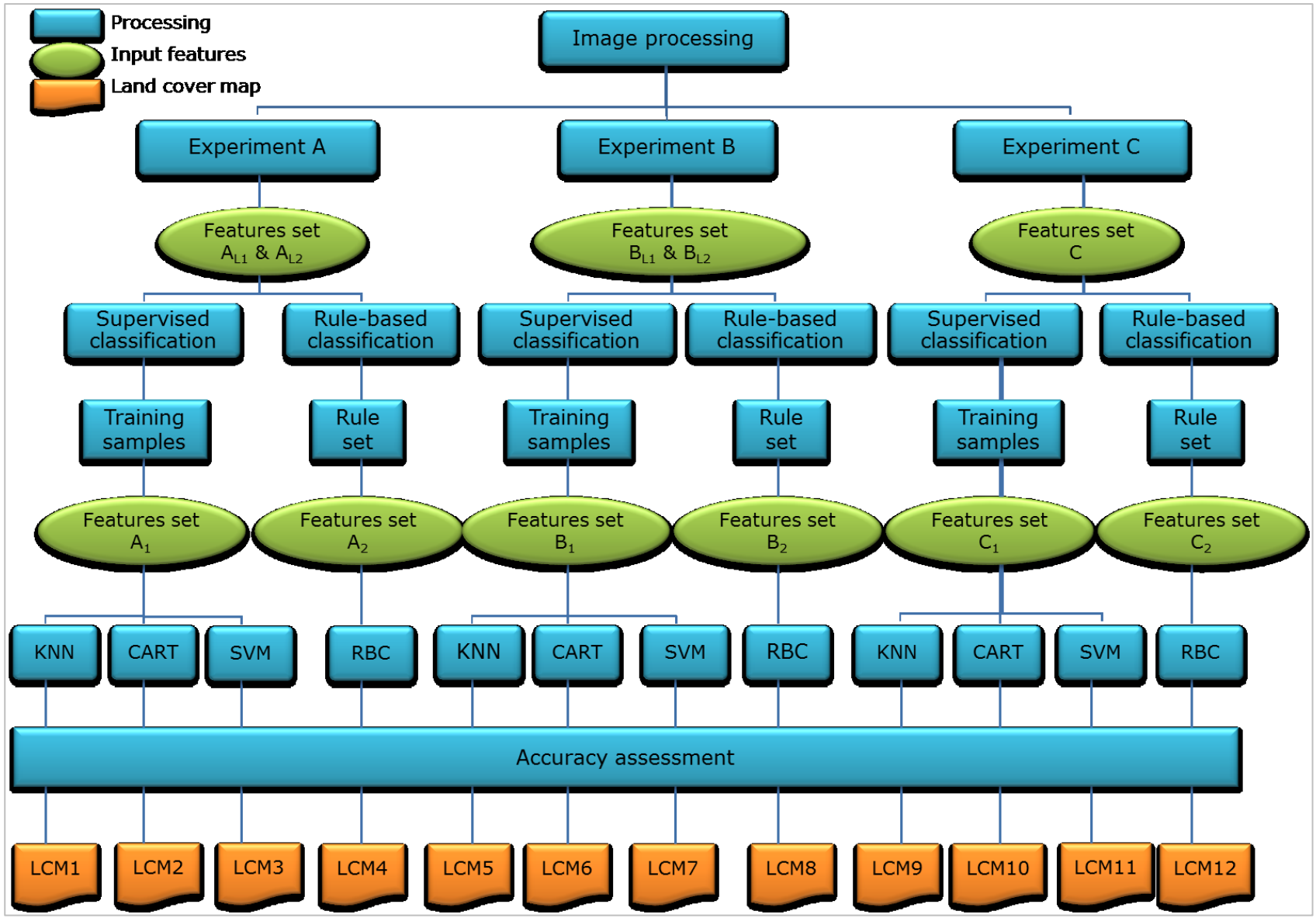

Figure 4.1 Rule-based and supervised image processing of GeoEye-1 imagery and the nDSM

4.3.1 Experiment A

Figure 4.2 defines the workflow of the segmentation process implemented in experiment A. That segmentation process was performed as follows:

1. Run the canny edge detection filter on the pan-sharpened GeoEye-1 image to generate the edge detection file which is used in the feature set A_{L2}.
2. Run the MRS using the feature set A_{L1} as input layers to generate the image objects;
3. Split the resulting image objects into elevated and non-elevated image objects using the nDSM threshold value of one metre.
4. Run the MRS region-grow algorithm to resize image objects for both elevated and non-elevated image objects.

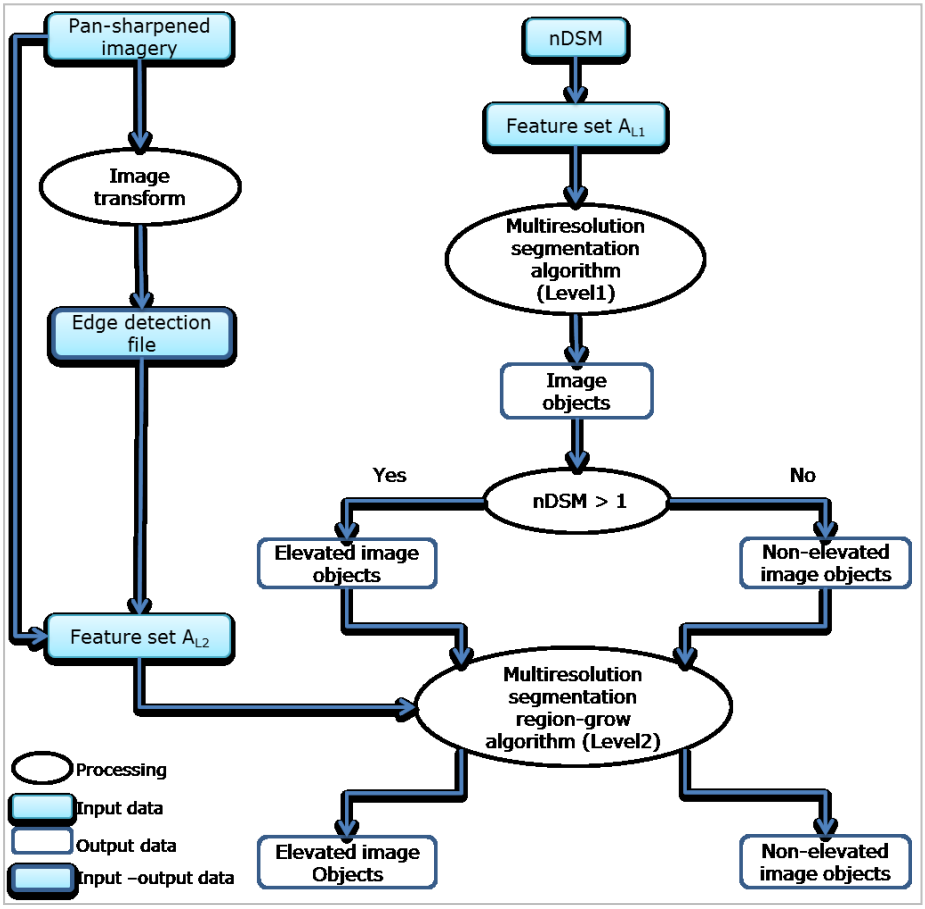

Figure 4.2 The segmentation workflow of experiment A

Table 4.2 indicates the respective weights and parameters values used for the segmentation process in experiment A. For the level 1 segmentation, i.e. using the MRS algorithm, a scale factor of five, shape value of 0.3 and a compactness value of 0.7 were used. For the level 2

segmentation, i.e. using the MRS region-grow algorithm, the scale factor was increased from five to 85 whereas the shape value and compactness value remained unchanged.

Table 4.2 Feature set weights and parameters used in the experiment A

Level	Feature set weights						Scale factor	Shape	smoothness
	Pan-sharpened GeoEye-1 bands				nDSM	Edge detection file			
	B	G	R	NIR					
1	0	0	0	0	1	0	5	0.3	0.7
2	1	1	1	1	0	1	85	0.3	0.7

4.3.2 Experiment B

Figure 4.3 defines the workflow of the segmentation process implemented in experiment B. The segmentation process was performed as follows:

1. Run the canny edge detection filter on the pan-sharpened GeoEye-1 image to generate the edge detection file which is used in the feature set B_{L2}.
2. Run the MRS using the feature set A_{L1} as input layers to generate the image objects;
3. Split the resulting image objects into elevated and non-elevated image objects using the nDSM threshold value of one metre.
4. Run the MRS region-grow algorithm to resize image objects for both elevated and non-elevated image objects.

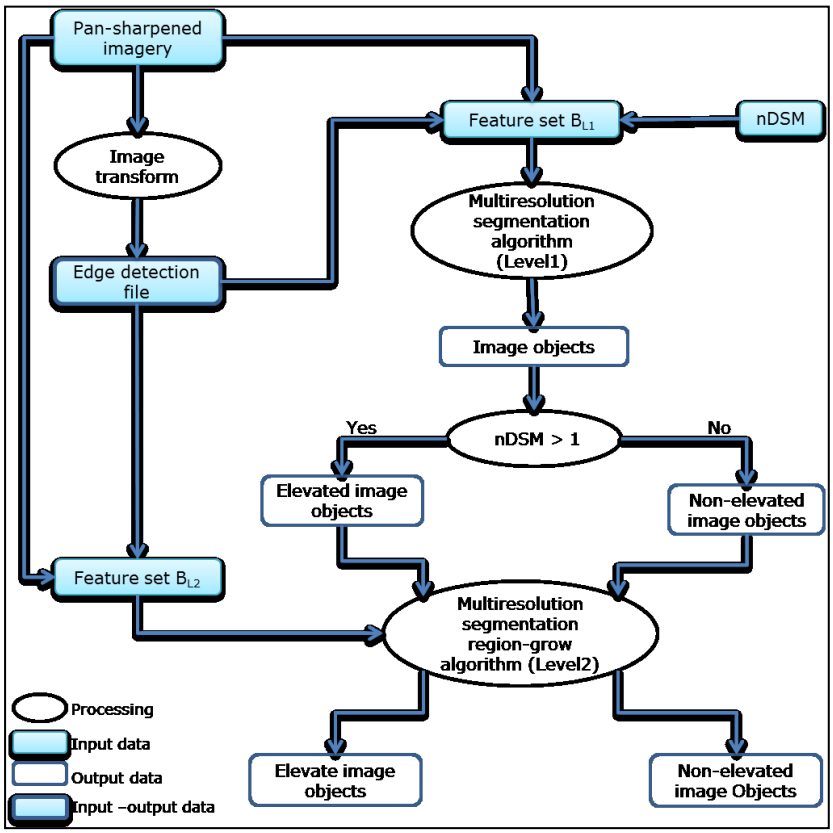

Figure 4.3 The segmentation workflow of the experiment B

Table 4.3 indicates the respective weights and parameters values used for the segmentation process in experiment B. For the level 1 segmentation, i.e. using the MRS algorithm, a scale factor of 30, a shape value of 0.3 and a compactness value of 0.7 were used. Moreover, the edge detection file and the nDSM were assigned a weight of five while the pan-sharp bands received a value of one. For the level 2 segmentation, i.e. using the MRS region-grow algorithm, the scale factor was increased from 30 to 85 whereas the shape value and compactness value remained unchanged.

Table 4.3 Feature set weight and parameters used in the experiment B

Level	Feature set weight						Scale factor	Shape	Smoothness
	Pan-sharpened GeoEye-1 bands				nDSM	Edge detection file			
	B	G	R	NIR					
1	1	1	1	1	5	5	30	0.3	0.7
2	1	1	1	1	0	1	85	0.3	0.7

4.3.3 Experiment C

Figure 4.4 defines the workflow of the segmentation process implemented in experiment B. The segmentation process was performed as follows:

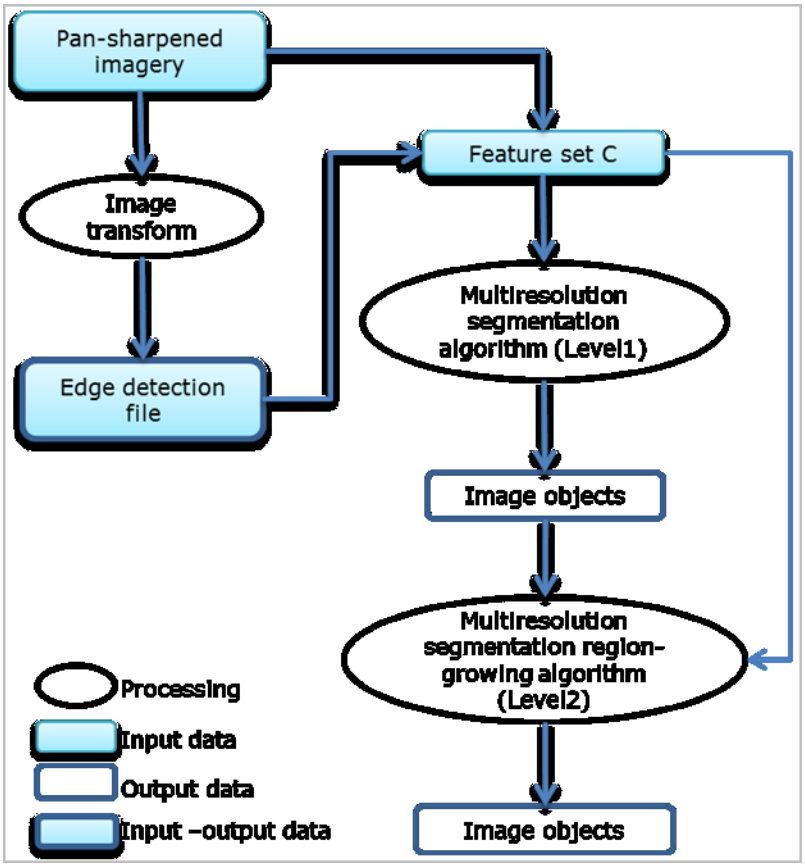

Figure 4.4 The segmentation workflow of experiment C.

Table 4.4 indicates the respective weights and parameters values used for the segmentation process in experiment C. For the level 1 segmentation, i.e. using the MRS algorithm, a scale factor of 30, a shape value of 0.3 and a compactness value of 0.7 were used. The edge detection file was assigned a value of 5 as in experiment B. For the level 2 segmentation, i.e. using the MRS region-grow algorithm, the scale factor was increased from 30 to 85 whereas the shape value and compactness value remained unchanged.

Table 4.4 Feature set weight and parameters used in the experiment C

Level	Feature set weight							
	Pan-sharpened GeoEye-1 bands				Edge detection file	Scale factor	Shape	Smoothness
	B	G	R	NIR				
1	1	1	1	1	5	30	0.3	0.7
2	1	1	1	1	1	85	0.3	0.7

4.3.1 Qualitative approach for assessing the segmentation

‘’There is no consistent means to establish if a given segmentation is appropriate or more correct than another due to a lack of a formal and accepted conceptual foundation to support the belief that a segmentation-derived object is an understandable representation of a structural or functional unit of the landscape’’ (Lein 2011: 11). Certainly, the main drawbacks of the segmentation algorithm are the artefact along the boundaries (Blaschke, Lang & Hay 2008). The method described in section 2.11 by Bouziani, Goita & He (2010) was not applied given that the reference segmentation was not available. Producing the reference data by digitising feature class in the aerial photograph was an option, but it ought to be not only time consuming, but also assessing the segmentation was not an objective of this research. Therefore, this study used the visual and subjective qualitative method to assess the specific arrangement of objects and how well they represent the target feature.

4.4 CLASSIFICATION METHODS

This section describes the land cover mapping using the rule-based and the supervised classification method. The land cover mapping used image objects products of the segmentation process. To implement the classification, the rule-based and the supervised classification approaches were respectively used in the three experiments A, B and experiment C.

4.4.1 Supervised classification

4.4.1.1 The training samples

The supervised classification used the user defined training samples or regions of interest (ROIs) selected during the training site process. In object-based environments, a region of interest pertains to image objects created during the segmentation process. ROIs were randomly collected across the entire high-resolution pan-sharpened GeoEye-1 imagery which provided the ability to visually identify data to be collected. More training samples were collected for the building class because of its variability and complexity. The training areas for any land cover class need to fully represent the variability of that class within an area. Shadows are less complex and less ROIs were therefore collected for that class. Other classes did not have particular properties and an average of 25 samples was collected for them.

4.4.1.2 Separability analysis

In order to assess the quality of ROIs collected and to identify appropriate features to best classify urban land cover, the separability analysis was carried out. That technique defined features that provided more accurate land cover information by measuring the similarities and differences of known ROIs in relation with input features. To calculate the separability for all experiments, the following features were used: the pan-sharpened GeoEye-1 bands, the NDVI, the NDWI for all experiments and an additional nDSM only for experiment A and B. The separability value lower than 1.9 indicated relatively high similarities between two classes. Moreover, the overlapping classes increased as the number of features decreased while the distance between classes increased with the number of features. Before the steps on running the supervised classification are described, the three classifiers are discussed briefly.

4.4.1.3 Classifiers

The *K nearest neighbour* (KNN) classifier is one of the simplest algorithms. According to Schowengerdt (2006), KNN assigns labels according to the majority label of k nearest-neighbour trainings pixels (Figure 4.5). The nearest object in Euclidian distance to a given sample will be assigned to the class characterizing that sample (Mott 2006).

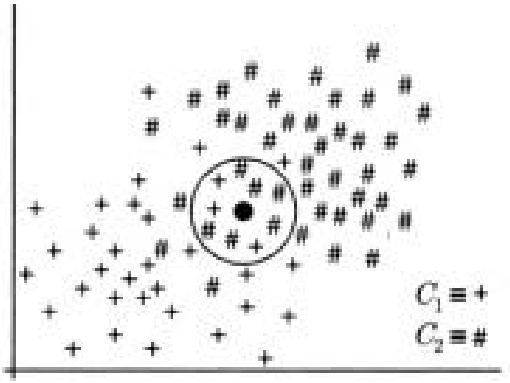

Source: Chanda & Majumder 2011

Figure 4.5 KNN supervised classification for k=9

The *classification and regression algorithm tree* (CART) is a popular and simple classification approach to multistage decision making. According to Leung (2010), CART is a decision trees that deals with both the classification and a regression problem (a combination of classification tree and regression tree). CART is a directed tree containing nodes that form a rooted tree. It has two different nodes: a terminal node, also called leave, has no interval and the second node called test node, has an interval (Tso & Mather 2001). CART splits the pace (or data) at the test node into two or more sub-spaces according to a discrete function of the input attribute value (Zhang, Feng & Jiang 2010). The performance of decision tree depends on how well the tree is designed. Figure 4.6 is an example of a tree structure comprising a root node at the top level, internal nodes which need to be further partitioned and a terminal node where partition is no longer required.

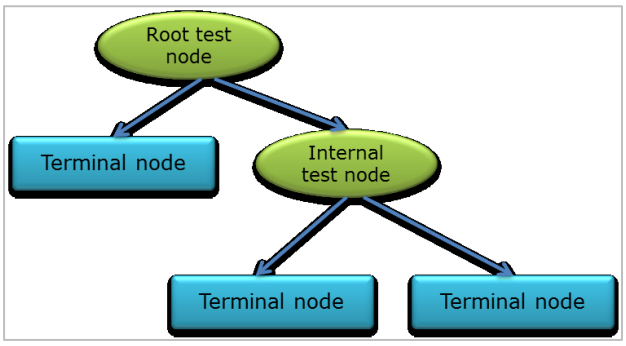

Figure 4.6 Tree structure

Support vector machine (SVM) is a supervised non-parametric statistical learning technique that assigns to a given test samples a class from a number of classes defined in the training samples (Mountrakis, Im & Ogole 2011). To discriminate objects that belong to one or few categories, SVMs use two key concepts to solve both the problem of large margin separation and the kernel function that compute the similarity between class information object (Ben-hur & Weston 2010).

A kernel function is introduced to map the non-linearly separable classes from the input space to a higher dimensional feature space, in which the non-linearly separable classes can be separated by an optimal linear hyperplane (Huang, Xie & Tay 2010). Margin separation consists of drawing a line as the separation boundary between distinct sets of objects (Figure 47). SVM performance depends on the choice of the type of kernel function that suits the training sample.

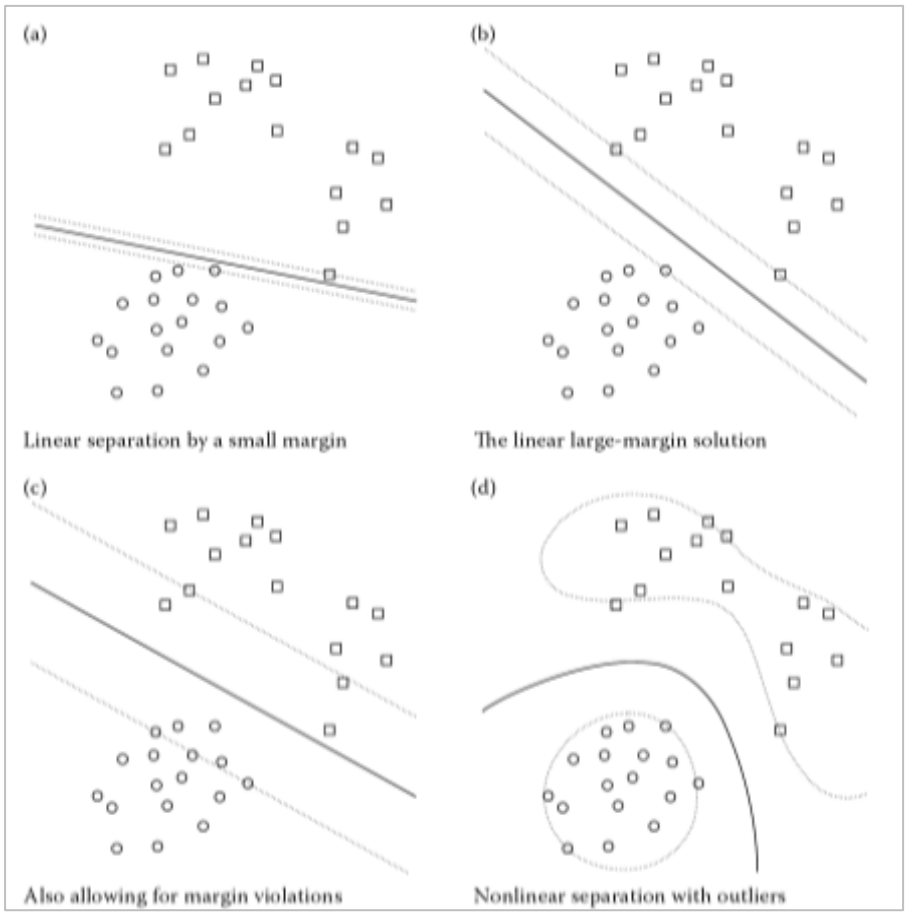

Source: Chen 2012: 41

Figure 4.7 An example of SVM linearly and non-linearly separable two class-data

4.4.1.4 Classification

Figure 4.8 describes the workflow of the supervised classification adopted in this study. For experiment A (Figure 4.8a) and experiment B (Figure 4.8b), feature set A_1 and B_1 respectively were used together with training samples, to classify elevated and non-elevated image objects. For experiment C (Figure 4.8c), feature set C_1 was used together with training samples for the classification of all image objects.

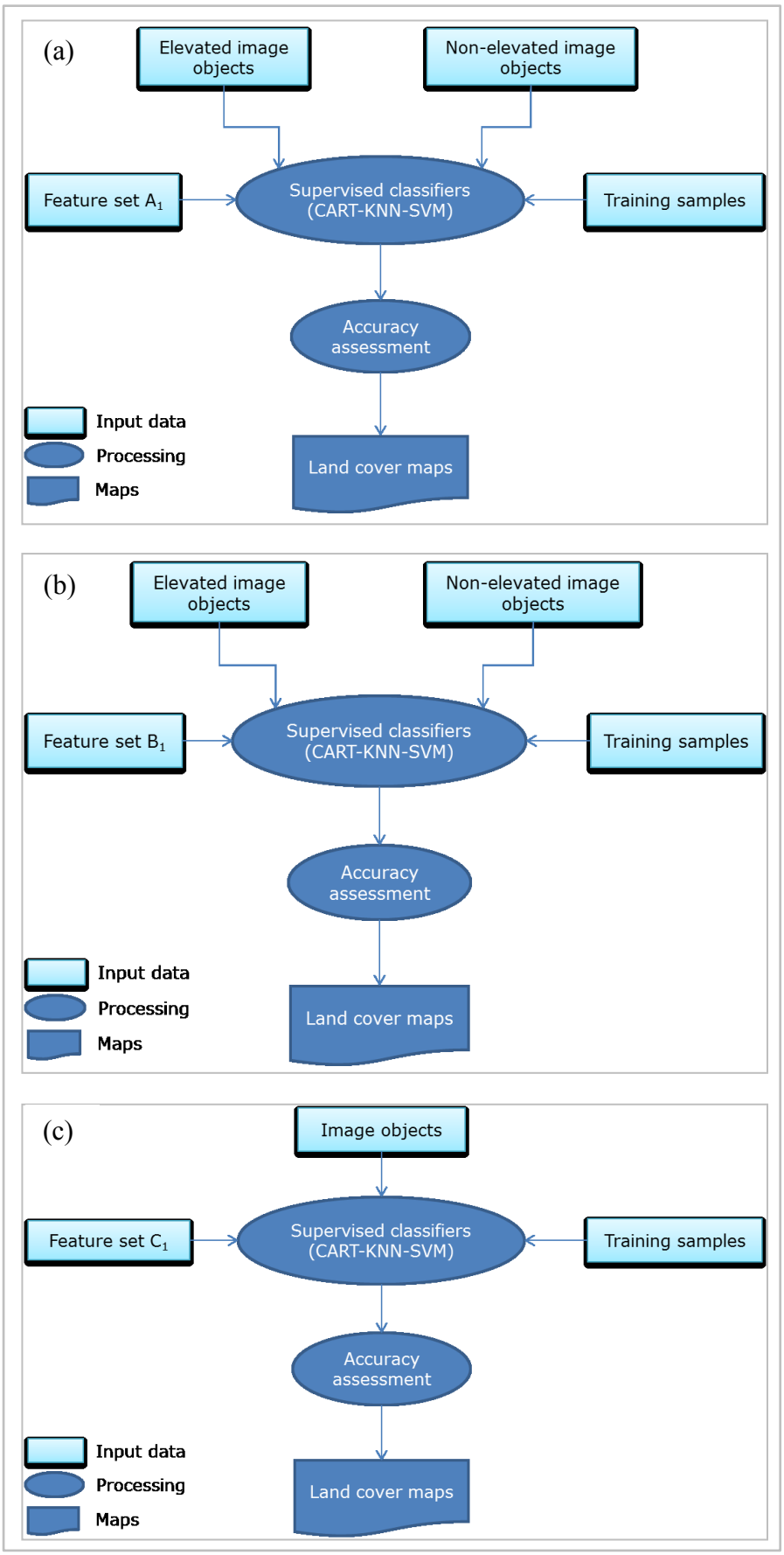

Figure 4.8 Workflow of the experiment A, B and C using the supervised classification

The key difference between the three experiments is the incorporation of a nDSM for experiment A and experiment B. No nDSM was used for the classification process in experiment C. For all three experiments, classification was undertaken using the KNN, SVM, and CART algorithms, to produce thematic maps defining the six land cover classes of interest in this study.

The default values were used in the different experiments conducted, given that eCognition inherently uses optimized hyperparameters for its machine learning algorithms (KNN. SVM, and CART). For SVM, the linear kernel was used as similarity function and produced better results than the RBF kernel. For the CART analysis, the default values used were: depth =0, minimum samples =0, and cross validation value of 3. For the KNN analysis, a k value of 1 was used.

4.4.2 Rule-based classification

4.4.2.1 Experiment A and B

Figure 4.9 describes the workflow of the rule-based classification used in this study. Experiment A (Figure 4.9a) and experiment B (Figure 49.b), using feature set A_2 and B_2 respectively, were used to classify elevated and non-elevated objects. Although several features were used for the classification (Table 4.1) the features indicated in Figure 4.9 had the most impact on the classification process. For example, NDVI was most important for differentiating trees from buildings. Similarly, brightness was used to classify shadow, whereas NDWI was used to differentiate waterbodies and impervious surfaces. Features such as homogeneity, standard deviation of nDSM, shape index, and rectangular fit were used to refine the classification. For example, the standard deviation of nDSM, brightness, and border to features were used to differentiate buildings from trees. Additionally, the features length/width, border to, distance to, and texture were used to refine the separation of impervious surfaces, grass, and waterbodies. For experiment A and B, the classification of GeoEye-1 imagery was done with an additional nDSM data.

4.4.2.1 Experiment C

Experiment C describes the rule-based classification from GeoEye-1 imagery (Figure 4.10). No nDSM was used consequently the RBC of experiment C required more complex rule sets. The features displayed enabled to extract significantly land cover information. For example shadows were extracted significantly using the brightness. Additionally, the classification of buildings, Waterbodies and grass were more effective with brightness, NDVI and NDWI respectively.

Other features such as textures (GLCM), geometry (i.e area and form) were used to refine the classification.

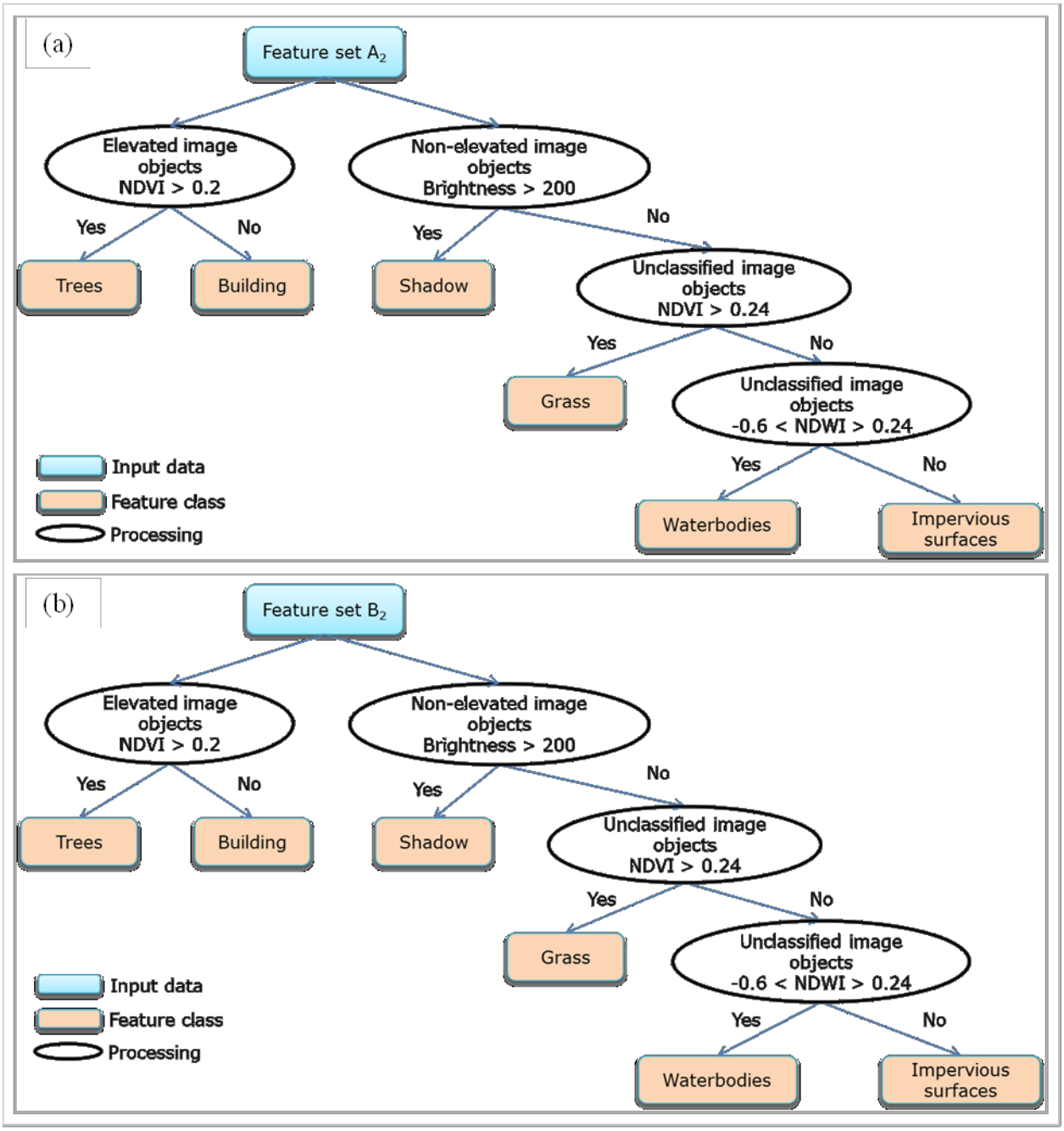

Figure 4.9 The classification workflow of experiment A and B using the rule-base method

For example, the geometric features (i.e. areas, density and form), texture (homogeneity) and border to, real border to enabled to enhance the classification of buildings. In addition, length/width, border to, real border to and GLCM were used to refine the discrimination of impervious surfaces from building. The key difference between experiment A, B and C is the use of a nDSM in the experiment A and B.

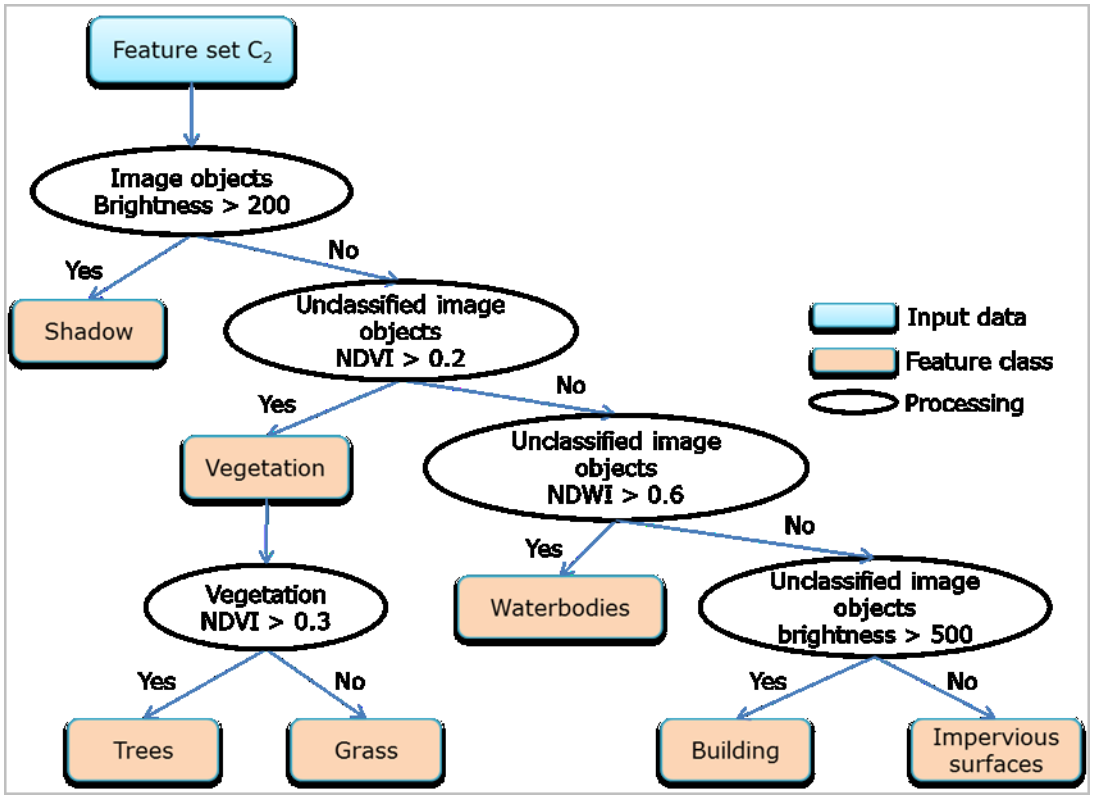

Figure 4.10 Workflow of the rule-based classification from GeoEye-1 imagery.

4.5 ACCURACY ASSESSMENT

Effective decision making requires accurate maps, or at least maps of known accuracy (Congalton & Green 2009) which provides information about the reliability the final classification output (Düzgün, Demirel 2011). Several sources of classification have been identified namely (1) the misidentification, excessive generalization, error in registration and variations in details in interpretation, (2) mixed pixels, landscape complexity and several key landscape variables. The land cover maps can have a value only if such maps have a calculated accuracy whereby the end users would estimate the reliability. The most used techniques by previous studies is the confusion matrix suggested by Congalton & Green (2009). The confusion matrix operates in a site specific or positional accuracy assessment basis which Congalton & Green (2009) defines as the appropriate selection of samples to estimate the statistical parameter of the population error occurring in the spatial data being assessed. The confusion matrix comprises two main components which are a kappa and the overall accuracy (OA) calculated by Congalton & Green (2009) as follow:

$$OA = \sum_{i}^{n} \frac{Xi}{n}$$ Equation 4-1

where X_i is the value of the i^{th} corrected classified sample units;

n is the number of sample units

And

$$Kappa = \frac{N \sum_{i=1}^{r} x_{ii} - \sum_{i=1}^{r} x_{i+} * x_{i+})}{N^2 - \sum_{i=1}^{r} (x_{i+} * x_{+i})}$$ Equation 4-2

where r is the number of rows in the matrix;

x_{ii} Is the number of observations in a row I and column I;

x_{i+} Are the marginal totals of row i

X_{+i} Are the marginal totals of column i

N is the total number of observations.

The kappa analysis is used in accuracy assessments to statistically determine if one error matrix is significantly different from another (Congalton & Green 2009). Additional details about the accuracy of the map are provided by the user and producer's accuracies. Gamba & Martin (2009) define the user and producer accuracies as: (1) the producer accuracy characterises the error of omission incurred when the classified map misses an area of urban land; and (2) the user accuracy reflects the error of commission measuring the number of pixels erroneously labelled like urban land

To assess the accuracy or validity of the maps, the visual inspection and the quantitative accuracy assessment approaches of the four methods proposed by Congalton & Green (2009), were used. The confusion matrix was computed followed by the estimation of the overall accuracy and the kappa statistic to measure the agreement between a standard assumed to be correct and a classified image of unknown quality (Campbell & Wynne 2011). The accuracy of the classification was computed by comparing the location and class of each ground-truth sample of the aerial reference image with the corresponding location and class of the same sample in the classified image.

The approach adopted for selecting reference samples is a combination of random and cluster sampling as described in Congalton & green (2009). Firstly, five hundred random points were generated in ArcGIS and converted in raster file. Secondly, the raster file of random points was

loaded to eCognition. The chessboard segmentation (Definiens AG 2007) was run on the aerial photographs at a scale of 1 for the manual collection of ground truth sampling clusters. Thereafter the polygon sample collection was implemented whereby manually collecting them pixel by pixel at every location where loaded random points were pinpointed. In other words, cluster samplings were generated by manually collecting pixels on the segmented aerial photograph that fall at the same location as the imported random points. Lastly, the created sample points were saved in eCognition TTAmax format and used to calculate the accuracy assessment for each land cover classification result. The confusion matrixes used to assess land cover maps were generated for all maps using the same ground-truth samples.

5 CHAPTER 5 RESULTS AND DISCUSSION

5.1 OVERVIEW OF RESULTS

The overall results of this study indicate that the incorporation of a nDSM into the segmentation and classification processes used for the extraction of urban land cover information from GeoEye-1 imagery, improved the overall classification accuracy. Additionally, the use of a nDSM enhanced the differentiation between spectrally similar features such as buildings and other impervious surfaces, thereby improving individual class accuracy. The level 1 segmentation was qualitatively assessed on the basis of how well elevated image objects were discriminated from non-elevated image objects, having using the region splitting approach, i.e. nDSM. The image objects produced from the level 2 segmentation were validated on the basis of how good they represented real world objects. The classification results were assessed both qualitatively, through visual interpretation of the classified images, and quantitatively, using a confusion matrix. The following sections provide the results of the nDSM creation, feature sets, segmentation, and classification, and discuss the results in the context of this study.

5.2 EVALUATION OF THE nDSM

Figure 5.1 shows the nDSM produced from the LiDAR dataset. The vertical accuracy calculated for the nDSM was 1.04 m, which is close to the standard. According to Liu, Zhang & Peterson (2009) the highest vertical accuracy achievable using LiDAR data is an RMSE of 15-50 cm. Additionally, the vertical accuracy of LiDAR data varies with factors such as flying height, laser beam divergence, location of the reflected points, LiDAR system errors including GPS errors and IMU, distance to ground-based station, and LiDAR data classification (filtering) reliability (Liu, Zhang & Peterson 2009). These factors directly / indirectly influence the overall accuracy of the resulting elevation model.

The bright areas in Figure 5.1 correspond to elevated features, whereas the dark areas correspond to non-elevated features. Very high buildings within the Cape Town CBD are clearly visible as the bright objects in the centre of the model. The two red circles correspond to artefacts that were produced when the nDSM was generated at the sea level. Well-known

structures such as the Cape Town International Convention Centre (CTICC) and the green point stadium in the upper left corner, can be easily identified.

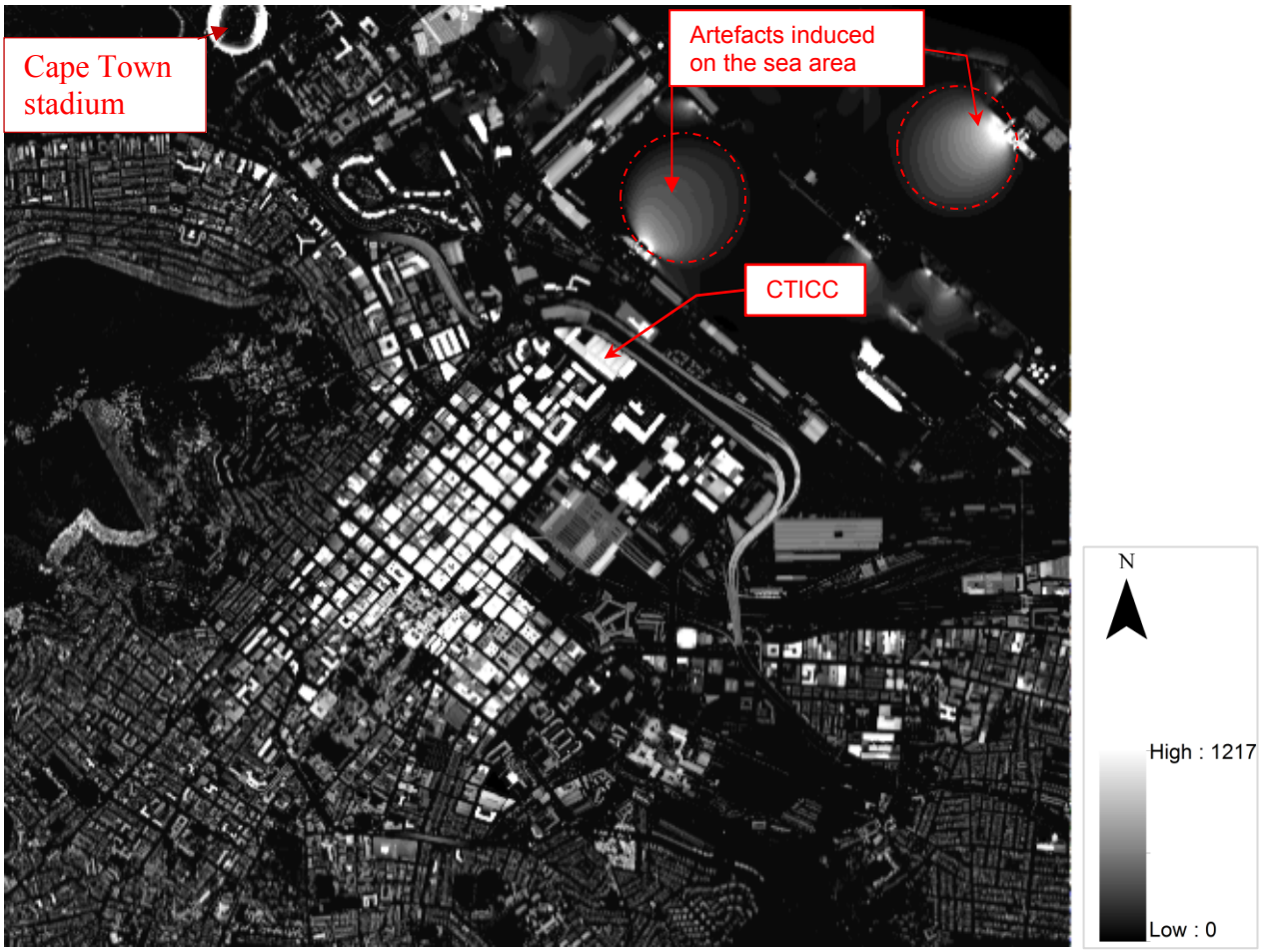

Figure 5.1 The nDSM of the study area and surrounding area produced from LiDAR data.

5.3 SEGMENTATION

5.3.1 Segmentation level 1

The results of the level 1 segmentation for experiment A and experiment B are displayed in Figure 5.2. The level 1 segmentation in experiment A produced image objects that could not be visually analysed, due to the small size of the image objects produced using a scale factor of 5. It is clear from Figure 5.2(a) that the ground features are not easily identifiable. Image objects produced for experiment B, however, are in line with the scale factor of 30 used, given their size. The validation of image objects results of segmentation level 1 depended on how accurate the output of the region splitting was. In other words, the region splitting output should ensure the integrity of elevated image objects versus non-elevated image objects. To

produce such result, a scale factor of 5 was used for the segmentation level 1 of experiment A whereas a scale factor of 30 was enough for the segmentation level 1 of experiment B to achieve the same result. The use of additional features in the segmentation (edge detection file, and pansharpened bands) for experiment B explained the difference of scale factor used.

To illustrate the difference in the output of the level 1 segmentation between experiments A and B, image objects were selected to represent real world features (Figure 5.2b). Experiment A required more objects (Figure 5.2a) given the small size of image objects and performed better on delineating the boundary of the real world features. These groupings of neighbourhood image objects, having similar spectral properties, correspond to man-made and natural real world objects. The selected image objects in Figure 5.2b illustrate the boundaries of waterbodies and footprint of buildings. For experiment C (Figure 5.2c), the level 1 segmentation produced a similar result to experiment B. This illustrates that the input of the nDSM into feature set B_{L1} did not impact on the level 1 segmentation of experiment B.

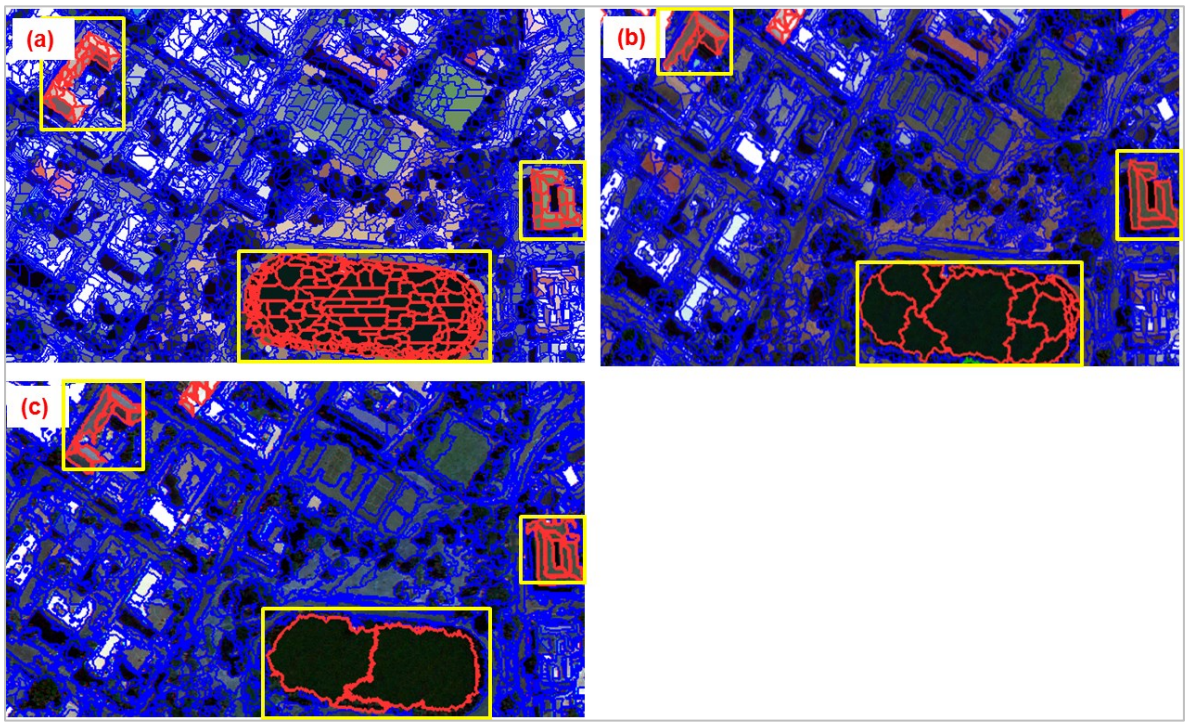

Figure 5.2 Segmentation objects of experiment A displayed in (a), image objects of experiment B in (b) and image object of experiment C in (c). Ground features are selected in red and in yellow boxes.

5.3.2 Region splitting of image objects using the nDSM

For experiments A and B, different nDSM thresholds were tested to discriminate elevated image objects from non-elevated image objects. For example, Figure 5.3a displays the buildings (coloured in blue) identified when a nDSM threshold value of two metres was used, with omitted buildings indicated with a red boundary. Similarly, some buildings in the vicinity of the CTICC could be successfully extracted using a nDSM threshold value of two metres, while others could not. A threshold value of two metres was however suitable for successfully extracting flat areas such as the CTICC and the north coast of Green point. Figure 5.3b shows that a portion of buildings were not successfully extracted using a nDSM threshold value of two metres. This was attributed to these buildings being segmented into several image objects having different mean height values due to the topography of the area.

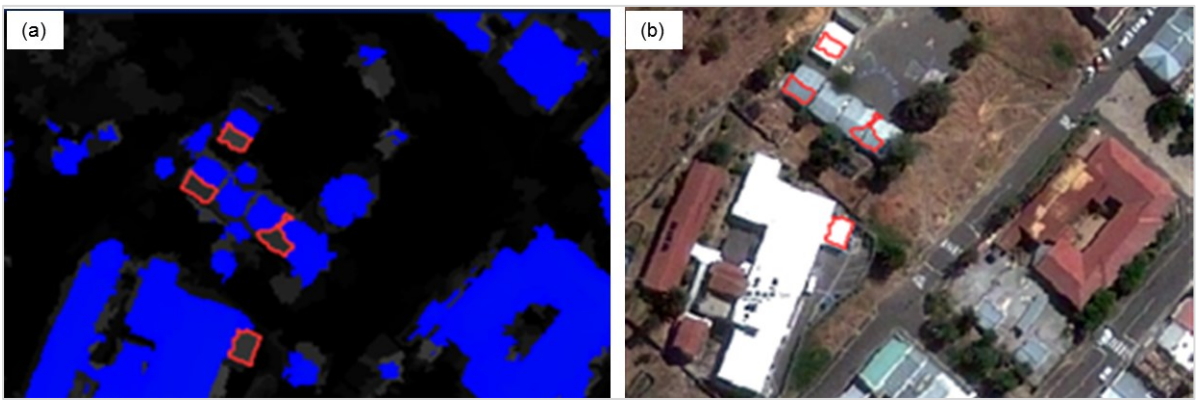

Figure 5.3 Feature extraction using a nDSM threshold value of two metres (a) and their corresponding real world features (buildings) (b).

To successfully extract buildings that were built on the slope of the mountain, a nDSM threshold value of one metre was used. This threshold value also discriminated a large number of elevated features across the study area, despite the variation in topography. Figure 5.4 illustrates the result of using a nDSM threshold value of one metre to split image objects into elevated and non-elevated image objects. For example, features such as small trees located around the dam (Figure 5.4c and 5.4f), were readily discriminated from non-elevated features. However, the gate, visible in Figure 5.4b and 5.4e was easily identifiable in experiment B but could not be readily identified in experiment A due to the smaller scale factor used. Although image objects produced at segmentation level 1 were relatively small,

the visual inspection of Figure 5.4 indicated that elevated objects are reliably distinguished from non-elevated objects.

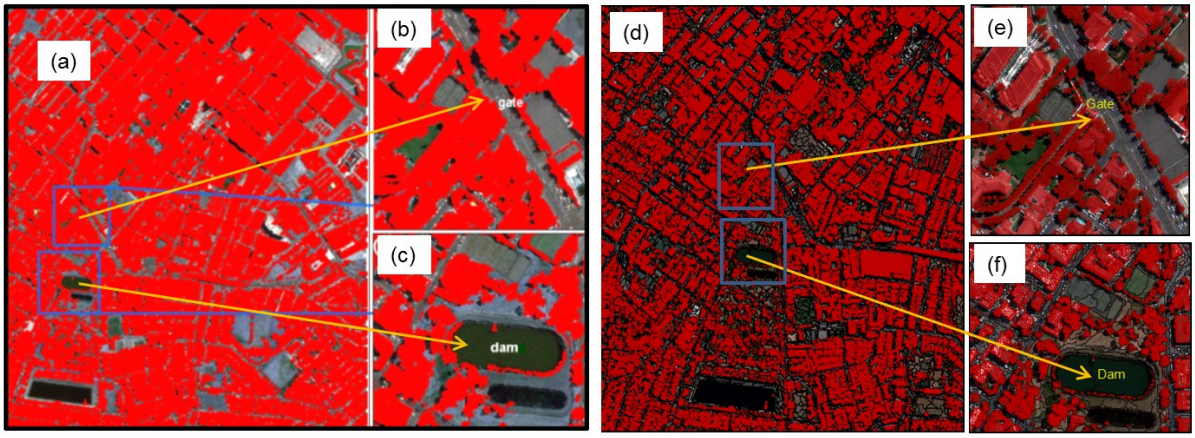

Figure 5.4 Region splitting results for experiment A (a) and experiment B (d). (b) and (e) show the extraction of the gate for experiment A and experiment B respectively, whereas (c) and (f) show the extraction of small trees for experiment A and experiment B respectively, using a nDSM threshold value of one metre.

Cape Town has a mixed topography characterised by mountains (Lions Head, Table Mountain and the Twelve Apostles) and flat areas around the CBD and Green Point. The extraction of buildings based on the nDSM threshold value was complex in areas of steep slopes. Choosing a low nDSM threshold value led to the extraction of infrastructure, such as bridges and covered parking areas that are not part of the building class. Selecting a constant nDSM threshold value to undertake region splitting presented challenges because all buildings had to be picked up, while avoiding features such as covered parking and bridges from being extracted as elevated structures. For example, to extract buildings in the vicinity of the CTICC, nDSM threshold values of two metres and three metres were tested. This allowed for the accurate extraction of trees and buildings since they are higher than their surroundings, which is relatively flat. Buildings could readily be extracted due to their average height of 30 metres. Haala & Brenner (1999) drew the same conclusion in a similar case study. However, when the threshold values of two and three metres were applied to areas on the mountain slope surrounding the centre of Cape Town, many buildings were excluded. This posed the need of reducing the threshold mean value of the nDSM to one metre as previously done by Brunn & Weidner (1997).

5.3.3 Segmentation level 2

For all three experiments, i.e. A, B, and C, the qualitative assessment of the image objects produced from the level 2 segmentation focused on evaluating how good image objects represented real world features. For all three experiments, the MRS region grow algorithm aggregated image objects thereby facilitating identification of real world features (Figure 5.5). Additionally, the output of the level 2 segmentation was similar for all three experiments, given that the same features were used to refine image objects produced from the level 1 segmentation.

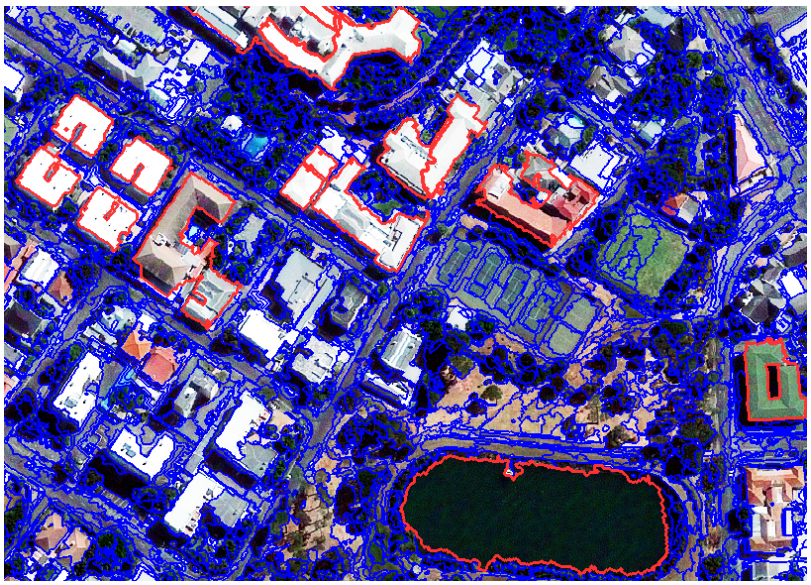

Figure 5.5 Example of image objects of the refinement process of experiment A

5.4 CLASSIFICATION

5.4.1 Separability analysis

The separability analysis performed prior to the classification process showed that the difference between classes increased with the number of features used (Figure 5.6). It is illustrated that the separability between classes increases as the dimension (number of features) increases. For example with one feature (dimension = 1), the separability is almost equal to zero. Figure 5.6 shows that with five features, the analyst gets a higher separability among different classes. As the CBD of Cape Town is highly developed, the scarcity of green areas and water bodies is more observable thus leading to a dominance of impervious

surfaces. Moreover, building and vegetation features (trees or grass) have a low separability measure due to green roofs having the same signature as trees and grass. Similarly, buildings with grey roofs, parking lots, and certain roads had a similar signature causing the low separability measure for buildings and impervious surfaces.

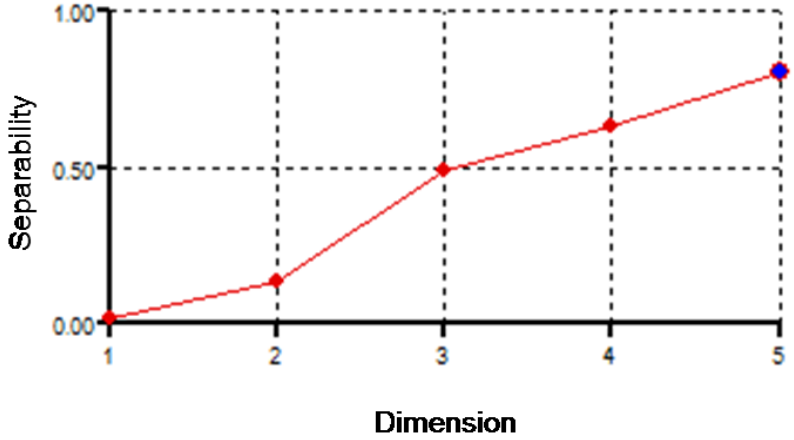

Figure 5.6 Separability of features as a function of the number of dimensions.

5.4.2 Quantitative assessment of urban land cover extraction

5.4.2.1 Supervised classification versus rule-based classification

Regarding the OA and kappa, the supervised classification produced the best result with an OA of 83% and kappa of 0.77 achieved using KNN (Table 5.1). However, the results of individual classes show that the RBC produced better results. For example Table 5.2 shows that the RBC produced constantly better results of buildings in terms of user accuracy (UA) and producer accuracy (PA) even though the highest accuracy was achieved using CART. The highest producer accuracy of 95% was achieved using CART as well as the lowest user accuracy. The UA and PA of other classes varied. No method in the basis of the PA and UA produced would be a better approach these land cover information. The SVM land cover accuracy extracted with a nDSM are almost identical to those of CART and KNN, but the accuracies of those without a nDSM are significantly lower, producing the poorest maps of all the classifiers.

Table 5.1 Overall accuracy and Kappa values for the three experiments

Segmentation approach	Split image objects using height information				Experiment C	
	Experiment A		Experiment B			
	OA (%)	Kappa	OA (%)	Kappa	OA (%)	Kappa
RBC	81.1	0.75	80.5	0.74	61.9	0.50
KNN	82.8	0.77	80.2	0.74	64.2	0.53
CART	80.6	0.75	74.9	0.67	61.7	0.5
SVM	80.4	0.74	81.5	0.76	49.3	0.32

5.4.2.2 Classification using the nDSM

The highest OA of 83 achieved by the KNN, and the lowest OA of 75 achieved using CART (Table 5.1) indicates that integrating the nDSM to the GeoEye-1 image classification produced land cover with a higher accuracy. On the other hand, without the nDSM, the highest OA for the GeoEye-1 image classification was 64 achieved using KNN. The Experiment C displays smaller values of OA and kappa ranging between 64% and 49% for OA and 0.32 and 0.53 for kappa. When classifying GeoEye-1 image without a nDSM, the OA and kappa decreased remarkably. This corresponds to a decrease of about 20% for each supervised classifier and for the RBC. For example, the land cover maps produced using KNN with the nDSM have the highest overall accuracy of 83% and a kappa of 0.77 which decreased for about 20 % when the same land cover is extracted without a nDSM.

The comparison of the user and the producer accuracy (UA and PA) in Table 5.2 also indicates that the land cover maps produced by the GeoEye-1 imagery using RBC, SVM, KNN and CART were less accurate than those produced after integrating a nDSM as additional data. For example the UA of building for experiment C varying between 40 and 68 and PA between 60% and 80%. After adding a nDSM to the classification (example of experiment A), the UA of buildings now varied between 80% and 93% whereas PA varied between 91% and 94%. Similarly for impervious surfaces in experiment C the UA varying between 13% and 67% while the PA varied between 5% and 49%. Compared experiment C to experiment A, the UA increased to value between 92% and 94% whereas the PA increased to values between 71% and 79%. All feature classes had their UA and PA increased from GeoEye-1 classification of experiment C to the classification of GeoEye-1 combined with the

nDSM (experiment A or B). This indicates a significant increase of accuracy to the urban land cover mapping of GeoEye-1 image using a nDSM as additional input data.

Table 5.2 User and producer accuracy of all classes for different classifiers based in the nDSM approach. The values in the table marked in red highlights the highest producer accuracies.

Classification approach	**Feature Classes**	**Experiment A**		**Experiment B**		**Experiment C**	
		UA	**PA**	**UA**	**PA**	**UA**	**PA**
RBC	**Building**	92.73	92.44	91.23	92.29	68.06	64.66
	Grass	58.99	91.28	69.72	76.01	40.59	62.56
	Impervious	93.99	70.79	88.3	76.55	66.95	48.52
	Shadow	18.05	49.73	12.42	45.73	51.67	29.62
	Trees	95.25	72.23	87.18	73.44	72.56	76.78
	Waterbodies	100	87.75	100	91.67	100	91.76
KNN	**Building**	83.39	94.10	78.75	93.47	62.9	79.32
	Grass	82.4	79.11	80.03	71.67	66.13	66.46
	Impervious	93.06	78.69	94.34	66.71	67.05	41.73
	Shadow	26.28	94.26	31.52	68.55	22.69	56.59
	Trees	92.43	73.57	87.58	82.68	79.4	66.19
	Waterbodies	90.83	82.54	39.9	91.92	37.8	97.1
CART	**Building**	84.17	91.82	74.80	94.53	59.09	62.46
	Grass	87.74	69.65	77.18	64.86	58.8	65.89
	Impervious	92.2	77.32	91.55	62.32	61.98	50.19
	Shadow	20.84	93.96	5.29	11.83	25.66	85.16
	Trees	89.9	75.76	78.88	73.29	81.11	67.56
	Waterbodies	34.79	63.1	41.52	73.46	76.47	91.76
SVM	**Building**	79.16	91.33	80.13	93.97	40.7	59.27
	Grass	82.37	79.11	84.16	70.7	62.09	67.61
	Impervious	93.06	79.01	93.67	69.98	13.83	5.63
	Shadow	23.08	93.96	28.41	79.57	36.4	67.31
	Trees	92.26	65.83	87.18	83.25	81.55	70.03
	Waterbodies	100	82.54	67.47	98.83	59.69	91.76

5.4.3 Qualitative comparison of the urban land cover maps

Figure 5.7 is an illustration of the quality of the land cover maps produced using the GeoEye-1 image and the nDSM. Two classes (buildings and waterbodies) were selected to appreciate without confusion how well different land cover information was extracted for the various classification methods tested. Swimming pool and building boundaries accurately delineated indicates that the RBC method performed well. This shows that waterbodies were best identified using the RBC in experiment A and B which produced similar land cover accuracy.

Figure 5.8 and 5.9 are displayed to visually evaluate the impact of the nDSM of the overall classification process. Figure 5.9 displays more structured building patterns than Figure 5.8. Therefore, the visual inspection of the two Figures shows a net difference between the land cover produced with GeoEye-1 imagery and that produced with the combined GeoEye-1 imagery and the nDSM.

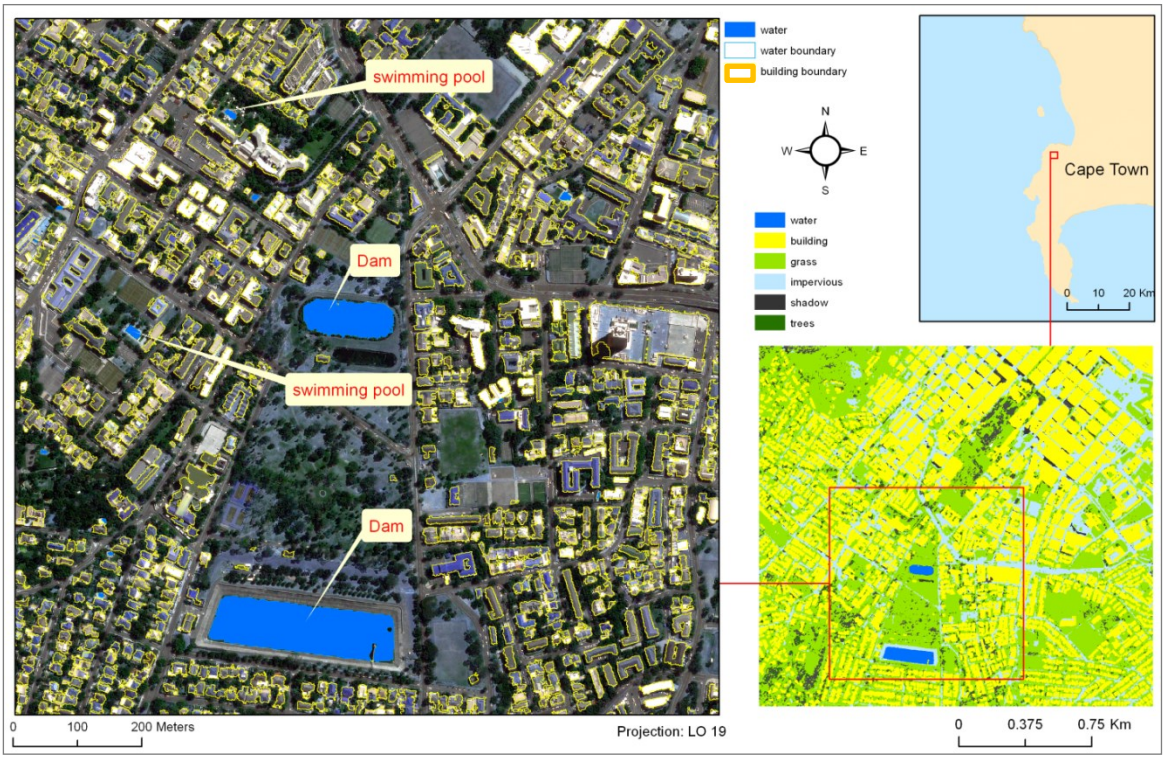

Figure 5.7 Building footprints information created using the RBC and the nDSM-based segmentation approach

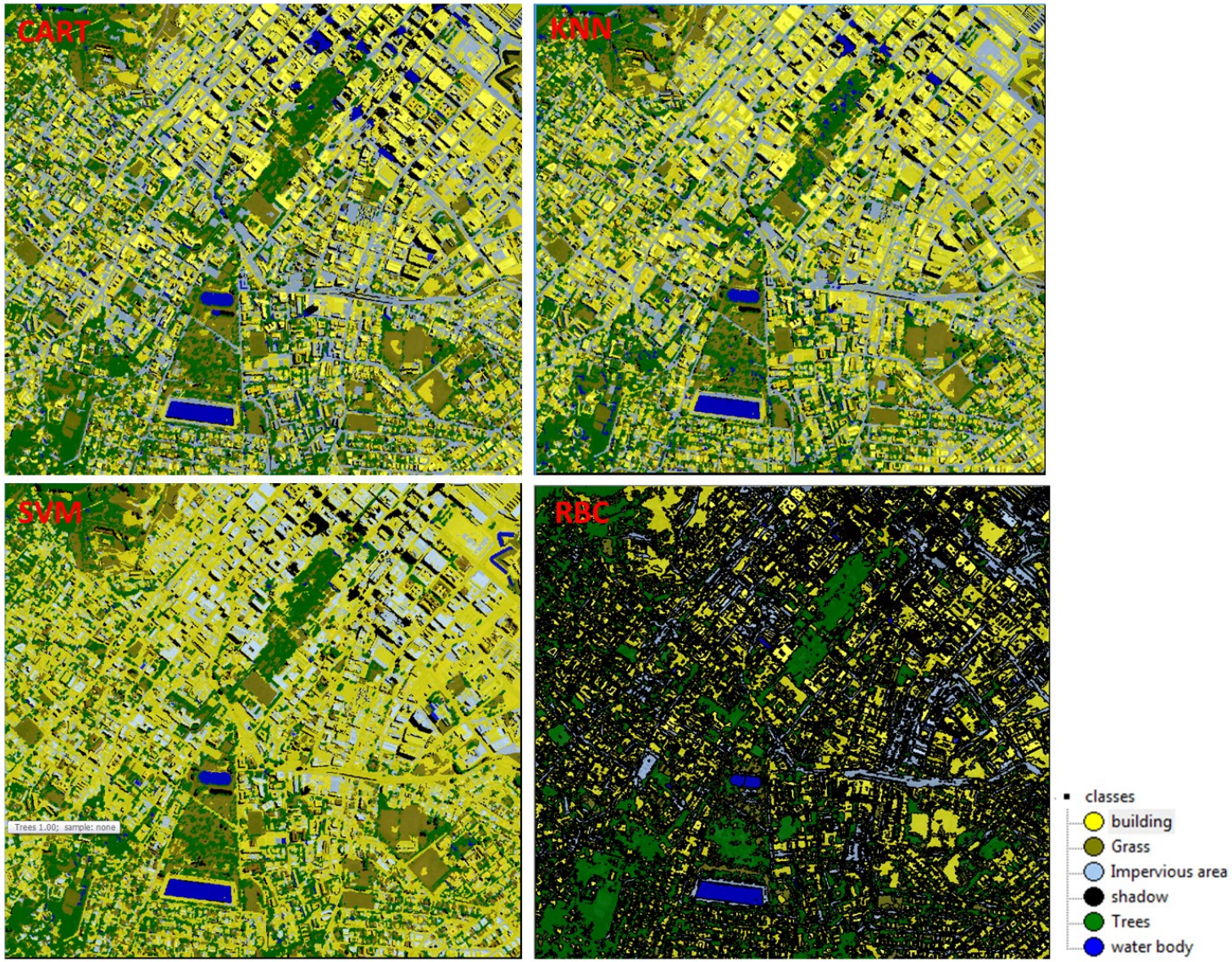

Figure 5.8 Urban land cover produced using GeoEye-1 imagery

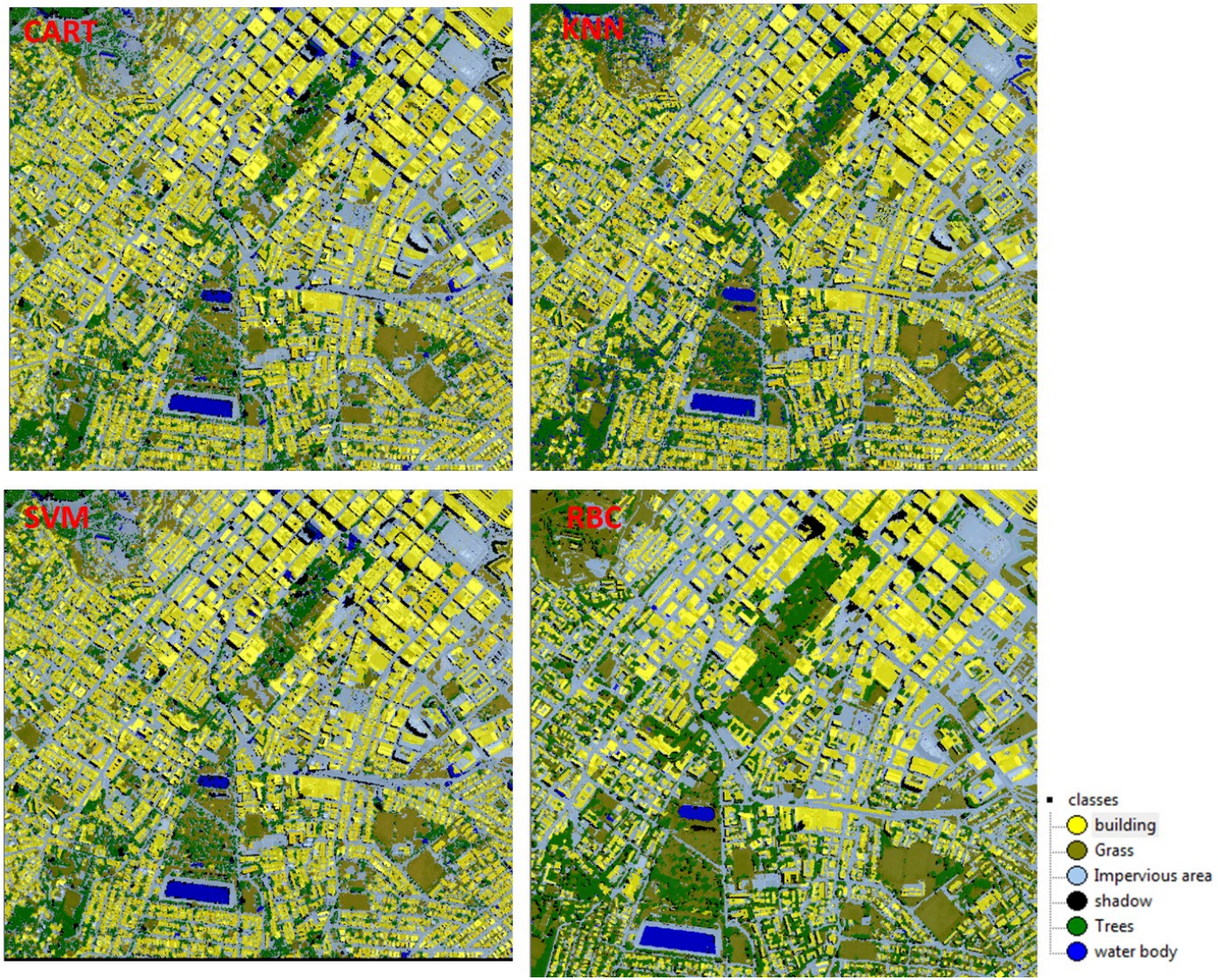

Figure 5.9 Urban land cover produced using GeoEye-1 imagery and the nDSM

5.4.1 Discussion

5.4.1.1 Impact of the nDSM versus non-nDSM

When including the nDSM in the RBC and the supervised classification, the overall accuracy and kappa increased respectively. When the nDSM was excluded, the overall accuracy and kappa ranged between decreased. The accuracies obtained were always about 20% higher when the DSM was included. Clearly the incorporation of the nDSM into the urban land cover extraction of Cape Town significantly increased the accuracy for the classification methods tested.

Without the nDSM, the misclassification not only occurred between image objects of similar height but also between image objects of different height (i.e., some buildings were misclassified as parking lots while others were misclassified as trees). Many impervious areas and buildings were misclassified to one another. Trees and grass were also misclassified to one another whereas for the classification approach using the nDSM, buildings and trees were misclassified to one another, shadow and water also were misclassified to one another. Consequently, misclassifications for the classification using the nDSM, only occurred among objects of the same category (elevated versus non-elevated). . The land cover maps produced by the two data approaches differ visually as is clearly observable when comparing.

The nDSM efficiently helped to remove shadow effects, visible on the GeoEye-1 imagery and to discriminate building structures accurately. All above ground shaded objects being higher than 1 meter in the GeoEye-1 image, were accurately mapped as feature that they are in the real world. Buildings and trees shaded by others high features had the same spectral properties as shadows. But, the use of the nDSM prevented to extract any shaded features as shadow due to the region splitting approach. The approach, which consists of splitting the scene first, to image elevated and non-elevated using the nDSM threshold, helped to correctly extract buildings and trees covered by shadows induced by other buildings or trees.

5.4.1.2 Impact of supervised classification

Quantitatively the KNN supervised classifier provided better result than the RBC, SVM and CART. The qualitative analysis of the land cover maps produced using the supervised classifiers showed errors that were not made by the RBC such as bridge and cover parking classified as building in experiment A and B, or as impervious in experiment C. The supervised classification is simple and fast to run producing accurate land cover. Impervious surfaces were exceptionally misclassified as water because samples of swimming pools selected as ROIs have the same spectral properties as impervious surfaces and buildings. Shallow swimming pools present the same characteristics as impervious surfaces (parking areas or roads) and buildings. Thus, selecting ROIs of swimming pools, leads to the misclassification of impervious surfaces and buildings as water bodies. Shaded parking areas were misclassified as water bodies for similar reasons.

5.4.1.3 Impact of rule-based classification

A fundamental purpose of maps is to convey information which is accurate and up to date. EO data are therefore eminently suitable for updating maps and the rule-based approach gives the means to produce accurate land cover images and quick access to-up-to date map information by means of automation. The NDWI implemented in the rule set improved the extraction of water bodies, particularly in classifications using the nDSM. The RBC makes it possible to extract swimming pools more accurately using the nDSM approach. The rule-based method not only facilitated the extraction of water bodies such as swimming pools, but also the differentiation of bridges and covered parking from building structures.

The rule-based extraction from GeoEye-1 imagery alone was more complex due to spectral similarities between various features. Shadow was first extracted together with shaded buildings and trees which could be avoided in the method using an additional nDSM. Another band combination that produces similar results as NDWI was also tested. In this band combination, the green band replaces the blue band in the original NDWI. The NDWI also helped to extract dark and green roof buildings.

The rule-based method is time consuming and complex but it has the advantage of creating additional rules to refine the classification results of previous rule sets. This process increases the classification accuracy by reducing the misclassifications. Appropriate implementation of indices

and the possibility of refining the classification result produced very accurate urban land cover maps even though the statistic accuracy was slightly low than the KNN.

Compared to the supervised CART classifiers, the accuracy for RBC was similar to CART's accuracy and higher than SVM's accuracy. However, the quality analysis revealed that the land cover maps produced by the RBC were more reliable than the land cover of the supervised classifiers. The RBC avoided misclassification of some buildings with green and dark roofs as trees. Such misclassifications were produced using the supervised classifiers whether the nDSM was used or not.

6 CHAPTER 6 EVALUATION AND CONCLUSION

6.1 SUMMARY OF THESIS

This research assessed the utility of a high resolution nDSM, produced from LiDAR data, for improving the extraction of urban land cover information from high resolution GeoEye-1 imagery within a GEOBIA environment. Three independent experiments were setup. For each experiment, two levels of image segmentation were undertaken using unique feature sets. Level I segmentation was undertaken to produce image objects that was later refined by a Level II segmentation and produce the final image objects to be classified. Two classification approaches were adopted in this study, i.e. a rule-based approach, and a supervised approach. For the supervised approach, three classification algorithms, namely KNN, CART, and SVM were tested. At last, the qualitative and quantitative analysis of the GeoEye-1 land cover results enabled to outline the effective increase in accuracy of the land cover induced by the integration of a nDSM to the classification process.

6.2 REVISITING THE OBJECTIVES IN THE CONTEXT OF THE RESULTS

The first objective of this research was to investigate appropriate methods for classifying urban land cover using GeoEye-1 imagery and a nDSM. The review of the literature suggested a nDSM approach that involved splitting the segmented image into elevated and non-elevated image objects using a nDSM threshold value. The region splitting approach did, however, result in some misclassification, for example of waterbodies such as swimming pools. This resulted from all swimming pools not being at ground level, but also occurring atop buildings or at mid-floor level. For the supervised classification, these swimming pools were classified as waterbodies. However, for the rule-based classification, such swimming pools were assigned to the building class given their location. This helped improve overall classification accuracy of the waterbodies class. For objective two, a high resolution (1 m) nDSM was generated using the LiDAR dataset. A vertical accuracy of approximately one metre provided a valid output that could subsequently be used for undertaking the urban land cover extraction. For objective three, it was found that the various classification techniques all produced good results. The land cover result produced through the segmentation using only the nDSM, was not significantly different from the land cover result produced from the segmentation using all input data (i.e. the four bands of GeoEye-1 imagery, the edge detection file, and the nDSM). For objective five, quantitative and qualitative analysis of the results, indicated that using the nDSM significantly

improved the accuracy of urban land cover extraction. The impact of the nDSM on the classification process could be evaluated at approximately 20 % increase in accuracy. The findings of this research indicate that the combination of the nDSM and GeoEye-1 satellite imagery constitutes an improved and effective approach for extracting detailed information of urban areas.

6.3 EVALUATION OF THE RESEARCH

This research not only evaluates the nDSM, it also compares rule-based versus supervised classification approaches. The supervised classification is simple and fast. It also produces good results regarding accuracy. However, details such as swimming pools, which represent water bodies in urban area, were often extracted as impervious areas, particularly when the nDSM were not included to the feature set used for the classification.

This study demonstrated the effectiveness of using a DSM to extract urban land cover information combined with high-resolution satellite imagery. The creation of new satellites with higher spatial resolutions offers great potential for creating a high-resolution DSM. The extraction of low-density features (individual trees and dwelling units) by this study highlights the effect of the nDSM for land cover extraction. Therefore, the current research further corroborates the results of previous studies (Hussain et al. 2011, Jiao 2012) that have combined satellite imagery with height information to extract urban land cover. However the comparative approach used here enabled to prove the usefulness of the nDSM, which they have not used.

In addition, this study shows that the RBC can reduce classification errors enabling the classification of complex features such as swimming pools and bridges and cover parking. However, it was found that the KNN classifier produced the highest accuracy for the land cover maps when combining the nDSM with the GeoEye-1 image as well as when only the GeoEye-1 image was used as input.

To evaluate the effectiveness of the nDSM, the accuracy of the land cover extracted with the combined nDSM and satellite imagery are benchmarked against the generated accuracy of the land cover extracted with the GeoEye-1 imagery alone. A rigorous comparison of the two extraction methods was achieved through a workflow that combined detailed quality control of the segmentation procedure with the assessment of the final extracted land cover maps. The following conclusions can be drawn about the findings:

- Land cover extraction that used a combination of a GeoEye-1 image and a LiDAR-based nDSM produced far better land cover maps of the studied part of the City of Cape Town than the extraction from the GeoEye-1 imagery alone.
- Regarding the two extraction approaches, the supervised classification method using the KNN classifier consistently produced better accuracies than the RBC. However, visual inspection of the results revealed the quality of the RBC land cover maps were better than the land cover maps extracted using the supervised classification.
- The nDSM enabled the definition of simple rules to generate a relatively accurate land cover map, whereas the RBC that only used the GeoEye-1 imagery input was much more complex and time consuming to develop.
- This research shows high potential for combining EHSR GeoEye-1 imagery with the nDSM to produce more accurate urban land cover maps (on the level of dwelling units) so facilitating knowledge and measurements of man-made features such as building footprint.

6.4 RECOMMENDATIONS

6.4.1 Generating urban land cover maps

The supervised classification produced accurate urban land cover maps over a rule-based method that was time demanding to produce similar results. A hybrid approach that combined both the supervised and the RBC methods can produce fast more accurate land cover information. The method can consist of running the supervised classification first and later refines the results using a rule set. In this case, the overall approach becomes faster as the rule-based will only focus on the fewer misclassified objects. An attempt of combining both a supervised and rule-based extraction is recommended for an expected fast and accurate land cover extraction.

The segmentation analysis and the visual assessment of less reliable image objects of segmentation (mainly those combining pixels of elevated features with the ground level's feature) has revealed that the production of such image objects prompted to the few mismatch between the nDSM and the GeoEye-1 pan-sharpened imagery.

The supervised classification can be improved by increasing the training sample of each feature class. Extending the training sample can enhance the results of supervised classification. But such extension is less effective, when dealing with a larger area and having to do ground truthing. The rule-based method may present more cost-effective alternative.

6.4.2 What further research is needed?

The focus of this study was to investigate the impact of the nDSM to the GoEye-1 image classification using OBIA and several classification methods. Further studies should investigate building robust rule sets in order to test their transferability to other study areas.

The resolution of the nDSM and GoeEye-1 image used in this study was one metre and 50 cm respectively. Although, the addition of a nDSM to the GeoEye-1 land cover classification increased the accuracy, further research could investigate the use of advance EHSR imagery such as WorldView 3 with 0.3 metre. The use of higher spatial resolution imagery and high spatial resolution nDSM can potentially enhance the accuracy of the urban land cover extraction.

6.5 CONCLUSION

This study found that the KNN supervised classifier produced land cover information with highest calculated accuracy. The rule-based enables the extraction of features such as swimming pools and bridges hardly differentiable by the supervised classifiers. In addition, the rule-based land cover maps present more accurate information with the visual inspection approach.

The quantity of feature sets involved in the segmentation does not necessarily imply a good segmentation output, and the EHSR imagery alone produces a reliable segmentation output.
Height information considerably increases the accuracy of land cover information. Therefore, producing land cover maps with an additional nDSM is more appropriate because it would optimise the accuracy, reduce the cost and the time.

Regarding individual land cover information, the RBC produced more accurate building footprints, waterbodies, trees and grass. The user and producer accuracy of these land cover information were higher for the RBC than for the three supervised classifiers. These results of individual land cover information indicate that the RBC is the best option for land cover extraction of buildings and others man-made features. The use of the RBC and three supervised classifiers was to ensure that the results remain identical when combining high resolution imagery with the nDSM. The result can possibly change if the same rule sets were used with or without the same data in a different study area. Further research is required to test the transferability of the rule sets. However, this study and previous research have found that

combining the high resolution nDSM with RS imagery always improved the accuracy of urban land cover regardless of the area used.

REFERENCES

Aggarwal CC 2014. *Data classification: Algorithms and applications*. New York : CRC Press Taylor & Francis.

Al-Khudhairy DHA, Caravaggi I & Glada S 2005. Structural damage assessments from Ikonos data using change detection, object-oriented segmentation, and classification techniques. *Photogrammetric Engineering and Remote Sensing* 71, 7: 1-13.

Alshennawy AA & Aly AA 2009. Edge detection in digital images using fuzzy logic technique. *World Academy of Science, Engineering and Technology* 51: 178-186.

American Planning Association 2006. *Planning and urban design standards*. John Wiley & Sons.

Asmare MF 2013. Airborne LiDAR data and VHR WorldView satellite imagery to support community based forest certification in Chitwan, Nepal. Master's thesis. Netherlands: University of Twente, Department of Geo-information Science and Earth Observation.

Awrangjeb M, Ravanbakhsh M & Fraser CS 2010. Automatic detection of residential buildings using LiDAR data and multispectral imagery. *ISPRS Journal of Photogrammetry and Remote Sensing* 65, 5: 457-467.

Awrangjeb M, Zhang C & Fraser CS 2013. Automatic extraction of building roofs using LiDAR data and multispectral imagery. *ISPRS Journal of Photogrammetry and Remote Sensing* 83: 1-18.

Baraldi A, Durieux L, Simonetti D, Conchedda G, Holecz F & Blonda P 2010. Automatic spectral-rule-based preliminary classification of radiometrically calibrated SPOT-4/-5/IRS, AVHRR/MSG, AATSR, IKONOS/QuickBird/OrbView/GeoEye, and DMC/SPOT-1/-2 Imagery—Part I: System Design and Implementation. *IEEE Transactions on Geoscience and Remote Sensing* 48, 3: 1299-1325.

Barnes CF & Burki J 2006. Late season rural land-cover estimation with polarimetric-SAR intensity pixels blocks and tree-structured Nearest Neighbour classifiers. *IEEE Transactions on Geoscience and Remote Sensing* 44, 9: 2384-2392.

Baud I, Kuffe M, Pfeffer K, Sliuzas R & Karuppannan S 2010. Understanding heterogeneity in metropolitan India: The added value of remote sensing data for analysing sub-standard residential areas. *International Journal of Applied Earth Observation and Geoinformation* 12, 5: 359-374.

Bauer ME, Loffelholz BC & Wilson B 2008. Estimating and mapping impervious surface area by regression analysis of Landsat imagery. In Weng Q (ed) *Remote Sensing of impervious Surfaces* 3-19. London: Taylor & Francis Group.

Béland M, Widlowski JL & Fournier RA 2014. A model for deriving voxel-level tree leaf area density estimates from ground-based LiDAR. *Environmental Modelling & Software* 51: 184-189.

Belgiu M Drăgu L & Strobl J 2014. Quantitative evaluation of variations in rule-based classifications of land cover in urban neighbourhoods using WorldView 2 imagery. *ISPRS Journal of Photogrammetry and Remote Sensing* 87, 2014: 205-215.

Ben-Hur A & Weston J 2010. A user's guide to support vector machines. In Carugo O & Eisenhaber (eds) *Data mining techniques for the life sciences*. New Jersey: Humana Press.

Ben-Hur A, Ong CS, Sonnenburg S, Schölkopf B & Rätsch G 2008. Support vector machines and kernels for computational biology [Online]. Available from: http://svmcompbio.tuebingen.mpg.de/ [Accessed 06 December 2012].

Bennett J 2010. *OpenStreetMap*. Birmingham: Packt Publishing Ltd.

Benz UC, Hofmann P, Willhauck G, Lingenfelder I & Heynen M 2004. Multi-resolution, object-oriented fuzzy analysis of remote sensing data for GIS-ready information. *ISPRS Journal of photogrammetry and remote sensing* 58, 3: 239-258.

Berger C, Voltersen M, Hese S, Walde I & Schmullius C 2013. Robust extraction of urban land cover information from HSR multi-spectral and LiDAR data. *IEEE Journal of Selected Topics in Applied Earth Observations and Remote Sensing* 6, 6: 1-16.

Bernhardsen T 2002. *Geographic information systems: an introduction*. 3rd ed. Canada: John Wiley & Sons.

Bhatta B 2010. *Analysis of urban growth and sprawl from remote sensing data*. Berlin: Springer-Verlag.

Bhattacharyya S & Dutta P 2012. *Computational intelligence for engineering, science, and business*. Hershey: Information Science Reference.

Blaschke T 2010. Object based image analysis for remote sensing. *ISPRS Journal of Photogrammetry and Remote Sensing* 65, 1: 2-16.

Blaschke T, Lang S & Hay G 2008. *Object-based image Analysis Spatial concepts for knowledge-driven remote sensing application*. Berlin: Springer.

Borghys D, Lacroix V & Perneel C 2002. Edge and line detection in polarimetric SAR images. In Kasturi R, Laurendeau D & Suen C (eds) *16 th International Conference on Pattern Recognition,* 929-924. Proceedings of the pattern recognition conference held 11-15August 2002, Quebec, Canada. Piscataway: Institute of Electrical and Electronics Engineers.

Borough of Mendham 2009. Zoning & Engineering Word Definition [online]. From http://www.mendhamnj.org/Cit-e-Access/webpage.cfm?TID=94&TPID=9888. [Accessed 06/08/2014].

Bouziani M, Goita K & He DC 2010. Rule-based classification of a very high resolution image in an urban environment using multispectral segmentation guided by cartographic data. *IEEE Transactions on Geoscience and Remote Sensing* 48, 8: 3198-3211.

Brennan R & Webster TL 2006. Object-oriented land cover classification of LiDAR-derived surfaces. *Canadian Journal of Remote Sensing* 32, 2: 162-172.

Brunn A & Weidner U 1997. Extracting buildings from digital surface models. *International Archives of Photogrammetry and Remote Sensing* 32, 3: 27-34.

Brunner D, Lemoine G, Bruzzone L & Greidanus H 2010. Building height retrieval from VHR SAR imagery based on an iterative simulation and matching technique. *IEEE Transactions on Geoscience and Remote Sensing* 48, 3: 1487-1504.

Burbridge S & Yun Z 2003. A neural network based approach to detecting urban land cover changes using Landsat TM and IKONOS imagery. In *2nd GRSS/ISPRS Joint Workshop on Remote Sensing and Data Fusion over Urban Areas*, 157-161. Proceedings of the 2nd GRSS/ISPRS Joint Workshop on Remote Sensing and Data Fusion over Urban Areas held 22-23 May 2003, Berlin, Germany.

Burnett C & Blaschke T 2003. A multi-scale segmentation object relationship modelling methodology for landscape analysis. *Ecological Modelling* 168, 3: 233-249.

Cai W, Liu Y, Li M, Zhang Y & Li Z, Wen-ting C, Yong-xue L, et al. 2010. A best-first multivariate decision tree method used for urban land-cover classification. In Liu Y & Chen A (eds) *2010 18th International Conference on Geoinformatics,* 1-5. Proceedings of the 18th International Conference on Geoinformatics held 18-20 June 2010, Beijing, China.

Campbell JB & Wynne RH 2011. *Introduction to Remote Sensing*. 5th ed. New York: Taylor & Francis

Campbell JB & Wynne RH 2012. *Introduction to remote sensing*. 6th ed. New York: Guildford Press.

Campbell JB 2006. *Introduction to remote sensing*. 4th ed. New York: Taylor & Francis.

Carbonneau P & Piegay H 2012. *Fluvial remote sensing for science and management*. Chichester: John Wiley & Sons.

Chan CH 2012. *Signal and image processing for remote sensing*. 2nd ed. Boca Raton: CRC Press Taylor & Francis.

Chanda B & Majumder DD 2011. *Digital image processing and analysis*. 2nd ed. NewDelhi: Asoke K. Ghosh.

Chang A, Eo Y, Kim Y & Kim Y 2013. Identification of individual tree crowns from LiDAR data using a circle fitting algorithm with local maxima and minima filtering. *Remote Sensing Letters* 4, 1: 29-37.

Charaniya A P, Manduchi R & Lodha SK 2004. Supervised parametric classification of aerial LiDAR data. In *Computer Vision and Pattern Recognition Workshop 2004,* 30-30, with CD-ROM.

Charaniya AP, Manduchi R & Lodha SK 2005. Supervised parametric classification of aerial LiDAR data. In Schmid C, Soatto S, Tomasi C (eds) *2005 IEEE Computer Society Conference on Computer Vision and Pattern Recognition (CVPR 2005).* Proceedings of the meeting held 20-26 June 2005, San Diego, CA, USA.

Charlton S & Kihato C 2006. Reaching the poor? An analysis of the influences on the evolution of South Africa's housing programme. Democracy and delivery: Urban policy in South Africa 252-282.

Chen F, Kusaka H, Bornstein R, Ching, J, Grimmond CSB, Grossman-Clarke S, Loridan et al. 2011. The integrated WRF/urban modelling system: development, evaluation, and applications to urban environmental problems. *International Journal of Climatology* 31, 2: 273-288.

Chen Y, Shi P, Fung T, Wang J & Li X 2007. Object-oriented classification for urban land cover mapping with ASTHER imagery. *International Journal of Remote Sensing* 28, 20: 4645-4651.

Chuvieco E, Li J & Yang X 2010. *Advance in earth observation of global change*. London: Springer.

Clode S, Kootsookos P & Rottensteiner F 2004. The automatic extraction of roads from LiDAR data. In Altan O (ed) *ISPRS Archives-Volume XXXVPart B7, 2004.* Proceedings of International congress held 12-23 July 2004, Istanbul, Turkey.

Clode S, Rottensteiner F, Kootsookos PJ & Zelniker EE 2006. Detection and vectorisation of roads from LiDAR data. *Photogrammetric Engineering & Remote Sensing* 1: 1-50.

Colditz RR, Schmidt M, Ressl R, Hansen MC & Dech S 2008. A method for selecting training data and its effect on automated land cover mapping of large areas. In Entekhabi D, Kerekes JP, Miller & Reising SC (eds) *IGARSS* 2008 - 2008 IEEE *International Geoscience and Remote Sensing Symposium,* 542-545. Proceedings of the International Geoscience & Remote Sensing Symposium held 6-11 July 2008 Boston, Massachusetts, USA.

Conchedda G, Durieux L & Mayaux P 2007. Object-based monitoring of land cover changes in mangrove ecosystems of Senegal. In Verhoest N, Bruneel S, Coppin P, Gabriëlle De Lannoy G, Verstraete W & Hoeben R (eds) 2007 *International Workshop on the Analysis of Multi-temporal Remote Sensing Images,* 1-6. Proceedings of a meeting held 18-20 July 2007, Leuven, Belgium.

Congalton R. & Green K 2008. *Assessing the Accuracy of Remotely Sensed Data: Principles and Practices*. 2nd Ed. Boca Raton: Taylor & Francis.

Cots Folch R, Aitkenhead MJ & Martínez Casasnovas JA 2007. Mapping land cover from detailed aerial photography data using textural and neural network analysis. *International Journal of Remote Sensing* 28, 7: 1625-1642.

Couloigner I & Ranchin T 2000. Mapping of urban areas: a multiresolution modeling approach for semi-automatic extraction of streets. *Photogrammetric Engineering and Remote Sensing* 66, 7: 867-874.

Cowling RM, MaCDonald IAW & Simmons MT 1996. The Cape Peninsula, South Africa: physiographical, biological and historical background to an extraordinary hot-spot of. The Cape Peninsula, South Africa: physiographical, biological and historical background to an extraordinary hot-spot of biodiversity. *Biodiversity & Conservation* 5, 5: 527-550.

Cox KR, Hemson D & Todes A 2004. Urbanization in South Africa and the changing character of migrant labour. *South African Geographical Journal* 86, 1: 7-16.

Craglia M, Gould M, Goodchild MF, Annoni A, Camara G, Kuhn W, Mark D, Masser I, Maguire D, Liang S, Parsons E 2008. Next-generation digital earth. A position paper from the Vespucci Initiative for the Advancement of Geographic Information Science. *International Journal of Spatial Data Infrastructures Research* 3: 146–167.

Cross C 2006. Attacking urban poverty with housing: Toward more effective land markets. Paper delivered to the urban land seminar, Muldersdrift, South Africa.

Dare PM 2005. Shadow analysis in high-resolution satellite imagery of urban areas. *Photogrammetric Engineering & Remote Sensing* 71, 2: 169-177.

Darwish A, Leukert K & Reinhardt W 2003. Image segmentation for the purpose of object-based classification. In *IGARSS 2003: Learning from Earth's Shapes and Sizes: 2003 IEEE International Geoscience and Remote Sensing Symposium*. Proceedings of International Geoscience and Remote sensing Symposium held 21-25 June 2003, Toulouse, France.

Definiens imagine 2007. *eCognition Developer 8.64.1 tour guide*. Munchen: Trimble Germany GmbH.

Definiens imagine 2011. *eCognition user guide.* Trimble Germany GmbH, Munchen, Germany.

Dennison PE, Brunelle AR & Carter VA 2010. Assessing canopy mortality during a mountain pine beetle outbreak using GeoEye-1 high spatial resolution satellite data. *Remote Sensing of Environment* 114, 11: 2431-2435.

Dey V, Zhang Y & Zhong M 2011. Building detection from Pan-sharpened GeoEye-1 satellite imagery using context based multi-level image segmentation. In Zhang J (ed) *2011 International Symposium on Image and Data Fusion (ISIDF 2011)*, 1-4. Proceedings of a meeting held 9-11 August 2011, Tengchong, Yunnan, China.

Dial G & Grodecki J 2002. Block adjustment with rational polynomial camera models. In *the 18th American Society of Photogrammetry and Remote Sensing (ASPRS),* 77-86. Proceedings of ASPRS Conference held April 22–26, Washington DC, USA.

DigitalGlobe, Inc. 2014. Mining [online]. Available on http://www.digitalglobe.com/industries/other-industries/oil-gas#oil-gas. [Accessed on 24 Mai 2014].

Donnay JP, Mike JB & Longley PA (eds). *Remote Sensing and Urban Analysis: GISDATA 9*. CRC Press, 2003.

Duadze SEK 2004. *Land use and land cover study of the savannah ecosystem in the Upper West Region (Ghana) using remote sensing.* Gottingen: Cuvillier Verlag.

Düzgün S & Demirel N 2011. *Remote sensing of the mine environment*. London: Taylor & Francis.

Dwivedi RS & Sreenivas K 1998. Image transforms as a tool for the study of soil salinity and alkalinity dynamics. *International Journal of Remote Sensing* 19, 4: 605-619.

Environmental Systems Research Institute (ESRI) 2014. Arc GIS desktop release. Environmental systems Research Institute.

Erdas 2011. ATCOR for Erdas Imagine 2011. Atlanta, Georgia, USA.

Erdas, Inc 2010a. Erdas Imagine Tour Guides. Atlanta, Georgia, USA.

Erdas, Inc 2010b. Erdas Imagine- Leica Photogrammetry Suite help (LPS). Atlanta, Georgia, USA.

Esch T, Taubenbock H, Chrysoulakis N, Duzgun HS, Tal A, Feigenwinter C & Parlow E 2013. Exploiting earth observation in sustainable urban planning and management—The GEOURBAN project. In *Urban Remote Sensing Event*. Proceeding of Joint Urban Remote Sensing Event (JURSE) held 21-23 April 2013, Sao Paulo, Brazil.

ESRI 2013a. What is a LiDAR, ArcGIS resources help 10.1[online help]. Online available: http://resources.arcgis.com/en/help/main/10.1/index.html#//015w00000041000000.

ESRI 2013b. 5 ways to use LiDAR more effectively [online ArcUser]. Online available: http://www.ESRI.com/ESRI-news/arcuser/summer-2013/5-ways-to-use-LiDAR-more-efficiently.

Eurosense 2011 .Urban green monitoring [online]. Available from http://www.eurosense.com/documents/your-application/energy-environment-agriculture/urban-green-monitoring.xml?lang=en-gb [Access 10 Mai 1012].

Fahsi A, Tsegaye T, Tadesse W & Coleman T 2000. Incorporation of digital elevation models with Landsat-TM data to improve land cover classification accuracy. *Forest Ecology and Management* 128: 57-64.

Feng D, Wang X & Liu Y 2008. An edge detection method for infrared image based on grey relational analysis. In *2nd International Symposium on Systems and Control in Aerospace and Astronautics*. Proceedings of a meeting held 10-12 December 2008, Shenzhen, China.

Feret J & Asner GP 2012. Semi-supervised methods to identify individual crowns of lowland tropical canopy species using imaging spectroscopy and LiDAR. *Remote Sensing* 4, 8: 2457-2476.

Fernandes LA & Oliveira MM 2008. Real-time line detection through an improved Hough transform voting scheme. *Pattern Recognition* 41, 1: 299-314.

Fitzgerald RW & Lees BG 1994. Assessing the classification accuracy of multisource remote sensing data. *Remote Sensing of Environment* 47, 3: 362-368.

Fowler RA 2001. The thorny problem of LiDAR specifications [online]. Available from http://www.lasermap.com/laserM/en/doc03.htm. [Accessed on September 2012].

Fraser CS, Dial G & Grodecki J 2006. Sensor orientation via RPCs. *ISPRS Journal of Photogrammetry & Remote sensing* 60, 3: 182-194.

Frédéricque B, Daniel S, Bédard Y & Paparoditis N 2008. Populating a building multi-representation database with photogrammetric tools: recent progress. *ISPRS Journal of Photogrammetry and Remote Sensing* 64, 4: 441–460.

Gamba P & Houshmand B 2000. Digital surface models and building extraction: A comparison of IFSAR and LiDAR data. *IEEE Transactions on Geoscience and Remote Sensing* 38, 4: 1959-1968.

Gamba P & Martin H (eds) 2009. *Global mapping of human settlement: experiences, datasets, and prospects*. Boca Raton: CRC Press Taylor & Francis.

Gamba P, Du P, Juergens C & Maktav D 2011. Foreword to the special issue on “Human settlements: A global Remote sensing challenge”. *IEEE Journal of Selected Topics in Applied Earth Observations and Remote Sensing* 4, 1: 5-7.

Gang Y, Fuzhou D, Wenhui Z, Wenji Z & Lianjun Z 2010. Building extraction in towns and villages based on digital aerial image by texture enhancing. In *18th International Conference on Geoinformatics*: *GIScience in Change*, 1-6. Proceedings of a meeting held 18-20 June 2010, Beijing, China.

Gatziolis D & Andersen HE 2008. *A guide to LiDAR data acquisition and processing for the forests of the Pacific Northwest*. US Department of Agriculture, Forest Service, Pacific Northwest Research Station.

Gaulton R & Malthus TJ 2010. LiDAR mapping of canopy gaps in continuous cover forests: a comparison of canopy height model and point cloud based techniques. *International Journal of Remote Sensing* 31, 5: 1193-1211.

Gehrke S, Morin K, Downey M, Boehrer N & Fuchs T 2010. Semi-global matching: An alternative to LIDAR for DSM generation. In *Canadian Geomatics Conference and the International symposium*. Proceedings of the 2010 Canadian Geomatics Conference and Symposium of Commission I held 15-18 June, Calgary, Alberta, CANADA.

Gentsos C, Sotiropoulou CL, Nikolaidis S & Vassiliadis N 2010. Real-time canny edge detection parallel implementation for FPGAs. In *2010 17th IEEE International Conference on Electronics, Circuits, and Systems (ICECS).* Proceedings of 17th IEEE International conference on Electronics, Circuits, and Systems (ICECS) held 12-15 December 2010, Athens, Greece.

Giri C, Ochieng E, Tieszen LL, Zhu Z, Singh A, Loveland T, Masek J & Duke N 2011. Status and distribution of mangrove forests of the world using earth observation satellite data. *Global Ecology and Biogeography* 20, 1: 154-159.

Grigillio D & Fras MK 2011. Classification based Building detection from Geoeye-1 image. In Stilla U et al. (eds) *Joint Urban Remote Sensing Event* (*JURSE* 2011), 381-384. Proceedings of the 2011 Joint Urban Remote Sensing event was held 11-13 April 2011, Munich, Germany.

Grodecki J 2001. Ikonos stereo feature extraction - RPC approach. In Congalton R (ed) *2001 American Society for Photogrammetry & Remote Sensing (ASPRS) Annual Conference, 23-27*. Proceedings of ASPRS Annual Meeting held 21-26 April, St Louis, Missouri, USA.

Gupta RP 2003. *Remote sensing geology*. 2nd ed. Berlin: Springer-Verlag.

Haala N & Brenner C 1999. Extraction of buildings and trees in urban environments. *ISPRS Journal of photogrammetry & Remote Sensing* 54, 2: 130-137.

Habib A, Ghanma M, Morgan M & Al-Ruzouq R 2005. Photogrammetric and LiDAR data registration using linear features. *Photogrammetric Engineering and Remote Sensing* 71, 6: 699-707.

Haklay M 2010. How good is volunteered geographical information? A comparative study of OpenStreetMap and Ordnance Survey datasets. *Environment and planning. B, Planning & design* 37, 4: 682-703.

Hermosilla T, Ruiz LA, Recio JA & Estornell J 2011. Evaluation of automatic building detection approaches combining high resolution images and LiDAR data. *Remote Sensing* 3, 6: 1188-1210.

Holland DA, Boyd DS & Marshall P 2006. Updating topographic mapping in Great Britain using imagery from high-resolution satellite sensors. *ISPRS Journal of Photogrammetry and Remote Sensing* 60, 3: 212-223.

Huang B, Xie C & Tay R 2010. Support vector machines for urban growth modelling. *Geoinformatica* 14, 1: 83-99.

Huang X & Zhang L 2011. A multidirectional and multiscale morphological index for automatic building extraction from multispectral GeoEye-1 imagery. *Photogrammetric engineering and remote sensing* 77, 7: 721-732.

Huang X, Zhang L & Gong W 2009. Information fusion of aerial images and LIDAR data in urban areas: vector-stacking, re-classification and post-processing approaches. *International Journal of Remote Sensing* 32, 1: 69-84.

Hussain E, Ural S, Kim K, Fu CS & Shan J 2011. Building extraction and rubble mapping for City Port-au-Prince Post-2010 earthquake with GeoEye-1 imagery and LiDAR data. *Photogrammetric Engineering and Remote Sensing* 77, 10: 1011-1023.

IgorPro 2014. Online from: http://www.wavemetrics.com/products/igorpro/imageprocessing/imagetransforms.htm. [Accessed 17/11/2014].

Ioannidis C, Psaltis C & Potsiou C 2009. Towards a strategy for control of suburban informal buildings through automatic change detection. *Computer, Environment and Urban Systems* 33: 64-74.

Iovan C, Boldo D & Cord M 2008. Detection, characterization, and modelling vegetation in urban areas from high-resolution aerial imagery. *Selected Topics in Applied Earth Observations and Remote Sensing* 1, 3: 206-213.

Jackson RD & Huete AR 1991. Interpreting vegetation indices. *Preventive Veterinary Medicine* 11, 3: 185-200.

Jayachandran A, Dhanashakera R, Anand OS & Ajitha JHM 2010. Fuzzy information system based digital image segmentation by edge detection. In *Computational Intelligence and Computing Research* (ICCIC), 1-5. Proceeding of a meeting Held 28-29 December 2010, Coimbatore, India.

Jiao J 2012. A random forest based method for urban land-cover classification using LiDAR data and aerial imagery. Master's thesis. Waterloo: University of Waterloo, Department of Geography.

Jin X & Davis CH 2005. Automated building extraction from high-resolution satellite imagery in urban areas using structural, contextual, and spectral information. *EURASIP Journal on Applied Signal Processing* 2196-2206.

Kabolizade M, Ebadi H & Ahmadi S 2010. An improved snake model for automatic extraction of buildings from urban aerial images and LiDAR data. *Computers, Environment and Urban Systems 34*, 5: 435-441.

Kasetkasem T & Varshney PK 2011. An optimum land cover mapping algorithm in the presence of shadows. *IEEE Journal of Selected Topics in Signal Processing* 5, 3: 592-605.

Kim J & Muller JP 2011.Trees and building detection in dense urban environments using automated processing of Ikonos image and LiDAR data. *International Journal of Remote Sensing* 32: 2245-2273.

Kitchin F & Oven W 2009. Land management and spatial planning in towns and cities. Paper presented on the urban landmark conference held 28-29 March, Midrand, Gauteng, South Africa.

Kliarchuk K & Collins D 2011. Evaluation of stereoscopic GeoEye-1 satellite imagery to assess Landscape and stand level characteristics. In Lichti DD & Habib AF (eds) *ISPRS Archives-Volume XXXVIII-5/W12, 2011*. Proceedings of workshop on Laser Scanning held 29-31 August, Calgary, Canada.

Kneubuhler M, Richter R, Schaepman M & Itten K 2005. Geometric and radiometric pre-processing of CHRIS/ PROBA data over mountain terrain. In Lacost H & Ouwehand L (eds) *3rd International workshop on radiation of high temperature gases in atmospheric entry*. Proceedings of the third ESA Chris/ Proba workshop held 21-23 March 2005, Venice, Italy.

Koc D & Turker M 2005. Automatic building detection from high resolution satellite images. In Kurnaz S (ed), *Recent Advance in Space Technologies, Space in the Service of Society, RAST 2005*, 617-622. Proceedings of 2nd International Conference on Recent Advance in Space Technologies, held 9-11 June 2005, Istanbul, Turkey.

Kodge BG & Hiremath PS 2010. Automatic open space area extraction and change detection from high resolution urban satellite image. *Foundation of Computer Science* 1: 76-82.

Kothari CR 2011. *Research methodology: Methods & techniques*. New Delhi: New Age International.

Krause G, Bock M, Weiers S & Braun G 2004. Mapping land cover and mangrove structures with remote sensing techniques: a construction to a synoptic GIS support of coastal management in North Brazil. *Environmental Management* 34, 3: 429-440.

Krauβ T, Reinartz P & Stilla U 2007. Extracting orthogonal building objects in urban areas from high resolution stereo satellite image pairs. In Stilla U, Mayer H, Rottensteiner F, Heipke C & Hinz S (eds) *PIA 07 Photogrammetric Image Analysis*. Proceedings of the Photogrammetric Image Analysis Conference (PIA) held 19-21 September 2007 Munich, Germany.

Kumar R 2014. *Research methodology: A step-by-step guide for beginners*. 4th ed. London: SAGE Publication Ltd.

Kumar S 2005. *Basics of Remote sensing and GIS*. New Delhi: Laxmi Publications.

Küsel A 2009. The South African urban renewal programme (URP): Development of rural/urban nodes in the context of migration. Paper delivered at the Urban-Rural Linkages and Migration Conference, Pretoria.

La Rosa D & Privitera R 2013. Characterization of non-urbanized areas for land-use planning of agricultural and green infrastructure in urban contexts. *Landscape and Urban Planning* 109, 1: 94-106.

Laliberte AS, Rango A, Hacstad KM, Paris JF, Beck RF, Mcneely R & Gonzalez AL 2004. Object-oriented image analysis for mapping shrub encroachment from 1937 to 2003 in southern New Mexico. *Remote Sensing of Environment* 93: 198-210.

Land info World Mapping, LLC 2013. GeoEye-1 high-resolution satellite imagery [online]. Available from http://www.landinfo.com/geo.htm [Accessed on September 1013].

Lein KJ 2011. *Environmental sensing: Analytical techniques for earth observation*. New York: Springer.

Leiss IA, Sandmeier S, Itten KI & Kellenberger TW 1995. Improving land use classification in rugged terrain using radiometric corrections and a possibility based classification approach. In Stein TI (ed*) IGARSS'95: Quantitative Remote Sensing for Science and Applications*. Proceedings of Geoscience and Remote Sensing Symposium held 10-14 July 1995, Firenze, Italy. Quantitative Remote Sensing for Science and Applications.

Lemmens M 2007. Airborn LiDAR sensors. *GIM international* 21, 2: 24-27

Leukert K, Darwish A & Reinhardt W 2004. Transferability of Knowledge-based classification rules. Paper delivered at the 3rd International eCognition User Meeting.

Leung Y 2010. *Knowledge discovery in spatial data*. Berlin: Springer- Verlag.

Li G, Lu D, Moran E & Batistella M 2013. Land Use/Land Cover Classification in the Brazilian Amazon with Different Sensor Data and Classification Algorithms. In Wang G & Weng Q (eds) *Remote Sensing of Natural Resources,* 111-123. Beijing: Taylor & Francis.

Li J & Jones J 2006. Classification using multiple and negative target rules. In Gabrys B, Howlett RJ & Jain LC (eds) *Knowlegde intelligent information and engineering systems*. Proceedings of the 10 th International conference, KES 2006 held 9-11 October 2006, Bournemouth, UK.

Li S, Zhang B, Gao L, Sun X 2009. Small objects detection of hyperspectral image in urban areas. *Urban Remote Sensing* 1:1-5.

Lia G, Lu D, Moran E & Batistella M 2013. Land Use/Land Cover Classification in the Brazilian Amazon with Different Sensor Data and Classification Algorithms. In Wang G & Weng Q (eds) *Remote Sensing of Natural Resources,* 111-123. Beijing: Taylor & Francis.

Liang S, Li X & Vang J 2012. *Advance remote sensing: terrestrial information extraction and applications*. San Diego: Elsevier Inc.

Liu D & Xia F 2010. Assessing object-based classification: advantages and limitations. *Remote Sensing Letters* 1, 4: 187-194.

Liu X, Kafatos M, Gomez RB & Goetz SJ 2003. Combining MISR, ETM+ and SAR data to improve land cover and land use classification for carbon cycle research. In *2003 IEEE Workshop on Advances in Techniques for Analysis of Remotely Sensed Data,* 80-85. Proceedings of the IEEE Workshop on Advances in Techniques for Analysis of Remotely Sensed Data held 27-28 October 2003, Greenbelt, Maryland, USA. Piscataway: Institute of Electrical & Electronics Engineers.

Liu X, Zhang Z & Peterson J 2009. Evaluation of the performance of DEM interpolation algorithms for LiDAR data. In Ostendorf B, Baldock P, Bruce D, Burdett M & Corcoran P (eds) *Proceedings of the Surveying and Spatial Sciences Institute: Biennial International Conference* held 22 September -2 October 2009, Adelaide, Australia. Surveying and Spatial Sciences Institute.

Liu Z, Cui S, Yan Q 2008. Building extraction from high resolution satellite imagery based on multi-scale image segmentation and model matching. Paper delivered at the second International Workshop on Earth Observation and Remote Sensing Applications, China.

Lu D & Weng Q 2006. Use of impervious surface in urban land-use classification. *Remote Sensing of Environment* 102, 1: 146-160.

Lu D & Weng Q 2009. Extraction of urban impervious surfaces from an IKONOS image. *International Journal of Remote Sensing* 30, 5: 1297-1311.

Lunetta RS, Knight JF, Ediriwickrema J, Lyon JG & Worthy LD 2006. Land-cover change detection using multi-temporal MODIS NDVI data. *Remote sensing of environment 105*, 2: 142-154.

Martin D, Fowlkes C Tal D & Malik J 2001. A database of human segmented natural images and its application to evaluating segmentation algorithms and measuring ecological statistics. In *Proceedings* of the *Eighth International Conference On Computer Vision* (*ICCV*-01), held July 7-14 July, British Columbia, Canada.

Masialetti I 2008. Assessment of time-series MODIS data for cropland mapping in the U.S. central great plain. Doctoral dissertation. Kansas: Graduate school of University of Kansas, Department of Geography.

Mather P, Koch M 2011. *Computer processing of remotely sensed images: An introduction*. 4th ed. Oxford: John Wiley & Sons.

Mbaabu PR 2012. AGB/Carbon mapping using Airborne LIDAR data and GeoEye satellite images in tropical forest of Chitwan-epal: a comparison of community and Government managed forests. Master's thesis. Netherlands: University of Twente, Department of Geo-information Science and Earth Observation.

McIver D K & Friedl, MA 2001. Estimating pixel-scale land cover classification confidence using nonparametric machine learning methods. *Geoscience and Remote Sensing* 1: 1959-1968.

Meguro Y & Fraser CS 2010. Georeference accuracy of GeoEye-1 stereo imagery: experiences in Japanese test field. *International Archive of the Photogrammetry, Remote Sensing and Spatial Information Science* 38, 8:1069-1072.

Meier P 2013. Introducing Micro Mappers for digital disaster response [online]. Available from http://irevolution.net/2013/04/13/micromappers-for-digital-disaster-response/. [Accessed 21 june 2013].

Meng X, Currit N & Zhao K 2010. Ground filtering algorithms for Airborne LiDAR data: a review of critical issues. *Remote Sensing* 2: 833-860.

MicroImages, Inc 2013. Georeference/rectify [online]. Available from http://www.microimages.com [Accessed 10 November 2013].

Mihleim LE, JonesJW & Barlow RA 2007. Development of an Impervious-Surface Database for the Little Black water River Watershed, Dorchester County, Maryland. Geological Survey

Mitchell AL, Milne A, Tapley I, Lowell K, Caccetta P, Lehmann E, Zhou ZS & Held A 2011. Key outcomes of the Tasmania 'National Demonstrator': A project for the GEO Forest Carbon tracking task. In Proceedings of the 34th International Symposium on Remote Sensing of Environment held in Sydney, 10-15 April 2011.

Mokhtarzade M, Zoej MV & Ebadi H 2008. Automatic road extraction from high resolution satellite images using neural networks, texture analysis, fuzzy clustering and genetic algorithms. In Proceedings of *The International Archives of the Photogrammetry Remote Sensing and Spatial Information Sciences* held 3-11 July 2008, Beijing, China.

Moran EF 2010. Land cover classification in a complex urban-rural landscape with QuickBird imagery. *Photogrammetric engineering and remote sensing* 76, 10: 1159-1168.

Mountrakis G, Im J & Ogole C 2011. Support vector machines in remote sensing: A review. *ISPRS Journal of Photogrammetry and Remote Sensing* 66, 3: 247-259.

Mountrakis G, Im J & Ogole C 2011. Support vector machines in remote sensing: A review. *ISPRS Journal of Photogrammetry and Remote Sensing* 66, 3: 247-259.

Myint SW, Gober P, Brazel A, Grossman-Clarke S & Weng Q 2011. Per-pixel vs. object-based classification of urban land cover extraction using high spatial resolution imagery. Remote Sensing of Environment 115, 5: 1145-1161.

Nain N, Laxmi V, Jain AK & Agarwal R 2006. Morphological Edge Detection and Corner Detection Algorithm Using Chain Encoding. Hamid R & Arabnia (eds) In *IPCV'06: The 2006 International Conference on Image Processing, Computer Vision, & Pattern Recognition*. Proceedings of the 2006 International Conference on Image Processing, Computer Vision, & Pattern Recognition held 26-29 June 2006, Nevada, USA.

Navulur K 2007. *Multispectral image analysis using the objects-oriented paradigm*. CRC Press/Taylor & Francis.

Netzband M, Stefanov WL & Redman C (eds) 2007. *Applied remote sensing for planning, governance and sustainability*. Berlin: Springer-Verlag.

Niemeyer J, Rottensteiner F & Soergel U 2014. Contextual classification of LiDAR data and building object detection in urban areas. *ISPRS Journal of Photogrammetry and Remote Sensing* 87, 152-165.

Owechko Y, Medasani S & Korah T 2010. Automatic recognition of diverse 3-D objects and analysis of large urban scenes using ground and aerial LIDAR sensors. Paper presented at the Conference of Optical Society of America on Lasers and Electro-Optics, held 16-21 Mai 2010, San Jose, California USA.

Patentstorm 2012. Inertial measurement unit with aiding from roll isolated gyro [online]. Available from: http://www.patentstorm.us/patents/5067084/description.html [Accessed 05 September 2012].

Pauleit S, Ennos R & Golding Y 2005. Modelling the environmental impacts of urban land use and land cover change—a study in Merseyside, UK. *Landscape and Urban Planning* 71, 2: 295-310.

Pesaresi M & Gerhardinger A 2011. Improved textural built-up presence index for automatic recognition of human settlements in arid regions with scattered vegetation. *Journal of selected topics in applied earth observations and Remote Sensing* 4, 1: 16-26.

Pidwirny M 2006. Introduction to Geographic Information Systems. Fundamentals of Physical Geography, 2nd Edition [online]. Available from: http://www.physicalgeography.net/fundamentals/2e.html [Accessed 15 January 2012].

Pinho CMD, Silva FC, Fonseca LMC & Montero AMV 2008. Intra-urban Land Cover classification from high-resolution images using the C4.5 Algorithm. *The International Archives of the Photogrammetry, Remote Sensing and Spatial Information Sciences* 37, 1: 695-700.

Pittman SJ, Costa B & Wedding LM 2013. LiDAR Applications. In *Coral Reef Remote Sensing* 145-174. Netherlands: Springer.

Potsiou C; Doytsher Y, Kelly P, Khouri R & McLaren R 2010. Rapid urbanization and megacities: the need for spatial information management. In *FIG Congress 2010 Facing the Challenges - Building the Capacity*. Proceedings of The XXIV FIG International Congress held 11-16 April 2010, Sydney, Australia.

Priestnall G, Jaafar J & Duncan A 2000. Extracting urban features from LiDAR digital surface models.*Computers, Environment and Urban Systems* 24, 2: 65-78.

Rahman AA, Boguslawski P, Gold C & Said MI 2013. Developments in multidimensional spatial data models. Heidelberg: Springs.

Ramesh A 2012. Response of flood events to land use and climate change. Dordrecht: Springer.

Ren Z, Zhou G, Cen M, Zhang T & Zhang Q 2008. A novel method for extracting building from LiDAR data -Fc-S method. *The International Archives of the Photogrammetry, Remote Sensing and Spatial Information Sciences* 37: 283-288.

Renslow M, Greenfiel P & Guay T 2000. Evaluation of multi-return LiDAR for Forestry applications. *Remote Sensing Applications Centre* 1: 1-19.

Reyers B, O'Farrell PJ, Cowling RM, Egoh BN, Le Maitre DC & Vlok JH 2009. Ecosystem services, land-cover change, and stakeholders: finding a sustainable foothold for a semiarid biodiversity hotspot. *Ecology and Society* 14, 1: 1-23.

Richmond B 2013. A huge Laser-Mapping project is redrawing America. Available from http://motherboard.vice.com/blog/a-huge-laser-mapping-project-is-redrawing-america. [Accessed October 2013].

Richter R. & Schläpfer D 2014. Atmospheric/topographic correction for airborne imagery. *DLR report DLR-IB*, 565-01.

Ros Gordon MN & Bertoldi A 2007. Overview of urban land as a commodity in South Africa. Paper delivered on Urban Land Visioning towards 2020 workshop held in May 2007.

Rottensteiner F & Briese Ch 2002. A new method for building extraction in urban areas from high resolution LiDAR data. In Proceedings of *ISPRS on Photogrammetry Computer Vision* held 9-13 September 2002 Graz, Austria, 1-7.

Rust K 2006. Analysis of South Africa's housing sector performance [online], housing finance africa. Available from: http://www.housingfinanceafrica.org/wp-content/uploads/2006/12/HSectorPerformanceDec.pdf [Accessed 10 October 2012].

Sabins FF 2007. *Remote sensing: principles and applications*. 3rd ed. Long Grove: Waveland Press.

Salehi B, Zhang Y, Zhong M & Dey V 2012. Object-based classification of urban areas using VHR imagery and height points ancillary data. *Remote Sensing 4*, 8: 2256-2276.

Samad AM, Haron NS, Karnadi MS & Maarof I 2009. A comparison of AIRSAR and SPOT imagery for land cover mapping. *Signal Processing & its Applications* 1: 93-97.

SANBI (South African National Biodiversity Institute) 2009. Updating land cover. SANBI: Pretoria.

Sawaya KE, Olmanson LG, Heinert NJ, Brezonik PL & Bauer ME 2003. Extending satellite remote sensing to local scales: land and water resource monitoring using high-resolution imagery. *Remote Sensing of Environment* 88, 1: 144-156.

Schoeman F, Newby TS, Thompson MW & Van den Berg EC 2013. South African national land cover change map. *South African Journal of Geomatics* 2, 2: 1-12.

Schowengerdt RA. 2006. *Remote sensing: models and methods for image processing*. Burlington: Elsevier.

Shackelford AK & Davis CH 2003. Urban road network extraction from high-resolution multispectral data. *Remote Sensing and Data Fusion over Urban Areas* 1: 142-146.

Shackelford AK 2004. *Development of urban area Geospatial information products from high resolution satellite imagery using advance image analysis techniques*. Publication Number: AAI3204336; ISBN: 9780542503122. Columbia: Dissertation Abstracts International 67, 1: 201-451.

Shrestha DP & Zinck JA 2001. Land use classification in mountainous areas: Integration of image processing, digital elevation data and field knowledge (application to Nepal). *International Journal of Applied Earth Observation and Geo-information* 3, 1: 78-85.

Shruthi RBV, Kerle N & Jetten V 2011. Objects-based gully feature extraction using high spatial resolution imagery. *Geomorphology* 134: 260-268.

Siart C, Bubenzer O & Eitel B 2009. Combining digital elevation data (SRTM/ASTER), high resolution satellite imagery (QuickBird) and GIS for geomorphological mapping: A multi-component case study on Mediterranean karst in central Crete. *Geomorphology* 112, 2: 106-121.

Small C 2003. High spatial resolution spectral mixture analysis of urban reflectance. *Remote Sensing of Environment* 88, 1: 170-186.

Smith MJ, Paron P & Griffiths JS (eds) 2011. *Geomorphological Mapping: methods and applications*. Oxford: Elsevier.

South Africa (Republic of) 2010. Land cover field guide: CSIR Satellite Application Centre/ Earth Observation Service Centre. Pretoria: Department of Rural Development and Land Reform.

Steiner FR Butler K & American planning Association 2012. *Planning and urban design standards*. s.l.: John Wiley & Sons.

Surveying and land information Department (SLID) 2011. An introduction to coordinate systems in South Africa. Durban: SLID.

Tarek R & Jurgens C (eds) 2010. *Remote sensing of urban and Suburban areas*. London: Springer.

Taubenböck H, Esch T, Wurm M, Roth A & Dech S 2010. Object-based feature extraction using high spatial resolution satellite data of urban areas. *Journal of Spatial Science 55*, 1: 117-132.

Theng LB 2006. Automatic building extraction from satellite imagery. *Engineering Letters*, 13, 3: 255-259.

Thompson M 1996. A standard land-cover classification scheme for remote-sensing applications in South Africa. *South African journal of Science* 92, 1: 34-42.

Tooke TR, Coops NC, Goodwin NR & Voogt JA 2009. Extracting urban vegetation characteristics using spectral mixture analysis and decision tree classifications. Remote Sensing of Environment 113, 2: 398-407.

Toth CK 2009. R & D of mobile LIDAR mapping and future trends. In *American Society for Photogrammetry and Remote Sensing Annual Conference 2009* (*ASPRS 2009*).

Proceeding of ASPRS Annual Conference held 9-13 March 2009, Baltimore, Maryland, USA.

Tueller PT 2006. Remote sensing technology for rangeland management applications. *Journal of range management 42,* 6: 442-453.

Turner W, Spector S, Gardiner N, Fladeland M, Sterling E & Steininger M 2003. Remote sensing for biodiversity science and conservation. *Trends in ecology & evolution 18,* 6: 306-314.

Van Niekerk A 2012. Developing a very high resolution DEM of South Africa. *Position IT* 55-60.

Varshney PK & Arora MK (eds) 2004. Advance image processing for remotely sensed hyperspectral data. Berlin: Springer.

Verburg PH, Van De Steeg J, Veldkamp A & Willemen L 2009. From land cover change to land function dynamics: a major challenge to improve land characterization. *Journal of environmental management* 90, 3: 1327-1335.

Viera AJ & Garrett JM 2005. Understanding inter observer agreement: the kappa statistic. *Fam Med 3,* 5: 360-363.

Vincent OR & Folorunso O 2009. A descriptive algorithm for sobel image edge detection. In *Informing Science & IT Education joint Conference,* 97-107. Proceedings of Informing Science & IT Education Conference held 12-15 June 2009, Macon, Georgia USA.

Vögtle T & Steinle E 2003. On the quality of object classification and automated building modelling based on laser scanning data. *The International Archives of Photogrammetry, Remote Sensing and Spatial Information Sciences* 34, 3: 1-7.

Wang O, Lodha SK & Helmbold DP 2006. A bayesian approach to building footprint extraction from aerial LiDAR data. In Pollefeys M, Danilidis K (eds) *2006 3rd International Symposium on 3D Data Processing Visualization and Transmission,* 192-1993. Proceedings of a meeting held 14-16 June 2006, Chapel Hill, North Carolina. Piscataway: Institute of Electrical and Electronics Engineers.

Wang Y 2009. *Remote sensing of coastal environments*. Boca Raron: Taylors and Francis group.

Ward JT 2008. *Realistic texture in simulated thermal infrared imagery*. Doctoral dissertation. New York: Rochester Institute of Technology, the Chester F. Carlson Centre for Imaging Science.

Wei Y, Zhao Z & Song J 2004. Urban building extraction from high-resolution satellite panchromatic image using clustering and edge detection. In Davis CH & Lukowski T (eds) *2004 IEEE International Geoscience and Remote Sensing Symposium Science for Society: Exploring and Managing a Changing Planet,* 2008-2010. Proceedings of

IGARSS 2004 IEEE International Geoscience and Remote Sensing Symposium Science for Society held 20-24 September 2004, Anchorage, Alaska, USA.

Weidner U 1997. Digital surface models for building extraction. In Gruen A, Baltsavias EP & Henricsson O (eds) *automatic extraction of man-made objects from aerial and space images* 193-202. Berlin: Birkhausser.

Wen X & Yang X 2008. An operational improvement of haze/clear line identification from satellite imagery on multi-resolution segmentation. In Zhou Q & Luo J (eds) *2008 Second International Symposium on Intelligent Information Technology Application (IITA),* 571-575. Proceedings of the second international symposium on Intelligent Information Technology Application held 21-22 December 2008, Shanghai, China.

Weng Q & Hu X 2008. Medium spatial resolution satellite imagery for estimating and mapping urban impervious surfaces using LSMA and ANN. *IEEE Transactions on Geoscience and Remote Sensing* 46, 8: 2397-2406.

Weng Q & Quattrochi DA 2006. *Urban remote sensing*. Boca Raton: Taylor & Francis Group.

Weng Q, Lu D & Schubring J 2004. Estimation of land surface temperature–vegetation abundance relationship for urban heat island studies. *Remote sensing of Environment* 89, 4: 467-483.

West PC, Narisma GT, Barford CC, Kucharik CJ & Foley JA 2010. An alternative approach for quantifying climate regulation by ecosystems. *Frontiers in Ecology and the Environment 9*, 2: 126-133

Wu H, Huang Q, Zhou L & Okutani I 2008. Identification of band reflectance for each category and land-cover classification using fuzzy least-squares method. In Ma J, Yin Y & Zhou S (eds) *Fuzzy Systems and Knowledge Discovery: fifth International conference,* 47-53. Proceedings of the 5th International Conference on Fuzzy Systems and Knowledge Discovery (FSKD '08) held 18-20 October, Jinan, China.

Wu X & Li Y 2010. Integrated method of building edge line feature extraction from aerial imagery and digital surface model. In Liu Y & Chen A (eds) 2010 *18th International Conference on Geoinformatics*. Proceedings of a meeting held 18-20 June 2010, Beijing, China.

Wulder MA & Franklin SE 2006. *Understanding forest disturbance and spatial pattern, Remote sensing and GIS approaches*. Boca Raton: CRC Press Taylor & Francis Group.

Wurm M, Taubenböck H & Dech S 2010. Quantification of urban structure on building block level utilizing multisensoral remote sensing data. In Michel U & Civco DL (eds) *Earth Resources and Environmental Remote Sensing/GIS Applications*. Proceedings of

International Society for Optic and Photonics (SPIE) held 11-14 October 2010, Songdo Convencia Incheon, Republic of Korea.

Yang X 2011. *Urban remote sensing: monitoring, synthesis and modelling in the urban environment*. Chichester: Wiley-Blackwell.

Yu H, Cheng G, GE X & Lu X 2011. Object oriented land cover classification using ALS and GeoEye imagery over mining area. *Transaction of Nonferrous Metals Society of China* 21: s733-s737.

Yuan F & Bauer ME 2006. Mapping impervious surface area using high resolution imagery: A comparison of object-based and per pixel classification. In *Annual Conference of the American Society for Photogrammetry and Remote Sensing 2006: Prospecting for Geospatial Information Integration*. Proceedings of ASPRS 2006 annual conference held 1-5 May 2006, Reno, Nevada.

Yuan F & Bauer ME 2007. Comparison of impervious surface area and normalized difference vegetation index as indicators of surface urban heat island effects in Landsat imagery. *Remote Sensing of Environment* 106, 3: 375-386.

Yuan F & Bauer ME 2007. Comparison of impervious surface areas and normalized difference vegetation index as indicators of surface urban heat island effects in Landsat imagery. *Remote Sensing of Environment* 106, 3: 375-386.

Yuan F, Sawaya KE, Loeffelholz BC & Bauer ME 2005. Land cover classification and change analysis of the Twin Cities (Minnesota) Metropolitan Area by multitemporal Landsat remote sensing. *Remote Sensing of Environment* 98, 2: 317-328.

Zhang J He C, Zhou Y, Zhu S & Shuai G 2014. Prior-knowledge-based spectral mixture analysis for impervious surface mapping. *International Journal of Applied Earth Observation and Geoinformation* 28: 201-210.

Zhang X, Feng X & Jiang H 2010. Object-oriented method for urban vegetation mapping using IKONOS imagery. *International Journal of Remote Sensing* 31, 1: 177-196.

Zhou W 2013. An object-based approach for urban land cover classification: Integrating LiDAR height and intensity data. *Geoscience and Remote Sensing Letters, IEEE* 10, 4: 928-931.

Zhou W, Troy A & Grove M 2008. Object-based land cover classification and change analysis in the Baltimore metropolitan area using multitemporal high resolution remote sensing data. *Sensors 8*, 3: 1613-1636.

APPENDICES

APPENDIX A: LAND COVER CLASSIFICATION SCHEME

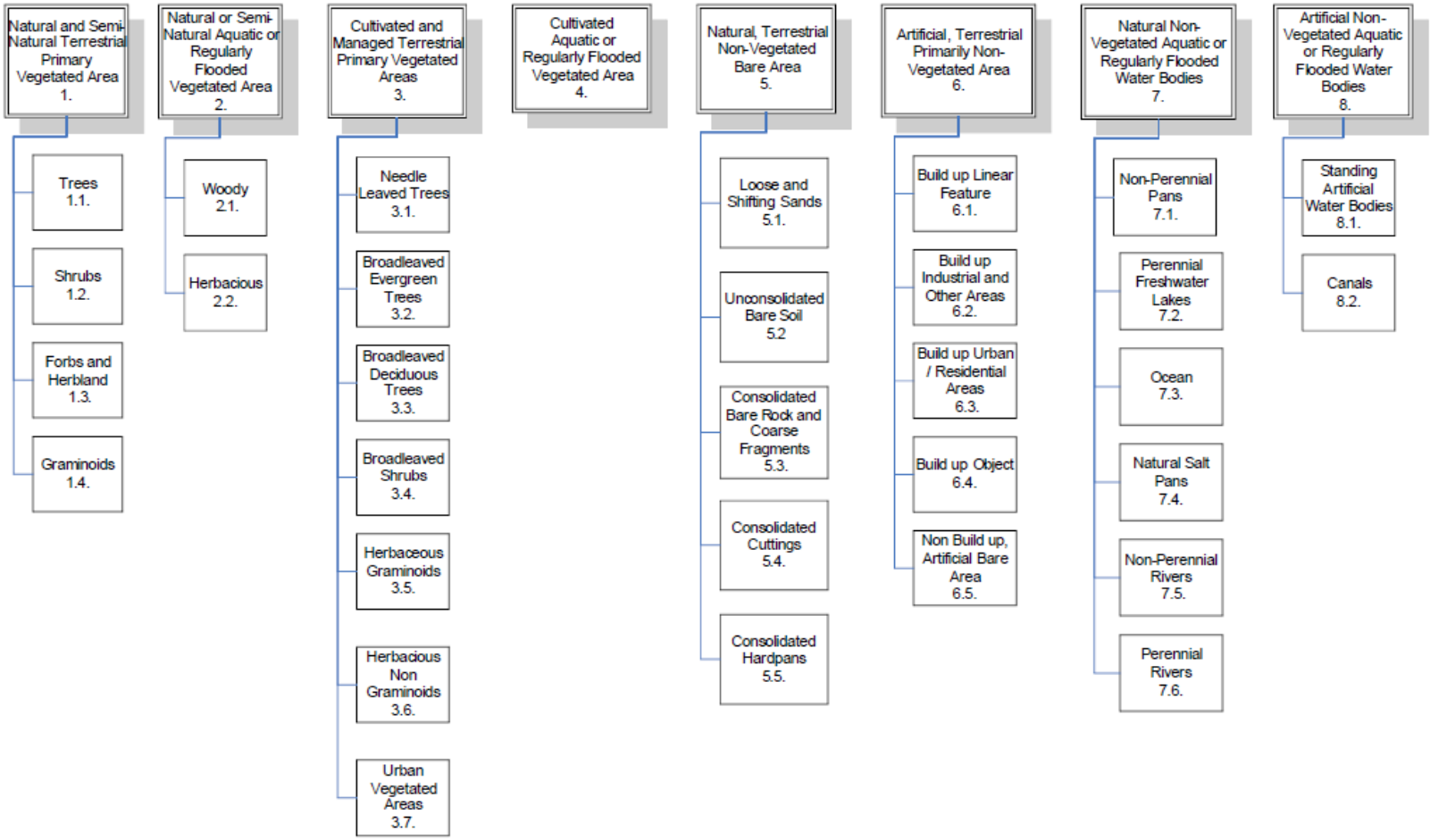

APPENDIX B: LAND COVER EXTRACTED

FIGURE B1 Urban land cover extracted from GeoEye-1 imagery and the LiDAR DSM using KNN

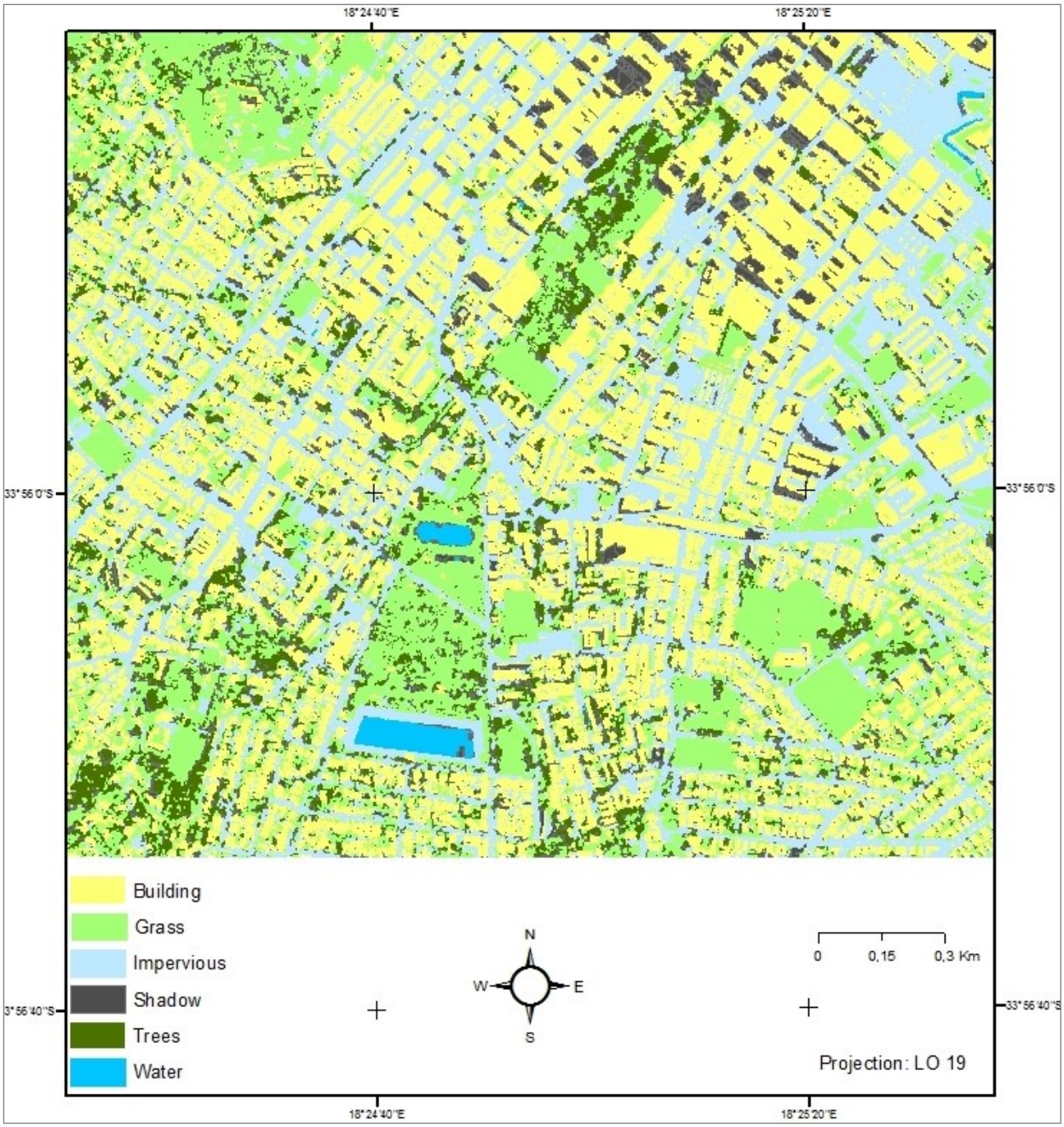

FIGURE B2 Urban land cover extracted from GeoEye-1 imagery using KNN

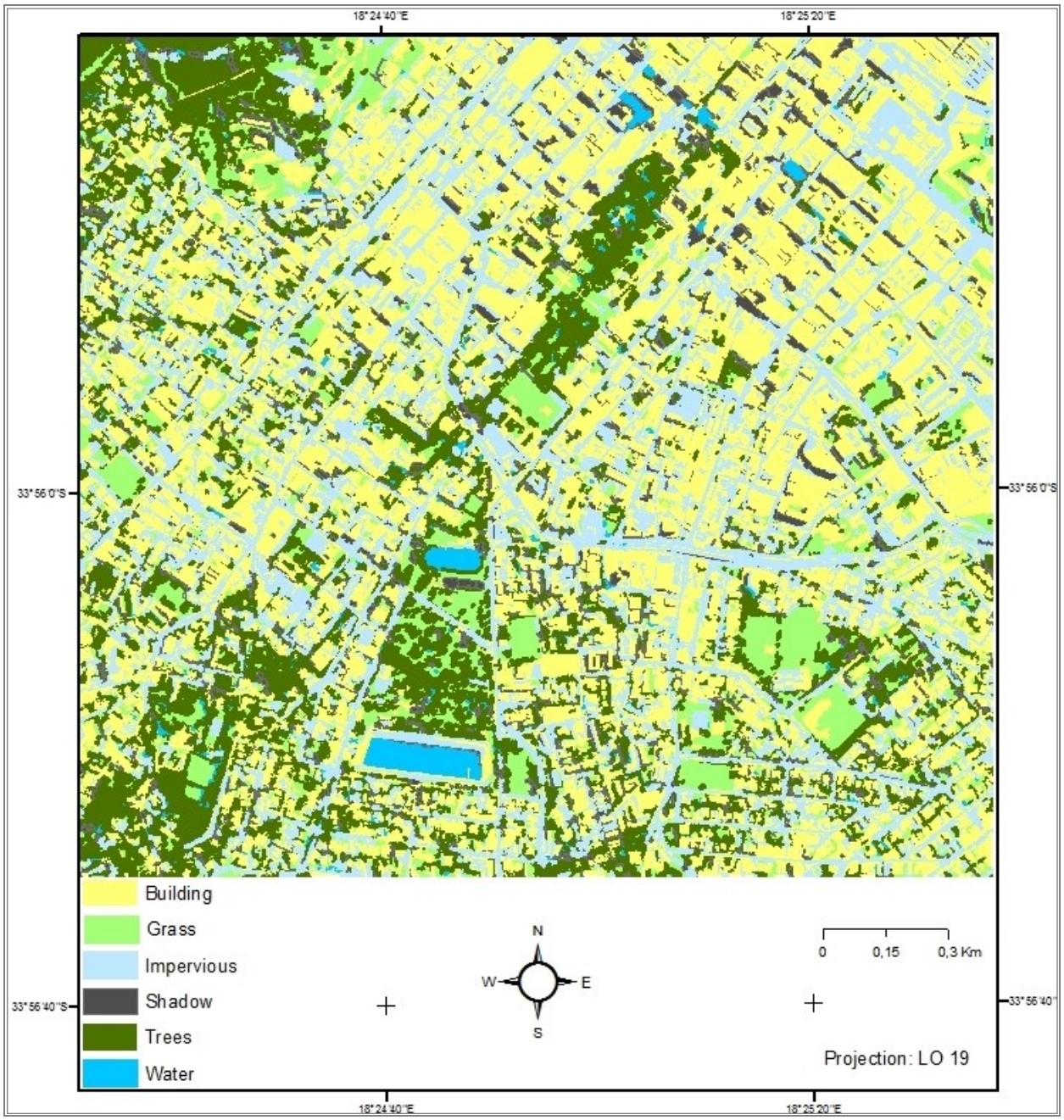

FIGURE B3Urban land cover extracted from GeoEye-1 imagery and nDSM using CART

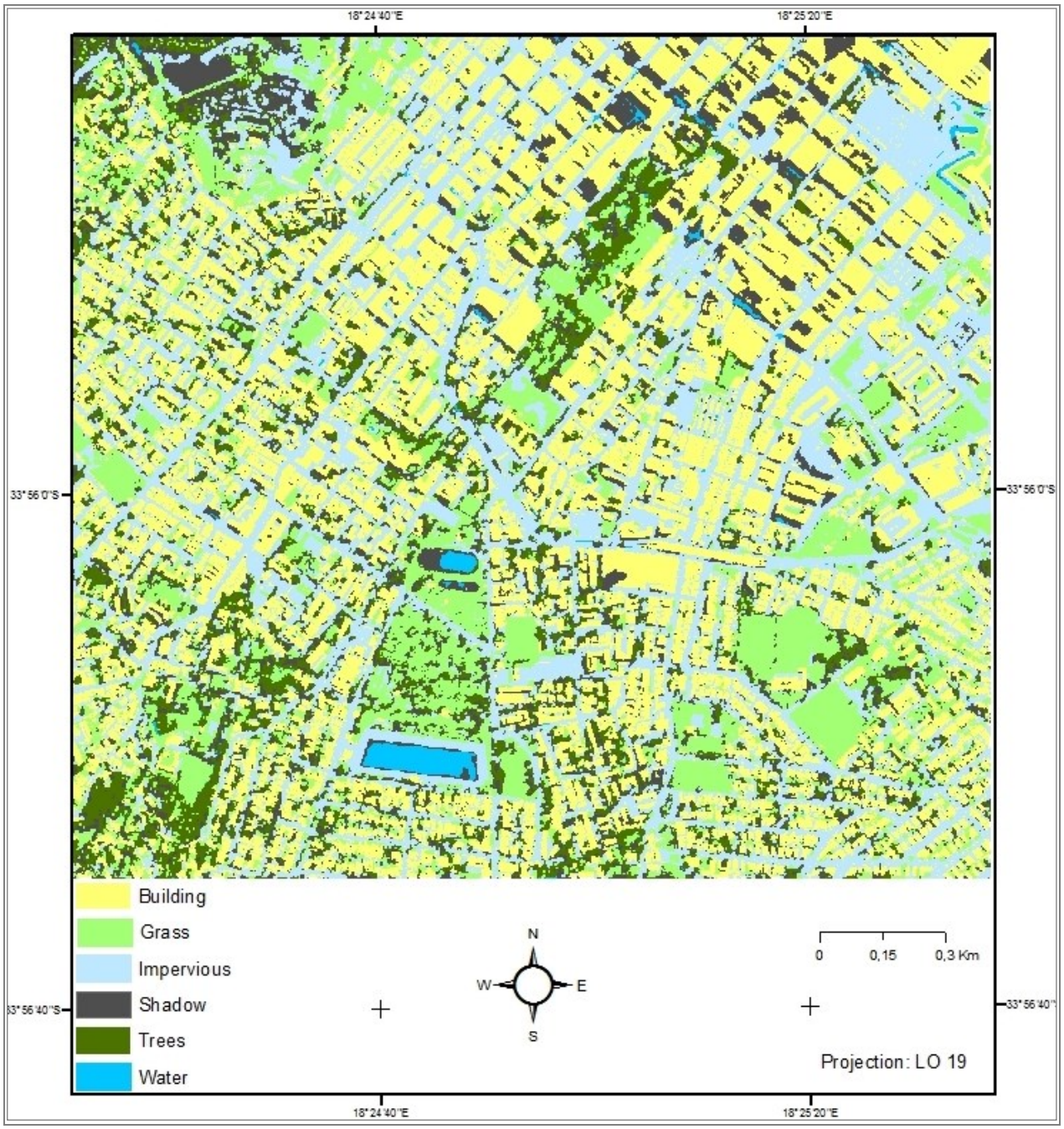

FIGURE B4 Urban land cover extracted from GeoEye-1 imagery using CART

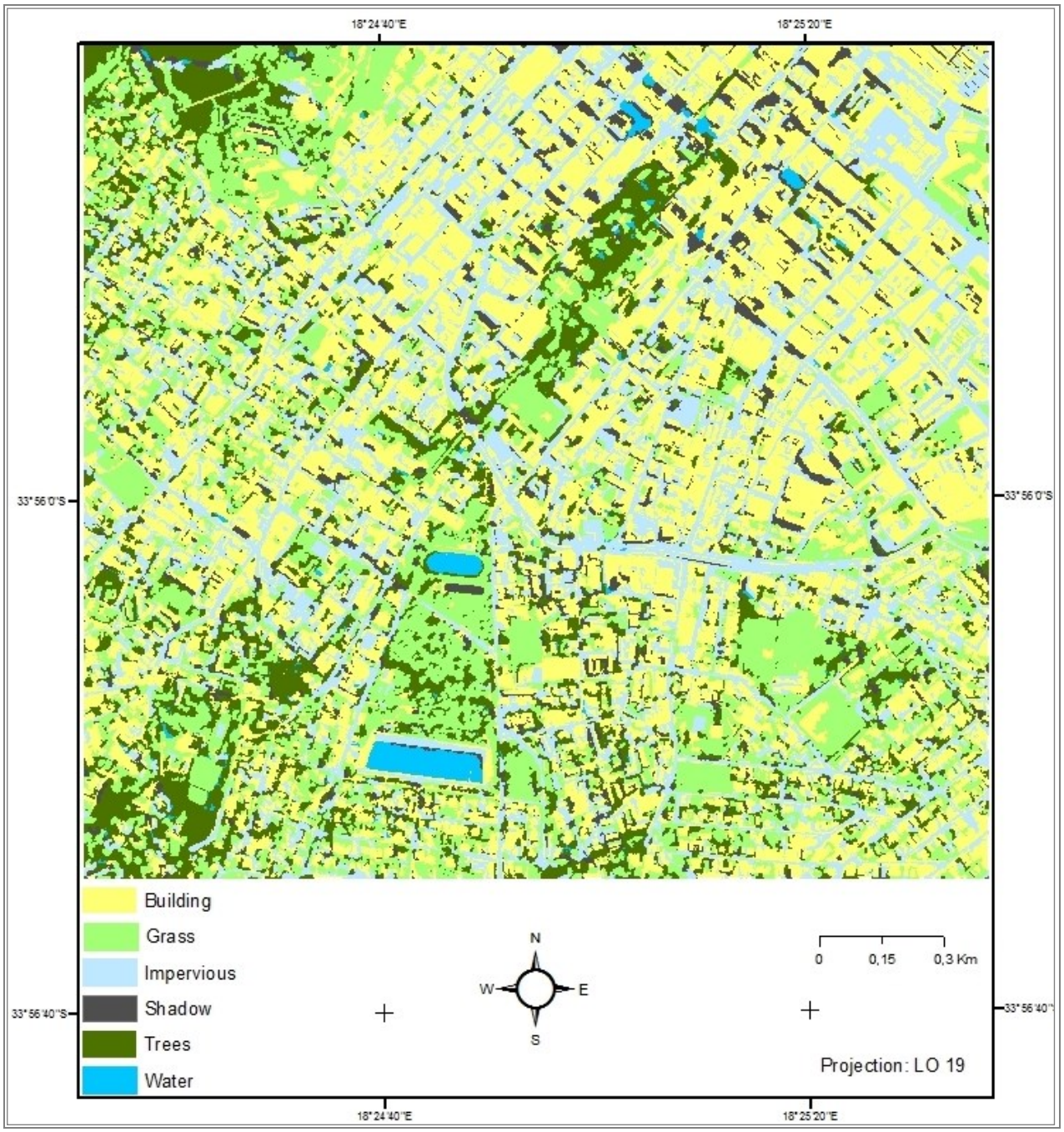

FIGURE B5 Urban land cover extracted from GeoEye-1 imagery and nDSM using SVM

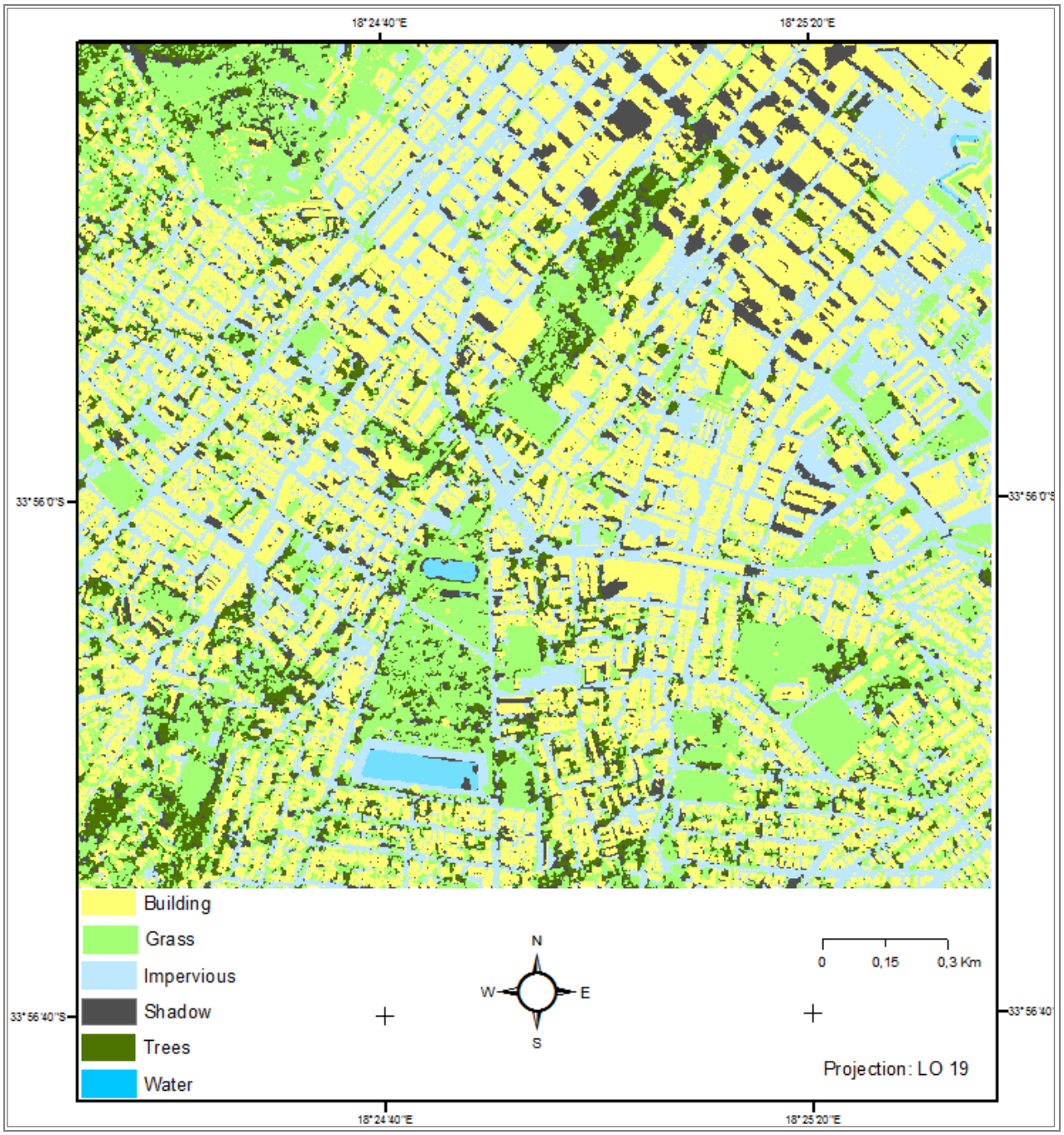

FIGURE B6 Urban land cover extracted from GeoEye-1 imagery and nDSM using The RBC

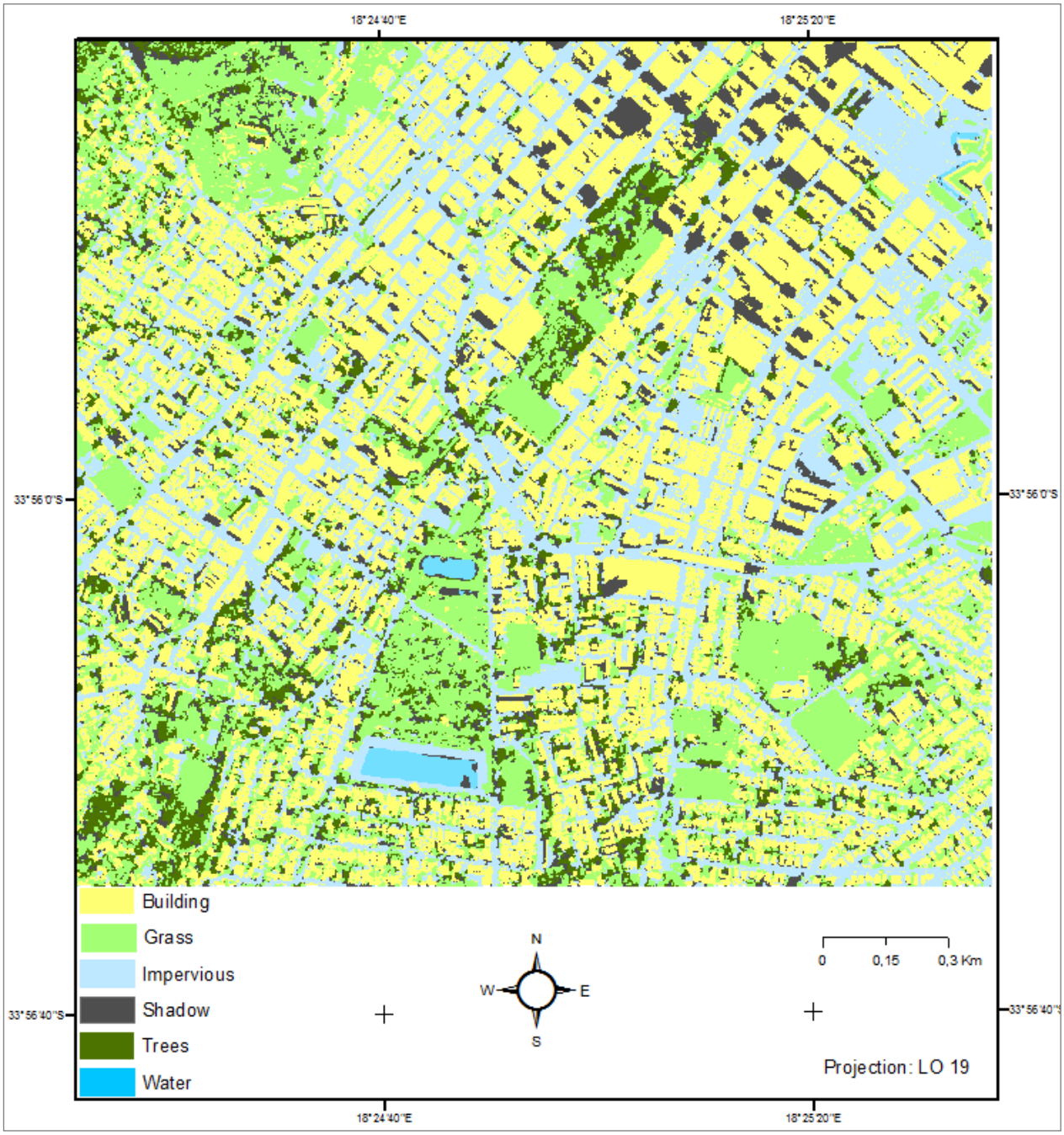

APPENDIX C: ACCURACY ASSESSMENT LAND COVER MAPS

Table C1Confusion matrix of the land cover maps produced with the GeoEye-1 imagery and the nDSM for experiment A

	Reference / classified	Building	Grass	Impervious areas	Shadow	Trees	Water	Total
Rule based	Building	5575	106	42	124	155	10	6012
	Grass	161	2647	1303	0	355	21	4487
	Impervious areas	125	27	3470	63	7	0	3692
	Shadow	97	56	78	185	609	0	1025
	Trees	73	64	9	0	2929	0	3075
	Water bodies	0	0	0	0	0	222	222
	Total	6031	2900	4902	372	4055	253	18513
	Producer accuracy	92.44	91.28	70.79	49.73	72.23	87.75	
	User accuracy	92.73	58.99	93.99	18.05	95.25	100.00	
	Overall accuracy		81.1		**Kappa**		0.75	
KNN	Building	5647	80	125	0	920	0	6772
	Grass	0	2341	397	0	103	0	2841
	Impervious areas	73	168	3859	11	15	21	4147
	Shadow	206	237	478	345	24	23	1313
	Trees	75	133	24	10	2956	0	3198
	Water bodies	0	0	21	0	0	208	229
	Total	6001	2959	4904	366	4018	252	18500
	Producer accuracy	94.10	79.11	78.69	94.26	73.57	82.54	
	User accuracy	83.39	82.40	93.06	26.28	92.43	90.83	
	Overall accuracy		82.8		**Kappa**		0.77	
CART	Building	5560	82	131	1	832	0	6606
	Grass	0	2061	238	0	50	0	2349
	Impervious areas	21	245	3792	11	23	21	4113
	Shadow	244	412	514	342	57	72	1641
	Trees	178	131	23	10	3044	0	3386
	Water bodies	52	28	206	0	12	159	457
	Total	6055	2959	4904	364	4018	252	18552
	Producer accuracy	91.82	69.65	77.32	93.96	75.76	63.10	
	User accuracy	84.17	87.74	92.20	20.84	89.90	34.79	
	Overall accuracy		80.6		**Kappa**		0.75	
SVM	Building	5530	134	131	11	1180	0	6986
	Grass	0	2341	398	0	103	0	2842
	Impervious areas	73	168	3859	11	15	21	4147
	Shadow	332	237	473	342	75	23	1482
	Trees	120	79	23	0	2645	0	2867
	Water bodies	0	0	0	0	0	208	208
	Total	6055	2959	4884	364	4018	252	18532
	Producer accuracy	91.33	79.11	79.01	93.96	65.83	82.54	
	User accuracy	79.16	82.37	93.06	23.08	92.26	100.00	
	Overall accuracy		80.4		**Kappa**		0.74	

Table C2 Confusion matrix of the land cover maps produced with the GeoEye-1 imagery and the nDSM for experiment B

	Reference / classified	Building	Grass	Impervious areas	Shadow	Trees	Water	Total
Rule based	Building	5567	56	115	95	269	0	6102
	Grass	174	2243	573	0	215	12	3217
	Impervious areas	162	175	3773	102	52	9	4273
	Shadow	12	230	398	166	531	0	1337
	Trees	117	247	70	0	2950	0	3384
	Water bodies	0	0	0	0	0	231	231
	Total	6032	2951	4929	363	4017	252	18544
	Producer accuracy	92.29	76.01	76.55	45.73	73.44	91.67	
	User accuracy	91.23	69.72	88.30	12.42	87.17	100.00	
	Overall accuracy		80.5		**Kappa**		0.74	
KNN	Building	5584	255	570	115	564	3	7091
	Grass	33	2052	432	0	47	0	2564
	Impervious areas	46	120	3118	2	1	18	3305
	Shadow	193	93	243	255	25	0	809
	Trees	118	322	32	0	3328	0	3800
	Water bodies	0	21	279	0	60	239	599
	Total	5974	2863	4674	372	4025	260	18168
	Producer accuracy	93.47	71.67	66.71	68.55	82.68	91.92	
	User accuracy	78.75	80.03	94.34	31.52	87.58	39.90	
	Overall accuracy		80.2		**Kappa**		73.80	
CART	Building	5647	291	557	86	965	3	7549
	Grass	12	1857	490	0	47	0	2406
	Impervious areas	54	198	2913	2	1	14	3182
	Shadow	60	137	489	44	49	52	831
	Trees	189	302	59	240	2950	0	3740
	Water bodies	12	78	166	0	13	191	460
	Total	5974	2863	4674	372	4025	260	18168
	Producer accuracy	94.53	64.86	62.32	11.83	73.29	73.46	
	User accuracy	74.80	77.18	91.55	5.29	78.88	41.52	
	Overall accuracy		74.9		**Kappa**		0.67	
SVM	Building	5614	226	537	74	552	3	7006
	Grass	12	2024	327	0	42	0	2405
	Impervious areas	65	148	3271	2	6	0	3492
	Shadow	171	114	400	296	61	0	1042
	Trees	110	351	32	0	3351	0	3844
	Water bodies	2	0	107	0	13	253	375
	Total	5974	2863	4674	372	4025	256	18164
	Producer accuracy	93.97	70.70	69.98	79.57	83.25	98.83	
	User accuracy	80.13	84.16	93.67	28.41	87.17	67.47	
	Overall accuracy		81.5		**Kappa**		0.76	

Table C 3Confusion matrix of the land cover maps extracted from GeoEye-1 imagery for experiment C

	Reference classified	Building	Grass	Impervious areas	Shadow	Trees	Water	Total
Rule based	Building	3885	165	1477	77	104	0	5708
	Grass	1167	1816	791	0	686	14	4474
	Impervious areas	881	11	2376	144	130	7	3549
	Shadow	19	15	47	93	6	0	180
	Trees	56	896	206	0	3062	0	4220
	Water bodies	0	0	0	0	0	234	234
	Total	6008	2903	4897	314	3988	255	18365
	Producer accuracy	64.66	62.56	48.52	29.62	76.78	91.76	
	User accuracy	68.06	40.59	66.95	51.67	72.56	100.00	
	Overall accuracy		61.90		**Kappa**		0.50	
KNN	Building	4795	318	2081	158	264	7	7623
	Grass	305	1972	258	0	447	0	2982
	Impervious areas	639	155	2045	0	211	0	3050
	Shadow	160	127	329	206	86	0	908
	Trees	132	388	165	0	2641	0	3326
	Water bodies	14	7	23	0	341	234	619
	Total	6045	2967	4901	364	3990	241	18508
	Producer accuracy	79.32	66.46	41.73	56.59	66.19	97.10	
	User accuracy	62.90	66.13	67.05	22.69	79.40	37.80	
	Overall accuracy		64.21		**Kappa**		0.53	
CART	Building	3776	407	1710	0	490	7	6390
	Grass	591	1955	226	0	539	14	3325
	Impervious areas	1171	141	2460	0	197	0	3969
	Shadow	371	107	353	310	67	0	1208
	Trees	136	356	135	0	2693	0	3320
	Water bodies	0	1	17	54	0	234	306
	Total	6045	2967	4901	364	3986	255	18518
	Producer accuracy	62.46	65.89	50.19	85.16	67.56	91.76	
	User accuracy	59.09	58.80	61.98	25.66	81.11	76.47	
	Overall accuracy		61.70		**Kappa**		0.50	
SVM	Building	3583	473	4055	119	560	14	8804
	Grass	700	2006	165	0	360	0	3231
	Impervious areas	1478	81	276	0	154	7	1996
	Shadow	187	56	165	245	20	0	673
	Trees	95	351	186	0	2794	0	3426
	Water bodies	2	0	54	0	102	234	392
	Total	6045	2967	4901	364	3990	255	18522
	Producer accuracy	59.27	67.61	5.63	67.31	70.03	91.76	
	User accuracy	40.70	62.09	13.83	36.40	81.55	59.69	
	Overall accuracy		49.33		**Kappa**		0.32	